THE UTILITY OF PHARMACOMETRICS IN DRUG DEVELOPMENT AND PHARMACOTHERAPY OF ANTIMICROBIALS

A DISSERTATION SUBMITTED TO THE FACULTY OF THE

UNIVERSITY OF MINNESOTA

BY

ALI AHMED ALHADAB

IN PARTIAL FULFILLIMENT OF THE REQUIREMENTS

FOR THE DEGREE OF

DOCTOR OF PHILOSOPHY

RICHARD C. BRUNDAGE, Advisor

MARNIE L. PETERSON, Co-Advisor

December 2017

DEDICATION

This work is dedicated to my beloved parents and family for their endless love, support and encouragement and to all advisers, mentors, teachers and individuals who helped me through my trainings.

ABSTRACT

Infectious diseases are a growing major public health concern due to the increase of antimicrobial resistance to current therapies and the lack of new drugs in development. As an alternative to developing new anti-infective drugs, my thesis research focuses on ways to optimize current antimicrobial therapies. This thesis aims specifically to utilize pharmacometric modeling and simulation that applies pharmacokinetic (PK) and pharmacodynamics (PD) principles to provide insights into ways to maximize drug effect while minimizing side effects and preventing resistance. Mathematical and statistical methods are used to develop integrated drug, body, and microbial models that quantify relationships among dose, plasma and tissue concentrations, and microbial killing. These pharmacometric models are then used to predict the outcome of various untested scenarios to select the optimal dosing regimens for confirmatory clinical testing.

A dose-finding study, named COAT, was conducted to assess the PK and microbiological efficacy of adjunctive sertraline for the treatment of cryptococcal meningitis (CM) in HIV-infected Ugandans. Plasma sertraline concentrations, fungal counts in cerebral spinal fluid, and survival outcome were modeled to characterize the dose-exposure-response-outcome relationships of sertraline as an antifungal. Sertraline PK was influenced by body weight and co-administration anti-retroviral therapy (ART) non-nucleotide reverse transcriptase inhibitors. The addition of sertraline to the standard induction therapy of Cryptococcus increased fungal clearance rate from cerebrospinal fluid 34-48% compared to COAT trial, a similar historical study in which patients received CM induction therapy without sertraline. The effect of sertraline on Cryptococcus fungal clearance was similar irrespective of the daily dose patients received

iv

(100 – 400 mg). The 2-week survival rates were lower for females and patients receiving sertraline 100 and 400 mg daily.

Further, a model-based meta-analysis of sertraline published PK studies in healthy adults were performed to estimate oral bioavailability, absorption and plasma clearance. Sertraline had super-proportional increase in exposure with dose attributed to the nonlinear increase of bioavailability with dose. The findings were then used to build and validate a physiological-based pharmacokinetic (PBPK) model in order to assess the potential clinical use of sertraline as an antimicrobial. PBPK oral stimulations indicated that therapeutic doses (50-200 mg) of sertraline do not produce clinical concentrations required for antimicrobial effects (MIC = 1 – 12 mg/L).

In addition, a population PK model of aminoglycoside antibiotic, amikacin, was developed in pediatric cancer patients and used to predict the probability of various dosing regimens to achieve PK-PD targets predictive of efficacy and toxicity. Simulation indicated ≥ 60 mg/kg administered once daily are expected to have a 97.5% probability in which the unbound $fC_{max}/MIC \geq 8$ is achieved in 80% of pediatric patients weighing 8-70 kg and the unbound $fC_{min} < 10$ mg/L in almost all patients. Furthermore, the population PK model was linked to an adaptive PD (ARPD) model of amikacin against *Pseudomonas aeruginosa* built using *in vitro* literature time-kill curve data to perform PK-ARPD simulation. The results suggested that amikacin 90 mg/kg given in two divided doses (45 mg/kg twice a day) will hit safety ($fC_{min} < 10$ mg/L) and efficacy ($fC_{max}/MIC \geq 8$) targets, and be associated with a lower rate of bacterial resistance evident by bacterial counts being below the limit of detection until day 7.

This thesis demonstrates the vital role of pharmacometric modeling and simulation in the rational selection of dose regimens of antimicrobial agents. The application of this tool in drug development process and clinical practice can guard against the costly late-stage failures and improve clinical outcomes of patient care, respectively.

TABLE OF CONTENT

LIST OF TABLES

LIST OF FIGURES

1   THESIS SCOPE AND OBJECTIVES

The scope of this thesis is to demonstrate the utility of pharmacometric modeling and simulation approach in informing drug development and optimizing pharmacotherapy of antimicrobials. The specific objectives are:

1. Review the role of pharmacometric-based analysis in improving drug development and pharmacotherapy of antimicrobial agents (Chapter 2).

2. Characterize the dose-exposure-response-outcome relationships of sertraline antifungal properties in HIV-infected patients and identify covariates that affect these relationships (Chapter 3).

3. Characterize sertraline pharmacokinetics in healthy subjects using a model-based meta-analysis (Chapter 4)

4. Assess the potential clinical use of sertraline as an anticancer and antimicrobial agent using a whole-body physiologically-based pharmacokinetic model (Chapter 5).

5. Optimize aminoglycoside antibiotic, amikacin, dose in children with cancer using the probability of achieving MIC-based PK-PD indices and dynamic PK-PD simulation approach (Chapter 6).

2   IMPACT OF PHARMACOMETRICS ON DRUG DEVELOPMENT AND PHARMACOTHERAPY OF ANIT-MICROBIALS

2.1   SUMMARY

While microbial resistance toward available therapies increases worldwide, the number of newly approved antimicrobial drugs decreases with very few ones in development pipelines. This alarming situation is attributed to the key triad of unproductive and inefficient drug development approach, inappropriate uses of anti-infective agents in clinical settings, and lack of interest of pharmaceutical industry in the antimicrobial sector. The latter is solved with economic incentive programs put in place to allure pharmaceutical companies to re-enter the field and to replenish the drought in antimicrobial pipelines. Pharmacometrics, on the other hand, is recognized and endorsed by regulatory agencies as the tool to address the first two causes. It streamlines the drug development process, de-risks investments, improves the economic viability, increases the probability of success, and accelerates drug approval. Pharmacometrics can also improve pharmacotherapy practice via the optimization of antimicrobial dosing regimens to maximize efficacy, minimized drug-related toxicity, and reduce microbial resistance. Additionally, it is applied to set antimicrobial susceptibility breakpoints, to guide formulary decision in health-care systems, and to establish infection treatment guidelines.

2.2   INTRODUCTION

Pharmacometrics is an emerging discipline that is gaining rapid popularity in pharmaceutical industry, regulatory agencies and academia due its potential to improve

drug development and the practice of pharmacotherapy. Yet, it remains greatly under-appreciated and under-utilized in both areas. This chapter aims to provide an overview about the shortcomings in drug development and pharmacotherapy, and to demonstrate how these limitations can be overcome by the application of pharmacometric modeling and simulation with a particular emphasis on anti-infective agents.

2.2.1 Problem

The development of a new drug is a very lengthy, costly, and risky process. On average, it takes 13 years for a drug to get the US Food and Drug Administration (FDA) approval for human use since the first discovery (1). Throughout each developmental phase, the number of drug candidates decreases exponentially and so does the costs associated with advancing the drug through the process. About 5% of drugs in development successfully complete the journey from the pre-clinical testing to the clinic that brings the total cost for each successful drug approval to at least $1 billion (2). Of all, the clinical failures, phase II and III studies are the most resource-wasting due to the high cost associated with them. Therefore, an innovative approach is warranted to reliably and quantitatively inform "go/no go" decisions before committing to more expensive studies. This will improve efficiency through resource conservation and reallocation to more promising development programs.

Furthermore, the investment in new drugs continues to increase over time and is currently reaching unsustainable levels. Drug development cost increased 14.3 fold from $0.179 billion in 1970s to $2.558 billion in 2010s and it touches $2.87 billion when accounting for post-approval phase IV commitments (3). There is no doubt that the

inefficient approach of drug development is a key driver for sky-rocketing costs, but it is not the sole contributing factor. Other factors play a role in this issue as well. It is likely that the low-hanging fruits have already been picked. The majority of pharmacological targets for the treatment of human diseases are already identified and targeted with drugs. Today, a greater depth of biological understanding, advanced methodologies and technologies, extensive experimentations, and innovative data modeling tools are required to pinpoint new promising targets and demonstrate its medical value in clinics. This in itself can bring the cost up and delay drug approval let alone the other factors, such as regulatory barriers (4).

For antimicrobials, the problem is even worse and the future looks darker for two main reasons. The first one is the rapid loss of anti-infective arsenal against infectious diseases due to the emergence of antimicrobial resistance (AMR). The outlook of the post-antimicrobial era will be the same as the pre-era. Human life will be significantly affected; many surgical and drug therapies will become limited; and life expectancy will become short once again. Currently, AMR claims 23,000 and 25,000 lives every year in the United States (US) and Europe, respectively (5). AMR also imposes higher economic burdens on health-care systems and patients. In the future, AMR infections are projected to be the number one killer as it was before the discovery of antimicrobials. A report shows that 10 million deaths and total global cost of $100 trillion are expected annually by 2050 (6). This is undoubtedly a global issue that requires immediate action because it is a matter of time before the crisis fully manifests. As a sign for what is coming, a pan-resistant bacterial infection by carbapenem-resistant Enterobacteriaceae (CRE) that was

not susceptible to any available antimicrobial drugs was recently reported in Nevada US and resulted in death (7).

While alarming resistance to anti-infective medications is quickly spreading, a fewer number of newly approved anti-infectives is available to treat AMR infections. This is the second reason that complicates the situation. For the past two decades, there was a constant decline in the number of FDA approved antimicrobials and the very few in development were taking longer times to get approved (8, 9). Additionally, the vast majority of approved drugs after 1985 are not of true clinical value because they lack novelty in mechanism of action. These drugs are synthetic re-engineering of existing ones with underlying resistance mechanisms already present, characterizing the so called "discovery void" period (10, 11).

In addition, drug development endeavors are heavily driven by financial reasons and feasibility more than critical needs. This is reflected on the differential availability of approved antimicrobial therapies and the ones in development. For example, there is a paucity of antifungals in development relative to antivirals and antibacterials (12–17). Likewise, there are more therapeutic classes to choose from for the treatment of bacterial and viral infections whereas therapeutic options are limited for fungal diseases even though the need for safer and more effective antifungals is substantial (18).

2.2.2   Causes

The low productivity and escalating cost of drug development is principally attributed to the use of an empirical statistical approach. It focuses on hypothesis-testing with minimum assumptions to answer a single "yes/no" question at a time to support

regulatory approvals while it largely ignores learning opportunities (19, 20). Also, the approach is often wrongly used in studies whose objectives are merely learning in which open-end questions are of interest, such as "what is the dose-response relationship in a patient population?", "what doses achieve desired effects?", "What dose achieves the maximum response", and "how does a disease change drug exposure?" (21). For example, three clinical studies were performed to determine the highest dose of liposomal amphotericin B associated with the maximal antifungal effect against invasive pulmonary aspergillosis. All concluded the lack of clinical therapeutic benefit with higher doses (22–24). The time, resources, and patient suffering from receiving high doses of a toxic drug, amphotericin B, could have been avoided altogether with one pharmacometric-based analysis that integrated pre-clinical and clinical data. The analysis was, in fact, performed and found there was no additional benefit expected with doses greater than 3 mg/kg/day (25). The analysis answers the right scientific question of interest whereas the three clinical studies answered a slightly different question because analyses were performed with the wrong objective in mind.

Another major limitation of the empirical statistical approach is the inability to leverage all relevant data collected from different sources throughout the development program as just mentioned with example above (19, 20). The approach is also prone to false-positive and false-negative findings due to uncertainty which leads to low statistical power that can be reduced further in case of multiple comparisons (26). To decrease uncertainty and increase power, a large trial with more patients can always be conducted. However, this will cost more and take longer duration of time to complete. Such decision

6

can consume the limited resources that could have been allocated to other development programs.

Similarly, anti-infective pharmacotherapy is practiced at suboptimal levels because clinical recommendations and guidelines are formulated based upon clinical studies analyzed with empirical statistical approaches. It is known with no doubt that sub-optimal use of currently available antimicrobials is a major contributor to the emergence of AMR we are facing today (27). Many older anti-infective agents were approved at suboptimal dosage regimens because the science of pharmacodynamics (PD) used to optimize therapies was simply not existent back then (28). The examples are many and amikacin, an aminoglycoside antibiotic, is a good representative one to list. It is FDA approved at 15 mg/kg in 1-3 divided doses (29–31). This dose is shown to be suboptimal and doses ≥ 40 mg/kg once daily are required to achieve good therapeutic outcomes in different patient populations (7, 31–33).

Another ripple effect of the empirical drug development approach is the selection of inappropriate dose. It is, in fact, the most common cause of failures in clinical development, either due to unsatisfactory efficacy (suboptimal doses) or unexpected adverse events (super-therapeutic doses) (36). Dose-ranging studies are first conducted to determine the range of safe doses for potential clinical use. These studies are mostly analyzed by a linear model, analysis of variance, or multiple pairwise comparisons to select a dose for confirmatory testing in subsequent trials that are likely carried out in parallel design and analyzed the same way. Generally, these empirical analyses are performed under the null hypothesis there is no dose-response relationship. Despite simplicity, rapidity and regulatory acceptability of these tests, they do not provide

information on the shape of individual dose-response curve; do not allow for dose interpolation; and have a strong tendency to select higher doses than required for optimal effect, especially in studies that have few number of patients and large variability in response (37, 38). This can certainly explain the clinical development failures caused by unexpected adverse events since studied doses are mostly super-therapeutic. Drugs that did not fail and received regulatory approval were likely required dose reduction. At least 20% of FDA-approved drugs between 1980-1999 had post-marketing dosage change in which 80% of the time was a dose reduction because of safety concerns (39).

In addition, the mean dose-response curve characterized by empirical statistics can be misleading of the individual curves (40). It is of greater clinical value to identify patient covariates that affect the dose-response relationship as "one dose fits all" is no longer preferred standard of care. Mechanistically, response is driven by drug exposure at the target site and modeling response a function of dose, rather than drug exposure, leads to overestimation of response variability (40). Not all patients receive the same doses will have the same exposures, thus, the over-estimated variability in this case represents the sum of drug exposure and response variability.

Like super-therapeutic dosing, the study of sub-optimal doses can also result in clinical development failures. This is the case in many failures of antimicrobial development programs. Ambrose looked at four different antibacterial programs that failed to get the FDA approval: daptomycin for the treatment of community-acquired (CAP), tigecycline and ceftobiprole for treatment of hospital-acquired pneumonia (HAP), and doripenem for the treatment of ventilator-associated pneumonia (VAP) (41). He showed that all were unsuccessful for one reason and that was the selection and study of

sub-optimal dose regimens in confirmatory pivotal trials. He concluded that a shift from frequentist statistical inferences to pharmacometric-based analyses would help to predict and avoid these costly failures.

Not only is sub-optimal dosing responsible for drug development failures, but also it compromises the efficacy of currently available antimicrobial therapies. As pointed out earlier, the inappropriate prescribing that include unnecessary treatment, wrong drug, wrong dose, wrong dosing frequency, or wrong treatment duration, increased the emergence of AMR. Again, pharmacometrics is suggested to be a promising tool to optimize anti-infective dosing to prevent or at least slow down the rate of microbial resistance (43, 44).

Despite the urgent need for new antimicrobials, fewer drugs are being developed because of the shifting interests in the pharmaceutical industry. This shift of attention started at the national level in 1966 when former Surgeon General of United States, William Stewart stated "it's time to close the books on infectious diseases, declare the war against pestilence won, and shift national resources to such chronic problems as cancer and heart disease" (45). It was a well-said statement that turns out to be true only for the time it was voiced when infectious diseases were easily treatable with efficacious antimicrobials that were abundant. Today, the situation is different because the effective antimicrobial armamentarium is scarce.

For pharmaceutical companies, it was not just a shift of attention. Rather, it was a search for a more lucrative sector with expected high profits (45). Chronic diseases, such as diabetes type II, cardiovascular diseases, and cancer, represented a true captive market since patients require life-long drug treatment as opposed to a short course of therapy that

9

can last usually for 2 weeks to clear an infection. The choice was really an easy one to make given the objective was a market with high profit potential.

Regulatory barriers also make drug development more expensive and extensive. Imposed obstacles includes bureaucracy, approval uncertainty, changes in clinical trial design and requirements, uncertainty regarding the magnitude drug effect, and poor bilateral communications (27, 46). The ultimate impact of these obstacles is the need for larger, more expansive trials to meet approval requirements. As an example, the approval of telavancin, a derivative of vancomycin, to treat HAP caused by Methicillin-resistant Staphylococcus aureus (MRSA) was delayed and made more expansive. The US FDA changed the only requirement to demonstrate non-inferior efficacy to vancomycin in clearing the infection to also show 28-day all-cause of mortality is not higher for telaavancin (47, 48). Not only was the change sudden, but also it was unrealistic as the patients who contract HAP are very sick, making it hard to know if the drug was the real cause of death, and HAP is relatively a rare infection. This additional requirement is a deterrent for companies since the need for larger pivotal trials to capture enough deaths to reach an acceptable statistical power are costly and unaffordable to many (45).

2.2.3 Solutions

Multiple countermeasures are taken to address the key triad causes of the problem: inefficient drug development approach; inappropriate uses of anti-infective agents in clinical settings; and lack of interest of pharmaceutical industry in the antimicrobial sector. Here, we focus only on the use pharmacometrics that address the

first two causes and the role of economic incentivization to replenish antimicrobial pipelines.

The urgent need for a scientific and quantitative approach to assess safety and efficacy of new drugs in faster time frames, with more certainty and at lower cost is recognized by FDA in the white paper titled "Innovation or Stagnation: Challenge and Opportunity on the Critical Path to New Medical Products"(49). In the same paper, the FDA also recognized and strongly endorsed pharmacometrics as a discipline to meet that need through the development and application of pharmaco-statistical models of drug efficacy and safety from preclinical and clinical data to improve drug development knowledge, management, and decision-making. This approach is termed a model-based drug development (MBDD) (19, 49, 50). To address limitations associated with the previous term and capture all potential impacts, the approach is currently named Model-Informed Drug Discovery and Development (MID3) and comprehensively redefined as "quantitative framework for prediction and extrapolation, centered on knowledge and inference generated from integrated models of compound, mechanism, and disease level data and aimed at improving the quality, efficiency and cost-effectiveness of decision making"(51).

The MBDD or MID3 approach was first pioneered by Lewis Sheiner who, with others, demonstrated the usefulness of pharmacometrics to enable knowledge-based decision making and increase drug development efficiencies across the continuum from discovery to commercialization (19, 50, 52). He also introduced the learning-confirming paradigm in which the aim, design and methods of analysis differ depending on whether the phase is learning or confirming. While confirmatory analysis requires few simple

assumptions to test predefined hypotheses using single-study data, exploratory analysis integrates all relevant information across multiple studies when needed and uses rich-assumption models based on known scientific information (physiology, pharmacology, pathophysiology, microbiology, etc) to increase knowledge about compound in development (52). The created knowledge is then used to inform "go/no go" decision making, such as to terminate the development program or to proceed with the next trial to confirm the knowledge and test new assumptions. Of note, a study can have both confirmatory and exploratory objectives, like phase II studies in which dose-response is confirmed and the optimal dose is explored to guide dose selection for future Phase III trials. So, drug development is really an iterative cycle of model-based learning and confirming to steer the compound from discovery to clinic in which knowledge about the compound is updated continuously and used to inform decision making, drug development strategies, and even labelling for approved drugs as shown in Figure 2-1(51).
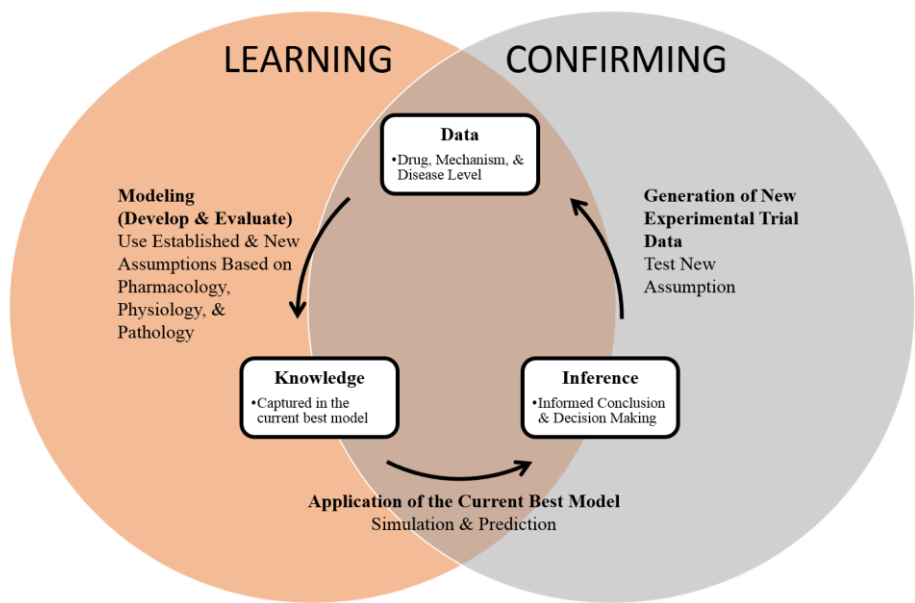
Figure 2-1: Learning and confirming paradigm.

To illustrate the process, the dose-response relationship knowledge in preclinical species is used to select an appropriate dose for a first in human phase I study in which the maximal tolerated dose is determined. Then, dose tolerability and efficacy is confirmed in small of group of patients (phase 2A). The cycle of learning and confirming can be repeated again in larger phase 2B and phase III studies when sufficient efficacy and lack toxicity are convincing to support the investment for full development. In phase 2B, the objectives are to explore the dose-response in larger number of target patients and to propose a dose that has acceptable benefit/risk. The ratio of benefit/risk is subsequently confirmed in a Phase III study to get marketing drug approval. Even though phase III is a confirmatory study, learning should be continued to assess factors that affect safety and efficacy to potentially identify special sub-populations that require different dosing recommendations (19).

To promote the appropriate use of antimicrobial therapies in clinics, several recommended steps are also implemented that include adaptation of antimicrobial stewardship programs, improving diagnosis, tracking prescriptions, prevention of infection and transmission, using combination therapies, and optimization of therapeutic regimens (53). The latter two can be easily achieved with the application of pharmacometrics to develop pharmacokinetic-pharmacodynamic models to describe the interrelated relationships of patient-drug-pathogen. After that, simulation is performed to explore dosing regimens and select the one that maximizes antimicrobial efficacy, minimizes drug-related adverse and reduces microbial resistance.

To address the lack of new antimicrobial development, incentive economic programs are enacted to attract pharmaceutical companies to intensify their research

efforts and replenish development pipelines. Under the US FDA Safety and Innovative ACT (FDASIA), the Generating Antibiotic Incentives Now (GAIN) act was signed into a law in 2012 and aimed to increase the profitability of pharmaceutical companies who develop new antibiotics (53, 54). The act provides 5-year of additional exclusivity and eligibility for fast-track and priority review status to expedite FDA approval. Since then, 39 antibiotics in development has gained the Qualified Infectious Disease Product (QIDP) designation under the GAIN act including 3 drugs (dalbavancin, tedizolid, and oritavancin) that were approved in 2014 (54). A similar program was also enacted in Europe for the same purpose called New Drugs for Bad Bugs (ND4BB) under the public-private Innovative Medicines Initiatives (IMI) (55).

As hoped, the concerted actions of countermeasures has eased the problem. Since the implantation of pharmacometric-based approach, improvements in drug development is recorded. Pharmacometrics has made a remarkable impact on streamlining the drug development process, de-risking investments, improving the economic viability, increasing the probability of success, and accelerating drug approval (50–52, 56). Pharmacometrics also plays a critical role in optimizing antimicrobial dosing regimens to suppress the development of microbial resistance. New pharmacometric-based dosing strategies for old antifungal and antibiotic agents are suggested and published but unfortunately the majority of dosing recommendations are not FDA-endorsed yet (11, 28, 57). Thanks to antimicrobial economic incentive programs, the number of approved anti-infective agents started to increase with 4 approved drugs in 2014 alone ending the decline that lasted for decades, and more drugs are now in development (12–17, 53). Measures put in place were impactful in addressing the triad causes, with

pharmacometric modeling and simulation is likely the most sustainable solution and impactful tool.

2.3   PHARMACOMETRICS

2.3.1   Definition and Principles

Pharmacometrics is the scientific discipline that applies mathematical and statistical methods to develop integrated physiology-drug-disease models to characterize the dose-exposure-response relationships, to quantify uncertainty of these relationships, and to rationalize decision-making in drug development and pharmacotherapy (58). It can also be described as a bridging science as it sets at the interface of many disciplines including and not limited to pharmacology, physiology, pharmacokinetics (PK), pharmacodynamics (PD), microbiology, pathology, data visualization, stochastic simulation, computational science, computer programing, and statistics (59). Pharmacometric models can be made simple (empirical) or complex (mechanistic) as needed to fit the purpose of modeling and simulation exercise. Empirical models, also known top-down approach, are data-driven while mechanistic models (bottom-up) aim to describe mechanisms of human physiology that require prior knowledge, and the combination of the two strategies is the middle-out approach (60). The development of pharmacometric models creates a powerful framework to facilitate multisource data integration for analysis and prediction to quickly explore untested scenarios for informing future decisions.

The application of pharmacometric-based analysis in infectious diseases relies on understanding the dynamic interactions between three components: patient, drug, and pathogen (Figure 2-2) (61). The patient-drug relationship is characterized by PK that describes the relationship between drug dosing and concentration-time profile in the body. PD links drug concentration to desired (drug-pathogen relationship) and undesired (drug-patient relationship) effects. PD also characterizes the decrease in microbial susceptibility upon drug exposure (pathogen-drug relationship). Microbial susceptibility is quantified by minimum inhibitory concentration (MIC) defined as the lowest drug concentration that inhibits visible growth of a pathogen *in vitro*. The patient-pathogen interaction represents immune response against the infective pathogen while the pathogen-patient interaction describes infection severity and physiological changes caused by the infection. These relationships are highly connected and a change in one relationship will trigger a change in the others. For example, a decrease in microbial susceptibility (increased MIC) is associated with more severe infection that causes physiological changes affecting the concentration-profile and drug exposure at the site of infection.
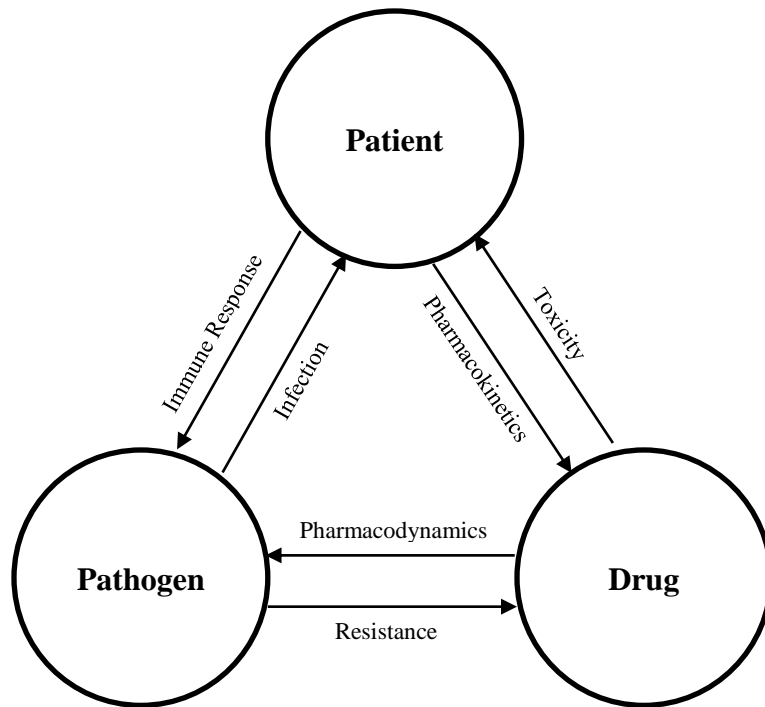
Figure 2-2: Triangle interaction between patient, antimicrobial agent, and Phogen.

A dose recommendation that fails to account for these intricate interactions in the triangle is more likely to result in suboptimal dosing leading to poor clinical outcomes and microbial resistance. Super-therapeutic doses can possibly increase resistance as patients become less adherent to therapy when they experience drug adverse events (55). Using either drug exposure or microbial susceptibility alone is insufficient to predict antimicrobial efficacy. Rather, hybrid parameters that consider PK and PD of the anti-infective agents are shown to be good surrogate endpoints of clinical outcomes and microbiological cure (11, 28, 57, 62–64).

These parameters are: the maximum free (unbound) drug concentration to MIC ratio (fCmax/MIC); the area under the free drug concentration-time curve to MIC (fAUC/MIC); and percent of time in the dosing interval when free drug concentrations are above MIC ($\%fT_{>MIC}$) as shown in Figure 2-3. These PK-PD indices are based on free drug concentrations at the site of infection because only free drug concentrations are

17

available to bind to targets in infective pathogens and produce microbiological effect.

Free plasma concentrations can be used instead when they are good surrogate markers for

concentrations at the site of infection. This is case for most antimicrobial agents but

certainly not all (28). Efficacy-linked PK-PD indices are also indicative of mode of

killing and optimal dosing strategy of an anti-infective drug. The efficacy of agents that

exhibit time-dependent killing with no post antimicrobial effect (PAE), characterized by

the persistent suppression of microbial growth even after concentration drops below MIC,

correlates with %fT>MIC and is maximized by prolonged infusion or small frequent

doses. On the other hand, drugs that have concentration-dependent killing with prolonged

PAE are optimized by large infrequent doses and their efficacy is linked to fCmax/MIC.

The last group of antimicrobial agents shows time-dependent killing with moderate to

prolonged PAE. Their effect is enhanced by dosing regimens that maximize overall drug

exposure relative to MIC as fAUC/MIC is the optimal predictive index.
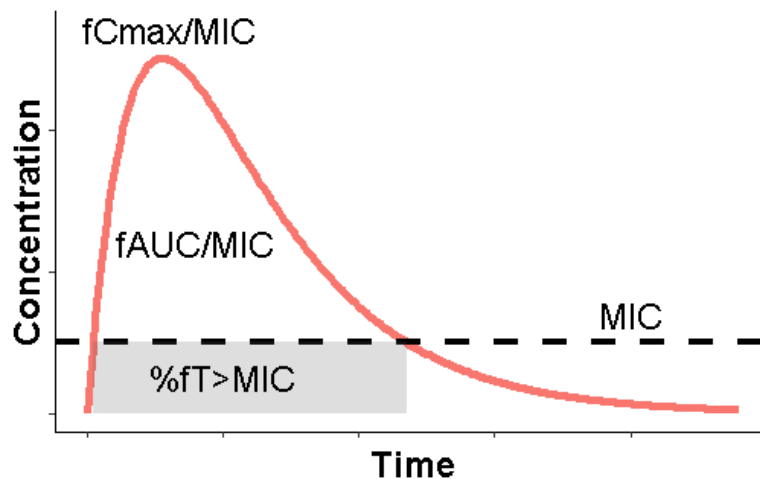
Figure 2-3: Efficacy-linked PK-PD indices of anti-infective agents

The PK-PD index for drugs in the same class is similar and so is the index target

magnitude even for different pathogens that is after accounting for difference in protein

binding between agents (65, 66). The predictive PK-PD index is determined in pre-

clinical animals using dose-fractionation studies in which the same total daily dose is

administered with different dosing intervals to break the correlations between the three

PK-PD indices (Figure 2-4) (57). When the most antimicrobial activity is associated with

the most fractionated dose, then %fT>MIC is likely the predictive index. The relevant

index is fCmax/MIC when the least fractionated dose has the most antimicrobial activity.

If the drug effect is the same regardless of the dose regimens, then efficacy is best

predicted by fAUC/MIC. In such studies, dosing schedule relative to the half-life of the

drug and whether or not the drug has PAE should be taken into considered to avoid

incorrect conclusions. Once this relationship is established, it can easily be extrapolated

to humans after accounting for species difference in physiology assuming the drug-

pathogen interaction is independent of the host. That means the concentration-effect

relationship in human is the same as in laboratory animals (18).
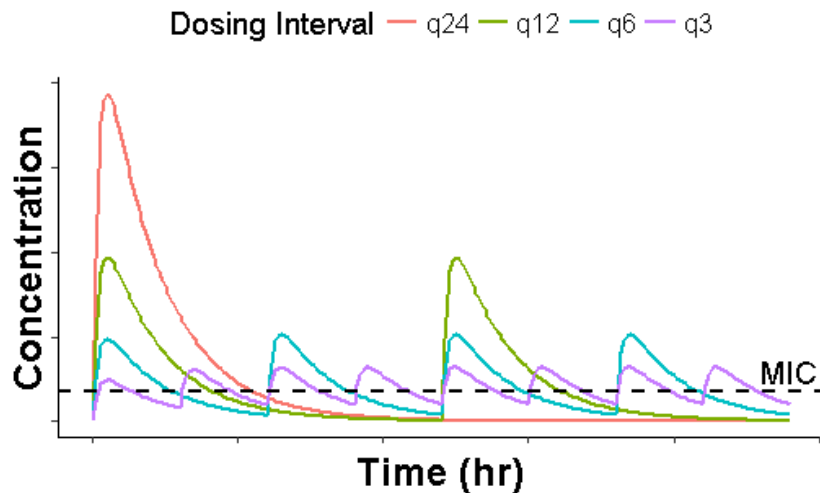
Figure 2-4: Effect of dose fractionation on concentration-time profile.

2.3.2 Acceptance

The Critical Path Initiative Report released in 2004 serves as the official FDA endorsement for the use of pharmacometric modeling and simulation in drug development (49). After that, multiple guidelines for industry are released to reflect the continuous support and encouragement for pharmacometrics use (67–70). The FDA specifically recognizes the role of the pharmacometric-based analyses to address the vexing problems in infectious diseases in a workshop co-sponsored in 2007 with Infectious Diseases Society of America (IDSA) (71). Similarly, pharmacometrics has gained the trust of the FDA counterpart in Europe, European Medicines Agency (EMA), to improve antimicrobial drug development (72). Unfortunately, the value of pharmacometrics in pharmacotherapy practice seems yet to be fully appreciated since the documented impact in literature is minimal.

However, the benefits of pharmacometric modeling and simulation is well-recognized by pharmaceutical industry, regulatory authorities, and academia (73). As a result, pharmacometrics becomes a hot topic in many conferences of pharmaceutical sciences and workshops since the early 2000s (20). Despite late adaptation, the use of pharmacometrics continues to grow with a substantial demand worldwide for scientists with pharmacometric skills (74). The implementation of pharmacometric-based approach by Pfizer led to an annual reduction in clinical trial budget of $100 million and increase in success rates of phase III and IV (56). This cost-saving was attributed to many factors but principally to early termination of development programs with unacceptable probability of success and studies for futility. Merck and 10 other large to mid-sized

pharmaceutical companies reported similar significant cost-saving through an impact on decision-making.

A recent FDA review (75) shows pharmacometric analyses are used to support drug approval and labelling decisions of more than 60% of New Drug Application (NDA) submissions between 2000 and 2008; dose labelling in 11% of submissions was based on pharmacometric analysis with no clinical trials conducted to assess efficacy; and 30% of submissions were assessed by independent pharmacometric analyses conducted by FDA reviewers. For example, FDA performed an independent exposure-response analysis of pooled data from two phase II and one phase III studies and recommended the approval of micafungin 150 mg dose instead of 100 mg for the treatment of esophageal candidiasis (76). Levofloxacin pediatric dose recommendation, 8 mg/kg twice day, for children following anthrax exposure was also based on an FDA independent pharmacometric analysis with no confirmatory studies (77).

Similar benefits can be achieved in pharmacotherapy practice and research upon the implementation of pharmacometrics. The efficiency of research, especially in investigator-led studies funded by government and public money, can be significantly improved. The involvement of scientists with proficiency in pharmacometrics in the design and analysis of studies can ensure the use of optimal doses, proper design, and correct analyses. Altogether can reduce cost, shorten duration, and maximize knowledge gain per study.

2.3.3 Advantages over Conventional Analyses

Pharmacometrics uses assumption-rich nonlinear mixed-effect modeling methods that may make frequentist statisticians feel uncomfortable. Yet, these assumptions are, in fact, an advantage rather than a deterrent for several reasons. The assumptions are based on established scientific principles in many relevant fields that include pharmacology, physiology, pathology, and microbiology (78). So, this characteristic is an advantage since it allows leveraging of prior knowledge accumulated over decades of research. The inclusion of such information allows our models to be more mechanistic and closer to reality. Of course, no model is perfect and each model should be weighed against the benefits. With that, assumptions can always be stated explicitly, debated openly, and tested rigorously.

In addition, pharmacometrics is a better approach to characterize complex biological systems because of the inherent nature of nonlinearity that cannot be adequately described with simple linear models. Biological systems also exhibit hysteresis in which two different measurements of effects can be observed for the same concentration. The temporal concentration-effect delay is a routine problem in pharmacometric data and it is easily modelled by delay differential equations or the incorporation of a transit, effect compartment, or indirect response model (79, 80). Another advantage is that pharmacometric model parameters have biological meanings associated with them even for parameters from empirical models. For example, small, hydrophilic, and highly protein-bound drugs that are eliminated renally tend to have clearance value close to the glomerular filtration rate and apparent volume of distribution similar to plasma volume. This exemplifies the usefulness of leveraging biological prior

information without which extrapolation of findings in one population to another, use of findings from one study to design the next, or application of findings directly in patient care would be difficult (81).

The pharmacometric-based approach often applies population mixed effects analysis that better estimates typical and individual values by quantifying between subject variability. On the contrary, traditional analysis tend pool data together, or ignore the correlation of data points within a subject leading to biased parameter estimates and inflated unexplained variability (81). Furthermore, pharmacometric-based analysis achieves significantly higher statistical power. It uses all longitudinal data instead of the end of trial observations that increases the signal to noise ratio (52, 82, 83). As a result, smaller and shorter in duration studies are required with pharmacometric-based analysis to achieve satisfactory power that translates to substantial cost-saving (56). For this reason, pharmacometrics is well-suited for the situation when only sparse data are obtained due to practical limitations or constraints in study design. The pharmacometric approach is a better fit with adaptive clinical trial design strategies that aim to maximize the information about dose-response curve via the strategic allocation of patients based on responses of earlier subjects (83). Lastly, pharmacometric-based analysis can be used effectively in both learning and confirming activities recommended by Sheiner (52, 83). Despite the advantage of pharmacometric-based analysis, it is unfortunately not yet widely implemented to reach it is full potential for several reasons.

2.3.4   Challenges for Implementation

The adoption of pharmacometric modeling and simulation by pharmaceutical industry had been delayed until more recently for multiple reasons. The first one is a multifaceted organizational concern due to uncertainty of outcomes and lack of experience (20, 83). Pharmaceutical companies were not sure whether the investment in the shift from traditional to pharmacometric-based approach would pay off in terms of greater productivity, cost-saving, and faster approval. Equally, they were fearful if such as a change would be approved and accepted by regulatory bodies. In addition, there was a lack of experience and trained personnel qualified to perform pharmacometric-based analysis. The unfavorable circumstance and natural resistance to the change is a typical response to every change in every discipline and the adoption of pharmacometrics by pharmaceutical industry represents one of many examples. These concerns are no longer valid because the pharmacometric-based approach received the endorsement of regulatory authorities and substantial benefits of the approach are already documented as mentioned earlier. Also, in response to the need of skilled manpower, academic departments in leading universities have established new graduate programs focused on pharmacometric and quantitative clinical pharmacology (84). The output of these programs is surely not enough to meet the substantial demand for pharmacometricians but it should not be a hurdle to widely implement the approach. Pharmaceutical companies also share the responsibility to train and educate their scientists about the principles of and technical skills required for the pharmacometric-based approach. This, in fact, is part of the upfront investments for such a transformation.

The other reasons limiting the pharmacometric-based analysis implementation are related to the approach itself. There are limitations to nonlinear mixed-effects modeling (NLMEM). One deterrent is the inability to quantify type I and II errors and this limitation remains to be addressed (83). Power calculation of NLMEM is another drawback that requires computationally-intensive Monte Carlo simulation and re-estimation with the planned model analysis to generate the distribution of test statistic (85). This is overcome with the development of newer and faster methods including Monte Carlo Mapped Power for the Wald test and parametric power estimation for likelihood ratio test (86, 87). In addition, violation of distributional assumptions of random effects for between subject and unexplained residual variabilities can render the model inappropriate and findings incorrect. To address this challenge, a semiparameteric approach is proposed to relax the assumptions on the distributions and add a flexibility to describe a wider range of distributions (88, 89). This is done using a transformation function where the parameter shape is estimated with the rest of model parameters. The distributional assumptions of uncertainty of model parameters are also important for interval estimates. Non-parametric methods already exist for NLMEM, such as bootstrapping and log likelihood profiling, but they lack diagnostics to judge their appropriateness and require intense computation. A new nonparametric sampling importance resampling technique was proposed to overcome the limitations of the existing methods and it is shown to be superior in cases of small datasets, highly nonlinear models, and meta-analyses (90).

Model building in NLMEM is typically data-driven and goes through a series of testing models before a final one is selected. This makes the model building process is

highly subjective and associated with an increased type I error that is not easily quantifiable (83). As a result, the use of NLMEM is not favored in confirmatory analysis since it requires model pre-specification to be fully described in advance. A proposal for full pre-specified model-based analyses in which model building is completely avoided or limited to a number of testing models with predefined selection criteria are suggested to ensure reproducibility and type I error control (91, 92). However, model pre-specification does not provide sufficient type I control when the predefined model is miss-specified. An alternative, multi-model approach (model-averaging), in which data are fit to a set of models and the weight of each model is adjusted based on how well it fits the data, is used to control type I error while safeguarding against model misspecification (83, 93).

2.3.5 Current Applications

There are many pharmacometric applications that span drug development continuum and pharmacotherapy across all therapeutic areas (44, 51, 78). Here, we only present the most common applications relevant to infectious diseases. Pharmacometrics is used to guide the rational selection of optimal dosing regimens in drug development: to maximize the success probability of clinical studies in the first time and to improve therapeutic outcomes of patient care in clinical settings. The optimal regimens are selected using stochastic (Monte Carlo) simulation-based methods. The first one is probability of target attainment (PTA) that aims to calculate the percentage of simulated patients with an estimated efficacy-linked PK-PD index equal to or greater than the target magnitude related to the antimicrobial efficacy against a pathogen with a certain MIC

(method 1) as shown in Figure 2-5 (55, 94) . Thus, PTA integrates the variability of

microbial susceptibility (MIC), the variability of drug exposure in the target patient

population characterized by a population PK model, and efficacy-predicting PK-PD

indices to quickly explore, via simulations, various dosing regimens and recommend the

one that is associated with the highest probability of achieving the PK-PD target. A

slightly modified PTA approach (method 2) that incorporates the uncertainty associated

with the PK model parameters, is also used. The modified PTA estimates the mean and

confidence intervals (CIs) of the PTA where the intersection of the horizontal line at the

PTA target value and the lower confidence represents the covered MICs by the dosing

regimen (Figure 2-5) (73, 95). This modified PTA method provides conservative

breakpoints that can be even more conservative by using a higher level of CI. Method 2 is

the approach used by the European Committee on Antimicrobial Susceptibility Testing

(ECAST) (11, 96) .
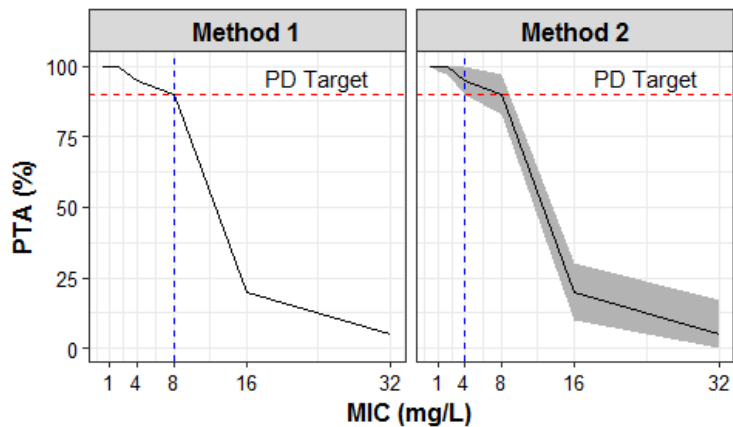
Figure 2-5: PTA methods to select optimal dosing regimens. Solid lines are the means

and shaded area is the 95% CI.

Despite the merits of the PTA method, it has major deficiencies arising from the

use of MIC-based indices. The MIC of a drug against a pathogen is determined after the

pathogen is exposed typically for 24 hr to a constant concentration of the drug that does

not reflect what happens *in vivo* (73, 97). So, MIC represents the net (snapshot) effect of microbial growth and killing over the incubation period and ignores the time-course relationships. Time-kill curve studies, on the other hand, provides more detailed information about the drug-pathogen interaction over time. The studies are designed to expose the pathogen to constant (static) or fluctuating (dynamic) drug concentrations to mimic *in vivo* scenarios. Time-kill curve data allow the use of pharmacometric-based analysis to develop an integrated PK-PD model to characterize the microbial growth and rate of killing as a function of both time and drug concentration. This approach allows one to identify the development of adaptive resistance of the pathogen upon drug exposure. This is a well-documented phenomenon for aminoglycoside antibiotics (42, 98). PK-PD modeling and simulation is the second method used to optimize doing regimens (Figure 2-6). It uses developed PK-PD models based on time-kill curve data and Monte Carlo simulation taking into account variability in both PK and PD to predict dosage regimens that result in microbial eradication (microbiological cure) (73).
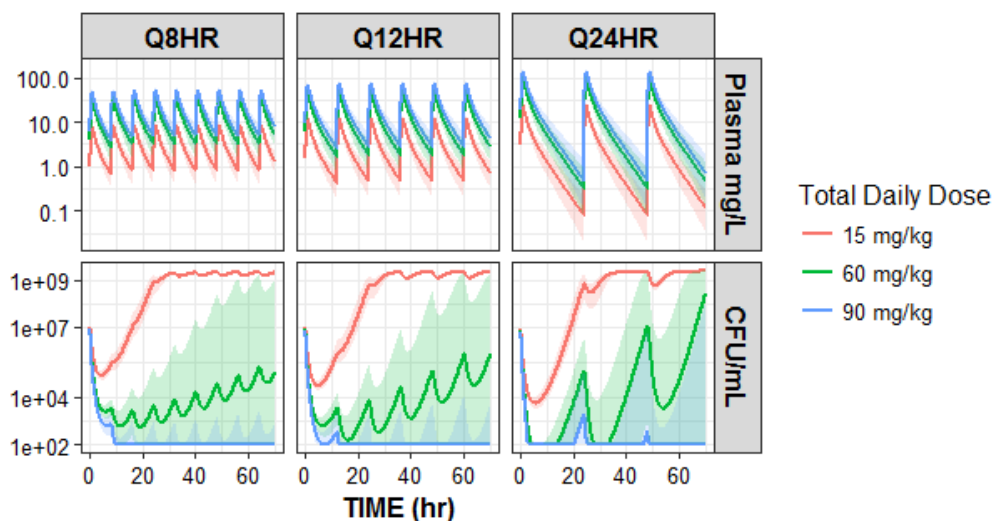
Figure 2-6: PK-PD modeling and simulation to guide dose selection. Solid lines are the mean and shaded areas are the 95% CI.

Pharmacometrics is also used to set antimicrobial susceptibility breakpoints. They serve as a guide for clinicians about the likelihood of treatment success for an antimicrobial agent against a micro-organism that is classified as susceptible, intermediate, or resistant (11, 78). The correct establishment of breakpoint is critical since it has significant clinical implications. Setting breakpoints higher than they actually are can lead to denying patients effective therapies. If higher breakpoints are used, it will expose patients to higher doses which may be toxic. On the contrary, therapeutic failure and microbial resistance may occur when the breakpoints are wrongly set lower than they actually are because the therapy would be suboptimal. The clinical breakpoint is set based on the efficacy-linked PK-PD indices to identify the highest MIC at which a subjective PTA target, usually $\geq 80\%$, is achieved for a given dosing regimen. It is the same PTA methods used for optimal dosing regimen selection (Figure 2-5).

Antimicrobial dosing recommendations are typically derived from PK-PD in healthy adults that do not apply to patients who have significantly altered physiology, such as critically-ill, renally- or hepatically- impaired, burn, sepsis, and pediatric patients (61). As shown figure 2, physiological changes as consequence of underlying disease states affect the PK of antimicrobial agents and drug exposure at the site of infection leading different PD effect. Therefore, different dosing recommendations are likely needed that take into consideration the altered PK in the target patients. This is where pharmacometrics comes in to use available data to characterize the altered PK or leverage prior information of diseased-induced physiological changes in the absence of data to guide dose recommendations for special populations. In the latter situation, physiologically-based PK modeling is commonly used and widely accepted by regulators

to explore the effect of intrinsic and extrinsic factors affecting drug efficacy and safety in patients (67, 78).

Lastly, pharmacometrics can guide formulary decisions and establish treatment guidelines. Again, it uses Monte Carlo simulation to estimate the cumulative fraction of response (CFR) for a specific drug regimen against a specific micro-organism given the population distribution of MIC. CFR is calculated as:

$$CFR = \sum_{i=1}^{n} PTA_i \times F_i$$

Where i represent the MIC dilution level, PTA is the probability of achieving PK-PD target, and Fi is the percentage of isolate at each MIC dilution level (99, 100). This method uses local and regional susceptibility data to compare the efficacies of different drugs or different doses of the same drug against different pathogens. Such information is then used with some economic considerations to inform formulary decisions in hospitals. Likewise, treatment guidelines are established based on the knowledge generated by pharmacometric-based approaches (101). These pharmacometric decision-guiding methods for antimicrobial therapies are now available in both mobile and electronic health record-embedded point-of-care platforms for the clinicians and antimicrobial stewardship personnel as an easy-to-used tool to individualize therapies and inform organizational decisions, respectively. One program is called PK-PD Compass developed by the Institute for Clinical Pharmacodynamics Technologies (Schenectady, New York, NY, USA) (102, 103). PK-PD Compass integrates population PK models, patient-specific characteristics, pathogen-specific susceptibility data, and Monte Carlo simulation to perform PK–PD target attainment analyses and select the optimal dosage regimens for a patient. Other similar platforms are available and currently in use as well.

2.4   CONCLUSION

Pharmacomteric modeling and simulation is emerging as a powerful discipline to rationalize and streamline drug development. Significant increase in drug development productivity and substantial reduction in cost are documented after the adoption of pharmacoemtric-based analysis by pharmaceutical companies. This is because of the advantages of pharmacometric-based analysis over the traditional statistical approach. With pharmacometrics, optimal doses are selected and studied for the first time in smaller and shorter in duration studies. It also allows the integration of data collected from different sources throughout the development program to maximize learning about the compound and inform decision making. Similar benefits can be achieved in pharmacotherapy practice and research when the pharmacometric approach is adopted. The efficiency of investigator-led studies can be improved by ensuring optimal doses are selected, studies are well-designed, and correct analyses are performed.

3 PHARMCOKINETICS-PHARMACODYNAMICS (PK-PD) OF SERTRALINE AN ANTIFUNGAL IN HIV-INFECTED PATIENTS WITH CRYPTOCOCCAL MENINGITIS

3.1 SUMMARY

The ASTRO-CM pilot study investigated the role of adjunctive sertraline for the treatment of HIV-associated cryptococcal meningitis in HIV-infected patients. This study is a secondary analysis of that study using a pharmacokinetic-pharmacodynamic modeling approach to provide insight into sertraline exposure-response-outcome relationships. To quantify the sertraline effect, estimated rates of fungal clearance of ASTRO-CM patients were compared to those in COAT, a similar study in which patients received standard *Cryptococcus* therapy of amphotericin B (0·7–1·0 mg/kg per day) and fluconazole (800 mg/day) without sertraline. Sertraline clearance was higher among antiretroviral therapy (ART) patients by more than 2-fold, resulting in lower drug exposure. However, ART was found to not affect fungal CSF clearance or survival of patients. Cumulative AUC of total sertraline concentration in the brain to MIC ratio was best correlated with the percent daily change in $\log_{10}$ CFU/mL. Sertraline significantly increased fungal clearance from CSF by 41.3% on average and the effect was found to be dose- and exposure- independent. This finding suggests that sertraline response might be mediated by different mechanisms than directly inhibiting the initiation of protein translation. This is supported by that fact that unbound sertraline concentrations are unlikely to reach MIC levels in the brain. Exploratory survival analysis showed female patients and those receiving 100 or 400 mg of sertraline daily had significantly lower 2-

week survival rate compared to patients receiving no or 200-300 mg sertraline daily. Altogether, study findings suggest sertraline doses greater than the maximum FDA-approved dose (200 mg/day) may not provide any additional benefits and come with greater risk of adverse events.

3.2 INTRODUCTION

Cryptococcal meningitis (CM) is an opportunistic fungal infection of the central nervous system caused by the pathogenic encapsulated yeast *Cryptococcus neoformans*. It is transmitted mainly by inhalation and commonly affects immunocompromised individuals, in particular those infected with human immunodeficiency virus (HIV) (104). In 1990s, the introduction of antiretroviral therapy (ART) significantly decreased the incidence and improved the long-term mortality of HIV-associated CM in western developed countries. However, in developing nations, CM burden remains unexpectedly high due to the lack of health care access (104–106). CM is one of the most common acquired immunodeficiency syndrome (AIDS)-defining infections in HIV-infected individuals with approximately 1 million new cases and 625,000 deaths every year worldwide (107). About 75% of these cases occur in HIV-infected people in Sub-Saharan Africa making *Cryptococcus* the 4th leading cause of death in the region (107). Globally, 10-week mortality rate is currently at least 35% and cerebral spinal fluid (CSF) sterilization at week 2 is achieved only in 60-70% of patients (108). Current drug therapies are expensive, toxic and not readily accessible, especially in resource-poor settings. These statistics highlight the critical unmet need for new safe, effective, affordable, and readily accessible antifungal therapies for CM treatment.

Sertraline (Zoloft®), a selective serotonin reuptake inhibitor commonly prescribed for the treatment of depression and other mental disorders, was shown to have an *in vitro* and *in vivo* fungicidal activity against *Cryptococcus neoformans* (109–111). The sertraline effect *in vitro* and animals was dose-dependent and believed to be mediated by the inhibition of protein synthesis of the fungus (109, 111, 112). Other mechanisms of action for sertraline antifungal activity are also suggested and include: non-specific lipophilicity-dependent cytotoxicity; membrane phospholipids disruption of acidic intracellular organelles; and elevation of plasma serotonin (5-HT) that is found to be biologically active against *Candida* and *Aspergillus spp.* and it could also be the case against *Cryptocccocus* (113–117). In addition, the effect of sertraline in combination with fluconazole, a major component of standard induction, consolidation, and maintenance phase therapy for CM, was synergistic against *Cryptococcus in vitro* and *in vivo* (109, 111, 118–120).

Previous findings suggest the potential use of sertraline in treating HIV-related CM given its favorable physiochemical, pharmaceutical, and therapeutic properties. Sertraline has high lipophilic characteristics that enable it to cross the blood brain barrier easily and concentrate in the brain at concentrations 10-57 times higher than in plasma (121). It can also help with depression, which is found to be a common co-morbidity in HIV-infected patients (122). More importantly, sertraline has a good safety profile: overdose situations are relatively safe and easily managed; drug-drug interactions are minimal which is an important advantage in this therapeutically complex setting; it is available as a less-costly generic formulation; it is orally bioavailable; and it has long half-life that allows once-daily dosing (123).

Based on the above compelling evidence and therapeutic properties of sertraline, our group hypothesized that the addition of sertraline to Amphotericin B and fluconazole would result in faster rates of fungal clearance from CSF and probably better clinical outcomes. To test this hypothesis, we conducted and authored the first-in human dose-escalating clinical trial to investigate the safety and efficacy of adjunctive sertraline for the treatment of HIV-associated CM (ASTRO-CM, NCT01802385) (108). This study is a secondary analysis of the ASTRO-CM pilot study using a pharmacokinetic-pharmacodynamic (PK-PD) modeling approach to provide insight into sertraline exposure-response-outcome relationships. An older study, COAT (Cryptococcal Optimal ART Timing), in which patients received standard CM therapy only was used as a comparison to quantify sertraline added effect on brain fungal clearance from CSF (124).

3.3   MATERIALS AND METHODS

3.3.1   Patients Cohort & Sampling Collection.

This study included a subset of HIV-infected Ugandans with CM from the ASTRO-CM pilot study, who had sertraline plasma concentrations measured (108). Venous blood samples were collected on days 1, 3, 7, 10 and 14 mostly within 8 hours after dose administration (**Figure 3-1**). Samples were analyzed using a high performance liquid chromatography (HPLC). Full details of study design and methods are presented in our previously published manuscript (108).
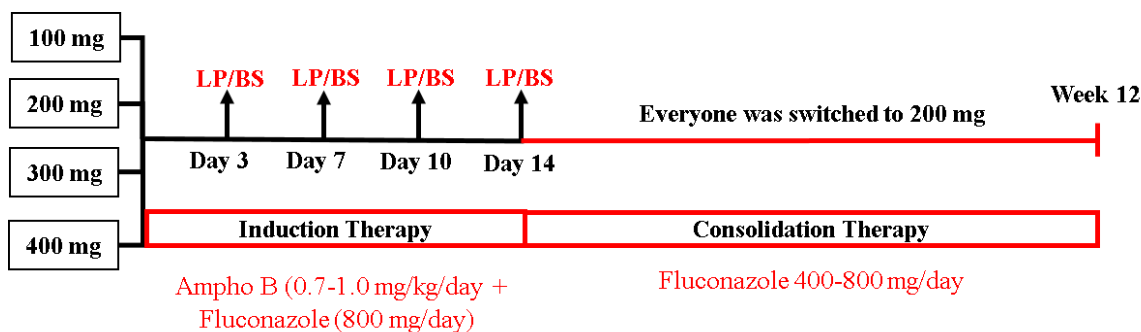
Figure 3-1: Study design of ASTRO-CM. LP is lumbar puncture and BS is blood sample.

3.3.3 Pharmacokinetic Analysis.

All sertraline plasma concentrations were fitted simultaneously using nonlinear mixed-effect regression methodology to a one- and two-compartment PK model with linear and nonlinear clearance. Between subject variability (BSV) was described by an exponential model and residual unexplained variability (RUV) was evaluated by proportional and combined error model. The effects of age, sex, weight, concomitant antiretroviral therapy (ART), parent-to-metabolite ratio (sertraline-to-desmethylsertraline ratio, RA), serum creatinine (SCr), and liver function enzymes (AST and ALT) were visually screened against Empirical Bayes parameter estimates of the base model. Potential covariates were then tested as linear and power models for continuous covariates and as a fractional change for categorical ones. The statistical significance of covariates was tested using the likelihood ratio test (χ^2, $\alpha = 0.05$, df = 1) which corresponds to at least a 3.84-point drop in objective function value (OFV, a measure of goodness of fits similar to a sum of squares). The criteria used to select the PK model were OFV, plausibility of parameter estimates, diagnostic plots and the prospective applicability of the model. The performance of the selected model was assessed by

36

prediction-corrected visual predictive check (pcVPC) (125) and parameter precision was evaluated by the sampling importance resampling (SIR) method (90).

There were missing data in weight, RA, and time of dose administration and blood draws. A single imputation was performed to replace missing weights with the median value of known weights based on sex (54 kg for male and 49 kg for female). Within a patient, RA, SCr, AST, and ALT were imputed with the last observation carried forward then the last observation carried backward. Missing dosing times were replaced by the frequent dosing time of patients while missing blood draw times were imputed by visit times when available or frequent blood draw times for other patients done on the same day. When there was no information to make reasonable imputation, records were excluded.

3.3.4   Predictive PK-PD Index Exploration.

This sub-analysis was limited to 115 patients who had fungal count quantifications in CSF and sertraline plasma concentration measurements. Quantitative CSF cultures were obtained by therapeutic lumber punctures using manometers at diagnosis, and on days 3, 7, 10, and 14. A described method was used for determining quantitative CSF cultures measured as CFU/mL (126). The empirical Bayesian estimates (EBEs) from the final PK model were used to simulate the sertraline brain concentration-time profiles using brain-to-plasma concentration ratios and to calculate standardized PK-PD indices: C_{max}/MIC, AUC_{24}/MIC, %$T_{>MIC}$ (121).

C_{max} is the highest (peak) concentration reached, AUC is the area under concentration-time profile, %$T_{>MIC}$ is the cumulative percentage of 24-hr period that the

concentration is above MIC. cAUC/MIC, the ratio of cumulative area under concentration-time profile to MIC, is not a commonly used PK-PD index but it was calculated to evaluate whether the drug effect was better associated with cumulative drug exposure. MIC is the minimum inhibitory concentration of sertraline against *Crypotococcus*, that was measured by broth microdilution in RPMI1640 media per protocol (127). When MICs of clinical isolates were undetermined, they were assumed to have the median value (4 mg/L).

All PK-PD indices are generally based on the free unbound plasma or tissue concentrations, and indicated by the prefix f. However, because unbound plasma concentrations were not measured in our patients, the prefix f was not used and total, instead of free, brain sertraline concentrations were predicted using the median value (16.5 fold) of total brain-to-plasma concentration ratios (121). Assuming that measured fungal CFU was only affected by previous doses, PK-PD indices were calculated after the last dose for C_{max}/MIC, AUC_{24}/MIC, $\%T_{>MIC}$ and up to the last dose given for cAUC/MIC. Drug effect was calculated as the percent change in $\log_{10}$ CFU/mL from the previous culture.

3.3.5   Fungal Count Analysis.

Fungal CSF counts from the ASTRO-CM pilot study and COAT trial were modeled together to determine the additional benefit of sertraline on brain CSF fungal clearance rate when added to standard induction therapy for 2 weeks (108). COAT is an earlier study that included similar patients from the same hospital, who were treated with the same regimen of amphotericin and fluconazole without sertraline (124). All CSF

fungal counts were log$_{10}$-transformed, rounded to nearest integer and fitted to a Poisson model (equation 3-1) (128).

$$P(Y_{ij} = n) = \frac{\lambda_{ij}^n}{n!} e^{-\lambda_{ij}} \qquad (3-1)$$

The probability of observing Y$_{ij}$ equal to n =0, 1, 2, … is determined by lambda (λ_{ij}), the mean fungal count for individual i occurring at fixed time-interval j and the factorial function (!) of n. λ_{ij} was further influenced by the preceding counts $f(\lambda_{i(j-1)})$ and time $f(t_j)$ (equation 2-2).

$$\lambda_{ij} = BASE_i . f(\lambda_{i(j-1)}). f(t_j) \qquad (3-2)$$

A three-state transition Markov model (MM) for an increase, decrease and no change in log$_{10}$ CFU/mL from the previous count was used to account for the correlation of data within a patient. Time effect was best modeled by a mono-exponential decline function with a separate random effect for each study (equation 3 – 3).

$$\lambda_{ij} = BASE_i. MM . e^{-[K_i + (1-SER).\eta_1 + SER.\eta_2).t_j]} \qquad (3-3)$$

MM is a multiplier factor for each Markov model state. SER is an indicator variable that equals 0 for COAT trial and 1 for ASTRO-CM study. K is an exponential constant for the daily decrease in fungal counts (day^{-1}). It was fixed to 1 for COAT trial and estimated for each dose arm (100, 200, 300, 400 mg/day) of ASTRO-CM study. This model parameterization was chosen to allow for easy comparison among different sertraline arms and standard induction therapy with no sertraline.

A different model parameterization was also used in order to characterize the dose-response relationship assuming sertraline has dose-dependent effect as supported by *in vitro* and animal studies. A common K value for both studies and a sertraline effect term described by a sigmoidal E$_{max}$ function were used (equation 3 – 4).

$$\lambda_{ij} = BASE_i \cdot MM \cdot e^{-[(K+\eta 1).t]} \cdot \left[1 - \frac{\left(\frac{DOSE}{MIC}\right)^{\gamma}}{D_{50}{}^{\gamma} + \left(\frac{DOSE}{MIC}\right)^{\gamma}} \right] \qquad (3-4)$$

D_{50} is the dose of sertraline to MIC ratio when sertraline effect is half maximal

and γ is a shape parameter for the dose-response curve. The final count model was

assessed by VPC and parameters uncertainty were estimated by SIR.

3.3.6 Survival Analysis.

This analysis was limited to patients included in the count analysis. Two-week

survival rate of patients from both (COAT & ASTR-CM) studies was modeled as time to

death using a time-varying exponential hazard function (equation $3-5$).

$$h(t) = \lambda_0 \cdot e^{\beta_o \times \ln(t)} \qquad (3-5)$$

λ_o is the baseline hazard and β_o is the shape parameter of the hazard function.

Based on whether covariates were time-invariant or time-varying, they were modeled,

respectively, as follows (129):

$$h(t) = \lambda_0 \cdot e^{(\beta_0 \times \ln(t) + \beta_{c1} \times covariate_1)} \qquad (3-6)$$

$$h(t) = \lambda_0 \cdot e^{\beta_0 \times \ln(t)} \cdot [1 + \beta_{c1} \times covariate_1(t)] \qquad (3-7)$$

The selected model was validated internally by VPC and distribution of parameter

uncertainty were estimated by SIR.

3.3.7 Software.

Nonlinear-mixed-effects, count and survival modeling analyses were performed

in NONMEM 7.3 (ICON Development Solutions, Ellicott City, MD) using various

ADVANs and estimation methods. The PK analysis was performed with ADVAN2

TRANS2 and FOCEI method; count analysis was done using PREDPP with FO

Laplacian method; and survival rates were estimated using ADAVN6 with FO likelihood

method. Data manipulation, imputation, and plotting were done in R (version 3.2.5). Perl-

speaks-NONMEM (PsN) was utilized to perform VPC and SIR analyses. The Pirana

interface was used to maintain and compare NONMEM and PsN runs (130).

3.4 RESULTS

3.4.1 Pharmacokinetic Model.

Weights of 45 unique patients (32 males and 13 females), 94 dosing times, and 19

blood draw times were imputed as described above. Nine observations below the lower

limit of quantification (1 ng/mL) were excluded. The final analysis included 335

sertraline plasma concentrations from 137 patients whose characteristics are summarized

in **Table 3-1**. A 1-compartment PK model with first-order absorption and elimination

adequately described the data. A combined proportional and additive error model was

preferred for the RUV. The absorption rate constant (K_a) was fixed to a literature value of

0.3 hr^{-1} because it was not estimable (131). Oral clearance (CL/F) and volume of

distribution (V/F) were allometrically scaled to a standard 70-kg person (equations $3 - 8$

& $3 - 9$).

$$\frac{CL}{F} = \theta_1 \times \left(\frac{Weight}{70}\right)^{0.75} \times e^{\eta_1} \qquad (3-8)$$

$$\frac{V}{F} = \theta_2 \times \left(\frac{Weight}{70}\right) \times e^{\eta_2} \qquad (3-9)$$

Table 3-1: Characteristics of patients included in PK analysis

	100 mg	200 mg	300 mg	400 mg	Total	P-value
Subjects, n	14	49	36	38	137	-
Male, n (%)	8 (57)	33 (67)	20 (56)	26 (68)	87 (64)	0.59
Age, mean (SD)	38 (7)	36 (8)	38 (8)	34 (8)	36 (7.8)	0.15
Weight, mean (SD)	54 (10.4)	52.7 (10.5)	50.8 (8.7)	52.2 (9.7)	52 (9.6)	0.72
ART, n (%)	8 (57)	23 (47)	12 (33)	14 (37)	57 (42)	0.34

The selected PK model included ART as a covariate on plasma CL/F, reducing the OFV by 40 points (p-value < 0.00001). On average, concomitant ART increased CL/F by 110% leading to lower drug exposure (**Figure 3-2**). The effect of ART was not different between patients receiving efavirenz- and nevirapine-based ART (result not shown). The diagnostic plots and pcVPC showed the model reasonably captured the observed data (**Figure 3-3** & **Figure 3-4**). The selected PK model parameters and their SIR-based uncertainty are presented in **Table 3-2**.
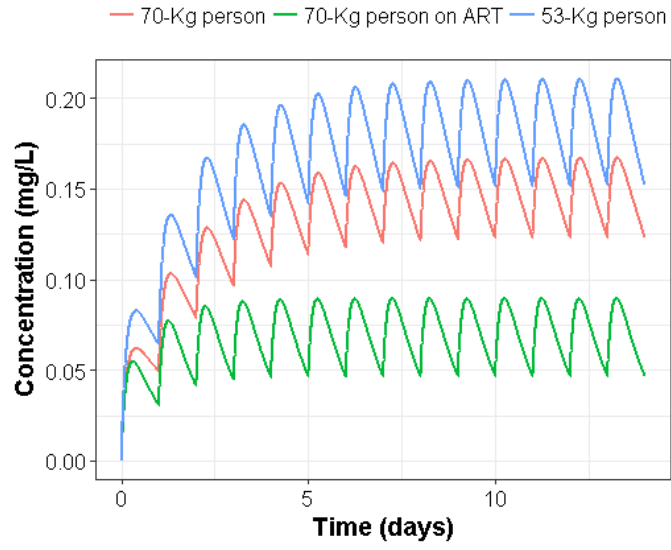
Figure 3-2: Effect of weight and ART on sertraline exposure
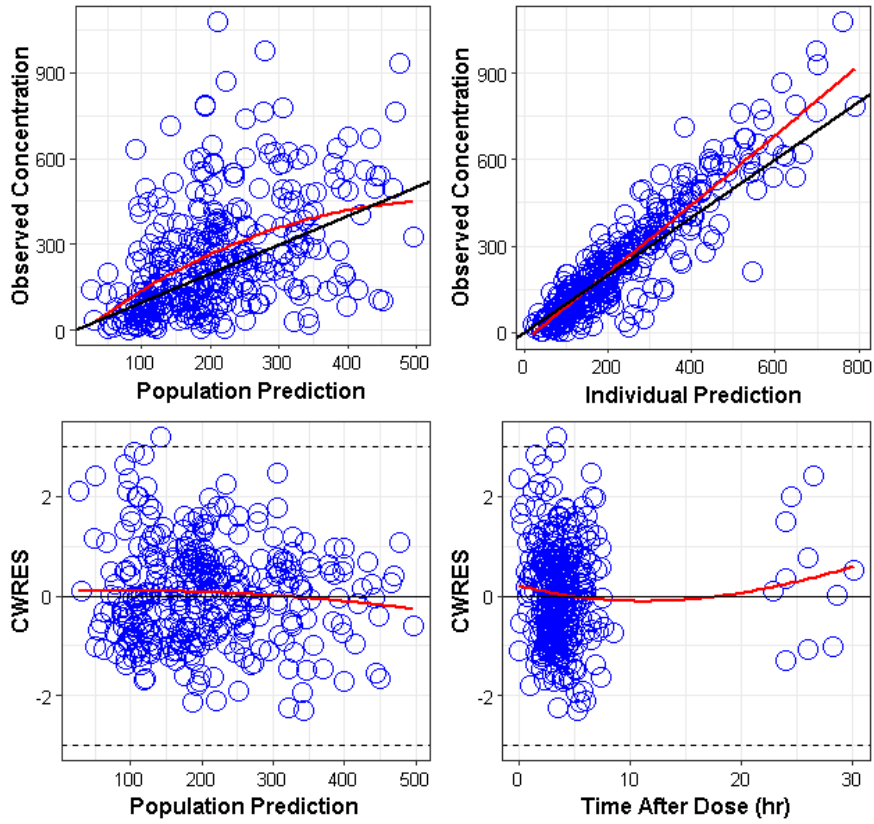
Figure 3-3: Diagnostic plots of the selected sertraline PK model. Red lines are Lowess

smoothers. CWRES is conditional weighted residuals.

43
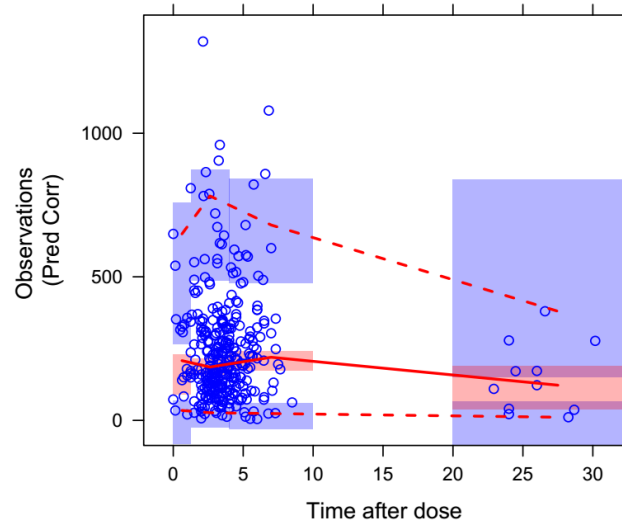
Figure 3-4: Prediction-corrected visual predictive checks of the selected sertraline PK model. Blue open circle represents the prediction-corrected concentrations, red solid and dashed lines represents the median, 5th and 95th percentile, respectively. Shaded areas are the simulated 95% CI of each percentile.

Table 3-2: Parameter estimates of the selected PK model of sertraline

Parameter	Estimate (RSE)	SIR median (95% CI)
CL/F*	55.7 (9)	56 (46 -67)
V/F*	2630 (11)	2649 (2092 – 3284)
ART_CL	1.1 (31)	1.16 (0.60 – 1.87)
K_a	0.3 FIXED	-
RUV_1	41.83 (74)	41.75 (23.57 – 60.54)
RUV2	11.4 (34)	11.6 (7 – 17.2)

* Parameters are allometrically scaled to a 70-kg person, CL/F (L/hr) and V/F (L) are oral clearance and volume of distribution, respectively, ART_CL is the fractional change in CL/F for patients receiving ART, K_a (hr^{-1}) oral absorption rate constant, RUV_1 & RUV_2 are the additive (SD) and proportional (%CV) components of residual unexplained variability. RSE is relative standard of error and SIR is sampling importance resampling.

3.4.2 Predictive PK-PD Index.

In vitro susceptibilities were determined for 151 clinical isolates (81 from ASTRO-CM and 70 from COAT) obtained from baseline CSF cultures from participants with a first episode of CM. The MIC distributions were comparable for both studies. The median (range) of sertraline MIC were 4 (1-8) µg/mL and 4 (1–12) µg/mL for ASTRO-CM and COAT clinical isolates, respectively. The undetermined MIC levels for the remaining 138 clinical isolates (34 from ASTRO-CM and 104 from COAT) were assumed to be 4 µg/mL.

PK-PD indices of ASTRO-CM patients calculated from the predicted total brain sertraline concentration-time profiles were plotted against the percent change in $\log_{10}$

CFU/mL that was not zero (**Figure 3-5**). There was no association between %T$_{>MIC}$ and

% change in log$_{10}$ CFU/mL. The change in fungal counts had a hockey-stick relationship

with AUC$_{24}$/MIC and C$_{max}$/MIC. cAUC/MIC index was the most predictive of the daily

percent reduction in fungal counts.
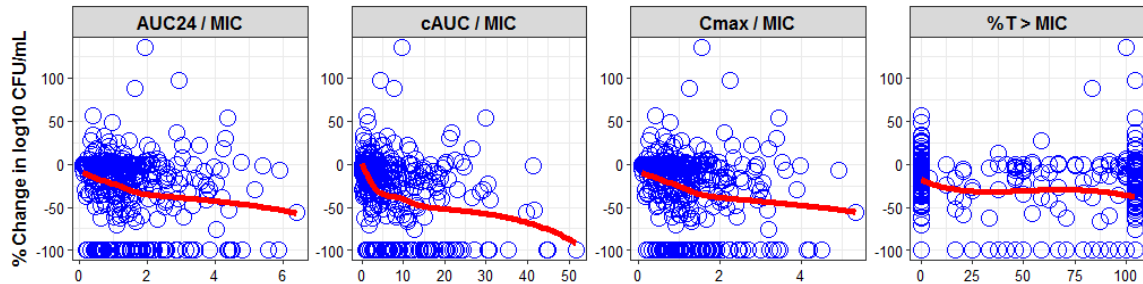
Figure 3-5: Association between the percent changes in log10 CFU/mL and sertraline PK-PD indices. Red lines are Lowess smoothers.

3.4.3 Rate of Fungal Clearance.

A total of 947 fungal count observations (491 from ASTRO-CM and 456 from

COAT) from 289 patients (115 from ASTRO-CM and 174 from COAT) were included in

the final analysis. The distribution of fungal counts and individual mean-variance

relationship were similar in the two studies, but ASTRO-CM had a slightly stronger serial

correlation of counts than COAT (**Figure 3-6**). ASTRO-CM treatment arms were

comparable except there were 10 patients in the 100 mg arm compared to 43, 32, and 30

patients in the 200, 300, and 400 mg arms, respectively.

No covariate was found to affect fungal counts. The selected model (equation 2-3)

found that the addition of sertraline to CM standard induction therapy significantly

increased CSF fungal clearance. The increase ranged from by 34-48% with an overall average of 41%.

The sertraline effect was similar irrespective of the daily sertraline dose our patients received (**Table 3-3**). The adequacy of the selected model was supported by the VPC in which model predictions reasonably captured the observed data (**Figure 3-7** & **Figure 3-8**). A differently parameterized model with fewer parameters (equation $3 – 4$), that was able to fit the data well and characterize a dose-response curve of sertraline, generated similar results. Compared to the first model (equation $3 – 3$), the second model (equation $3 – 4$) had a higher AIC but comparable VPC plots (results not shown). Modeling results were also similar when un-rounded $\log_{10}$-transformed were fitted (results not shown).
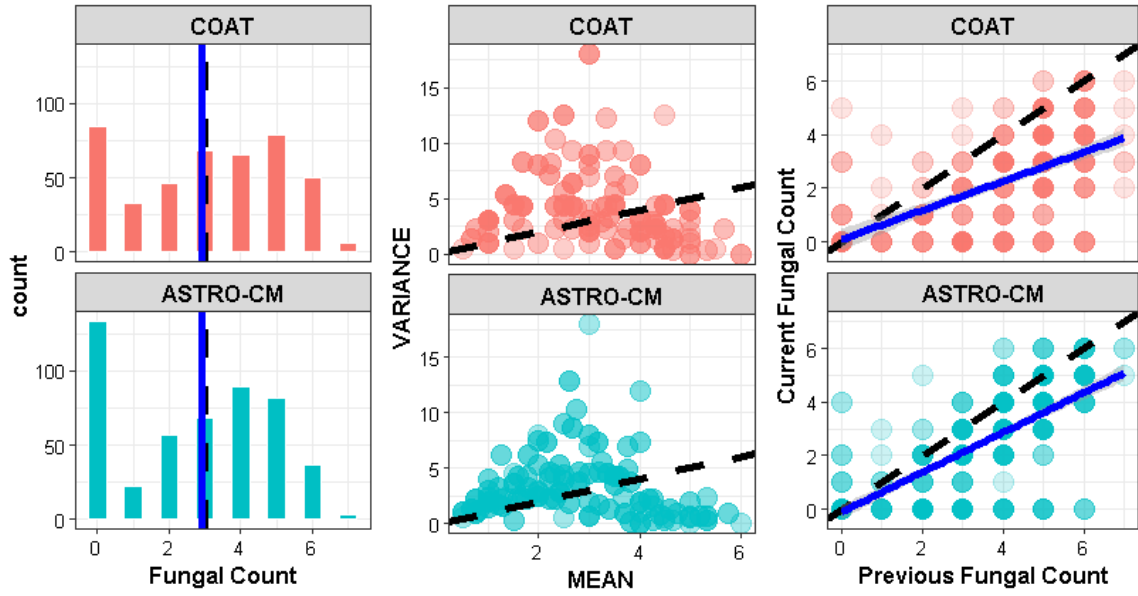
Figure 3-6: Characteristics of observed fungal counts. The left panel is a count distribution plot; middle panel is a mean-variance plot; the right panel is a serial correlation of counts. All plots are stratified by study: COAT top and ASTRO-CM bottom. Dash black line and solid blue line represents mean and median in the distribution plot, respectively. Dash black line is identity line in the mean-variance and serial correlation of count while blue solid line is a linear regression line. The slope of the regression line indicates the strength of serial correlation of count.

Table 3-3: Parameter estimates for the selected count model

Parameter	Estimate (RSE)	SIR median (95% CI)
λ	4.43 (2)	4.43 (4.22 – 4.62)
MM 1	1.56 (4)	1.56 (1.41 – 1.71)
MM -1	1.15 (4)	1.15 (1.03 – 1.28)
K- 0	1 FIXED	-
K-100	1.41 (28)	1.44 (0.72 – 2.29)
K-200	1.42 (15)	1.46 (1.08 – 1.90)
K-300	1.34 (18)	1.38 (0.97 – 1.89)
K-400	1.48 (18)	1.51 (1.08 – 2.03)
BSV1 in K	0.074 (14)	7.5 % (5.58 – 9.41)
BSV2 in K	0.14 (13)	14.3% (11.3 – 17.3)

λ ($\log_{10}$ CFU/mL) is the population mean count, MM 1/ MM -1 is the fractional increase and decrease in mean count from the previous one, K (day^{-1}) is the rate of daily decrease in fungal count for a given daily sertraline dose, and BSV1 and BSV2 (SD) are the between subjective variability in K for COAT and ASTRO-CM, respectively. RSE is relative standard of error and SIR is sampling importance resampling.
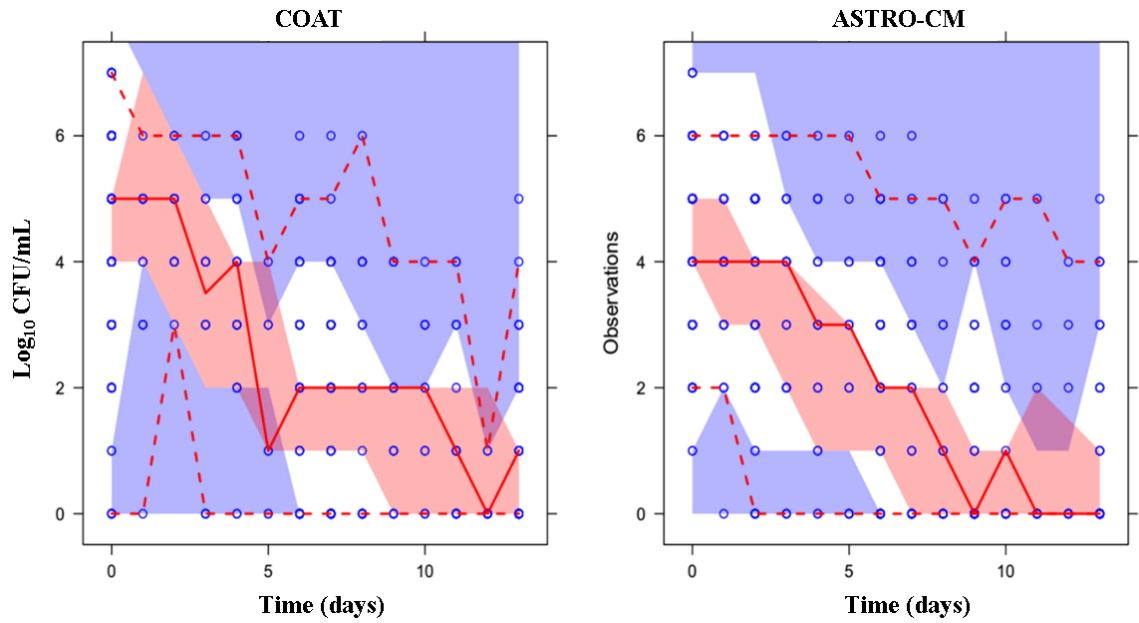
Figure 3-7: Mean fungal count over time visual predictive checks stratified by study. Blue open circles are the observed counts. Solid and dash red lines represent the median, 5th and 95th percentiles of the observed data. The shaded red and purple areas are simulated 95% CI for the median, 5th and 95th percentiles.
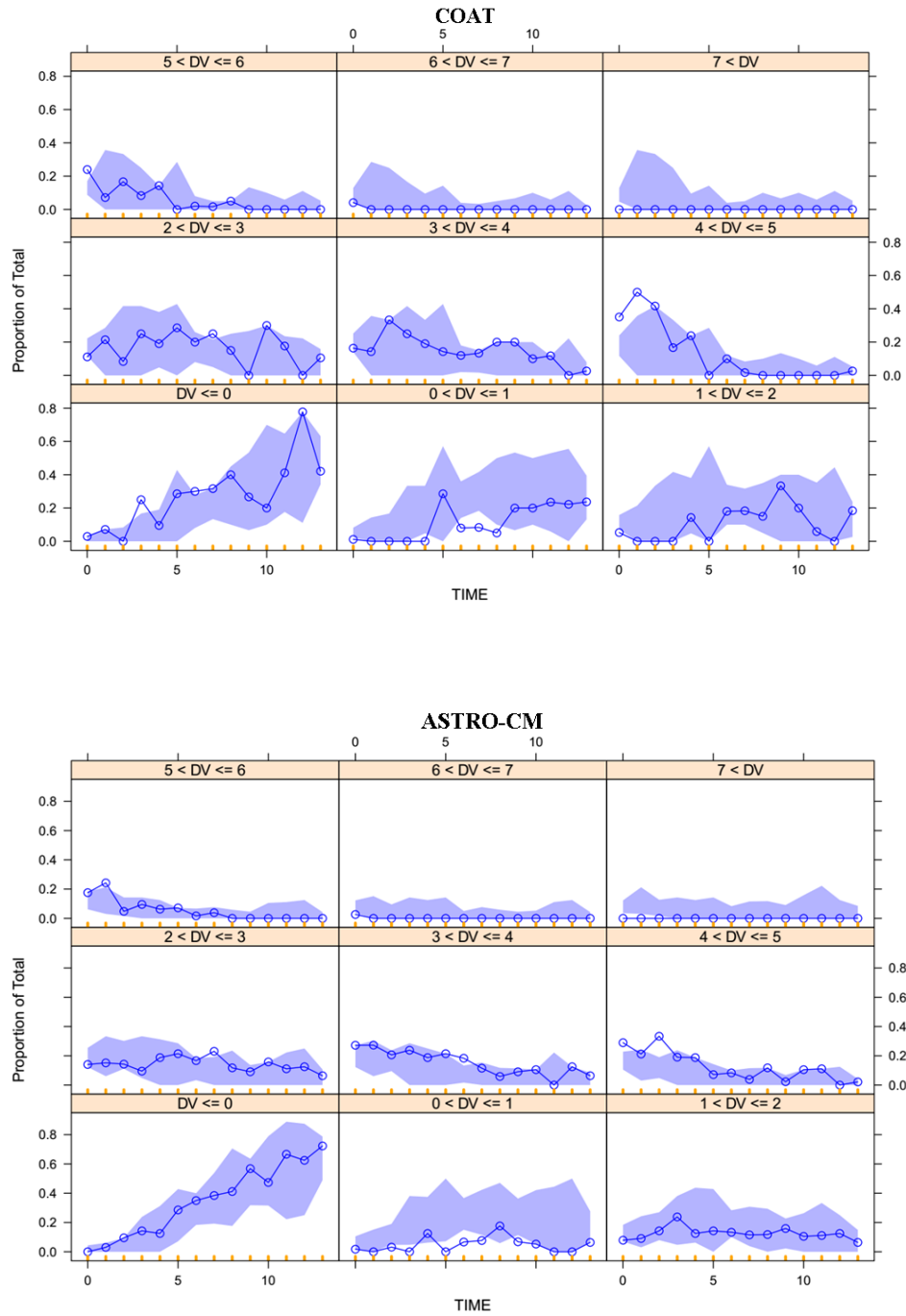
Figure 3-8: Categorical visual predictive check stratified by study and count. The blue dotted line and purple shaded area specify the proportion of observed data and simulated 95% CI, respectively.

3.4.4 Survival Rate.

The selected survival model found that hazard of death was significantly influenced by sex and sertraline daily dose as follows:

$$h(t) = \lambda_0 \cdot e^{(\beta_0 \times \ln(t) + \beta_{sex} \times SEX + \beta_{DOSE} \times DOSE_{100/400})} \qquad (2-7)$$

SEX equals 0 for female and 1 for male. $DOSE_{100/400}$ is 1 for those patients receiving 100 or 400 mg and 0 otherwise. Inclusion of sex reduced OFV by 13.9 points (p-value < 0.0005) and subsequent inclusion of $DOSE_{100/400}$ resulted in additional drop of 6.24 points in OFV (p-value < 0.02). The exponentiation of β's coefficients revealed that the hazard ratio of male to female is 0.25 and patients receiving 100 or 400 mg of sertraline daily to those receiving no sertraline, 200 or 300 mg daily is 2.92 (**Table 3-4**). The internal validation by VPC confirmed the model adequate (**Figure 3-10** & **Figure 3-10**).

Table 3-4: Parameter Estimate of survival model

Parameter	Estimate (RSE)	SIR median (95% CI)
λ_0	0.0367 (17)	0.0365 (0.0241 – 0.0473)
β_0	2.32 (16)	2.30 (1.61 – 3.25)
SEX_{male}	-1.38 (29)	-1.38 (-2.20 – -0.695)
$DOSE_{100/400}$	1.07 (38)	1.03 (0.25 – 1.82)

λ_0 is the baseline hazard, β_0 is the shape parameter of the hazard function, SEX_{male} and $DOSE_{100/400}$ are exponential coefficient to describe the effect of being male and receiving 100 or 400 mg of sertraline daily on the baseline hazard. RSE is relative standard of error and SIR is sampling importance resampling.
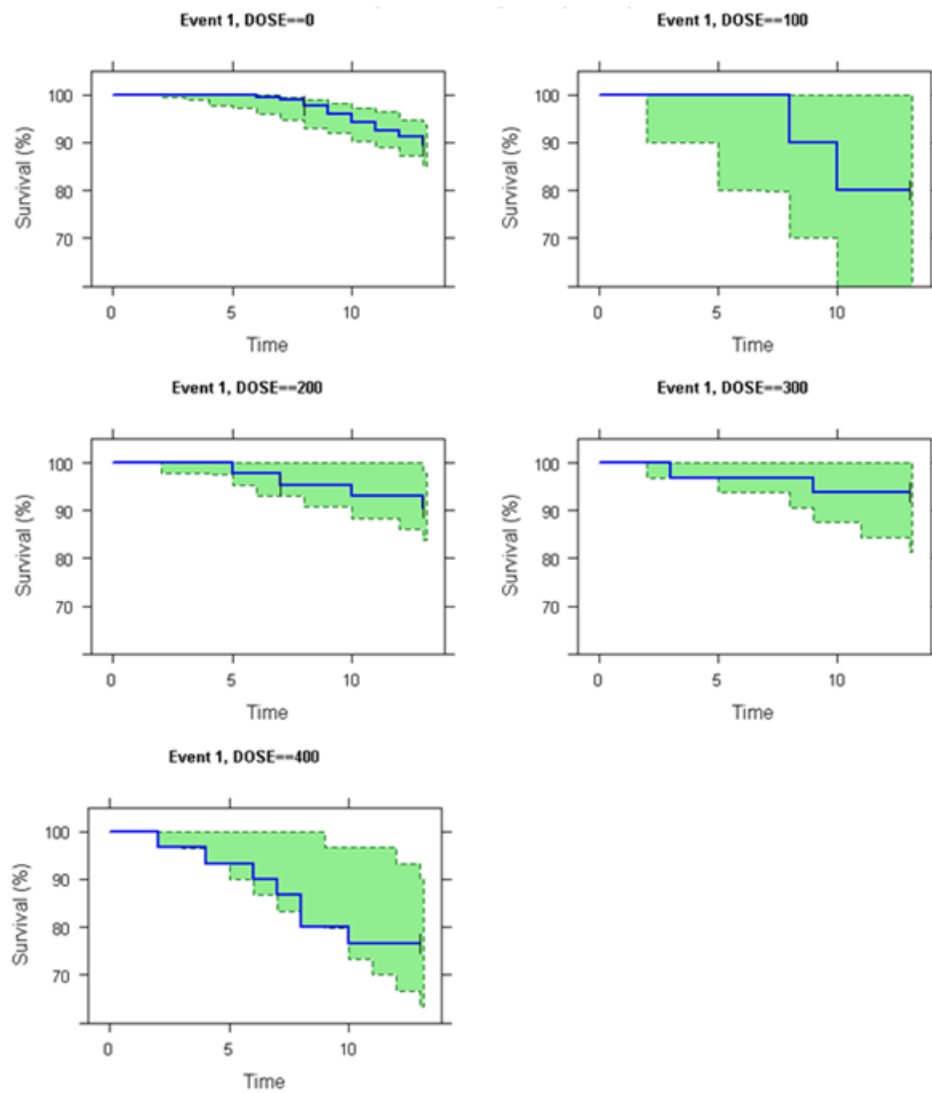
Figure 3-9: Kaplan-Meier plots for time to death stratified by dose. This is

comparison of observed data (blue line) to the 95% prediction interval of the simulated data
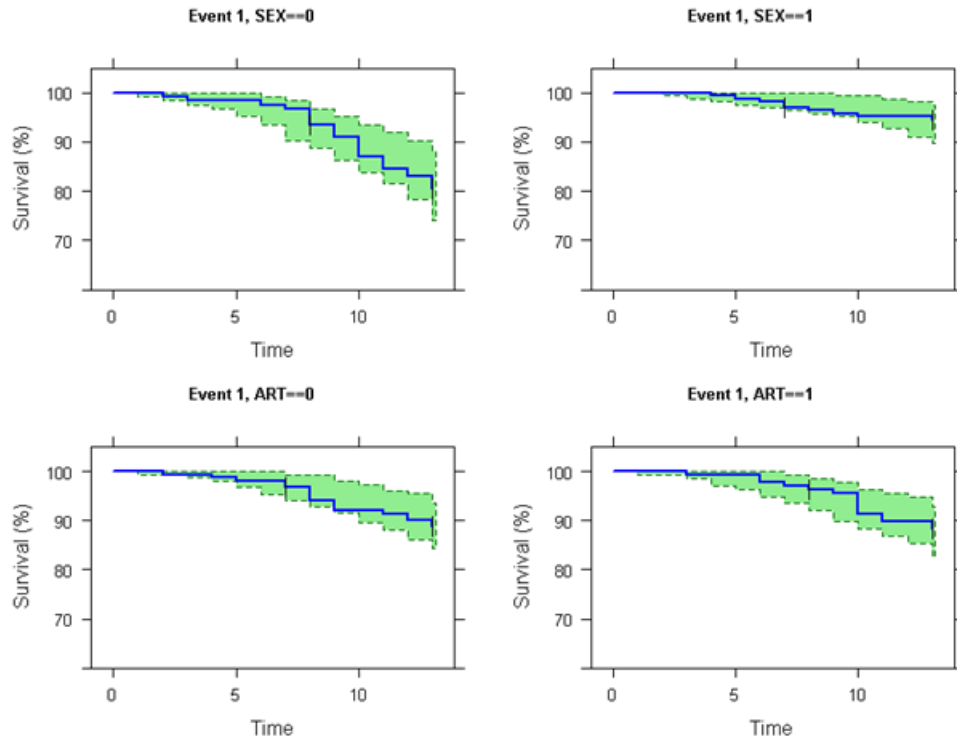
(green area).

Figure 3-10: Kaplan-Meier plots for time to death stratified by SEX and ART. Female and no ART are 0. This is comparison of observed data (blue line) to the 95% prediction interval of the simulated data (green area).

3.5 DISCUSSION

The co-administration of ART increased sertraline oral plasma clearance by > 2 fold, resulting in lower drug exposure. Yet, ART was found to not affect fungal clearance from CSF or survival of patients. Of the PK-PD indices explored, cAUC/MIC of total sertraline concentrations in the brain was the most predictive index of percent daily change in $\log_{10}$ CFU/mL. The addition of sertraline to the CM standard induction therapy increased the rate of CSF fungal clearance on average by 41%, and the effect was similar across dose arms. We also found that female patients and those receiving 100 or 400 mg of sertraline daily had lower 2-week survival rate.

Estimated sertraline clearance was similar to what was previously published, but the volume of distribution was 2-3 fold lower even after adjusting for body weight (132, 133). The difference in volume of distribution can possibly be explained by the disease state and race given that our patients were HIV-infected and sub-Saharan Africans. Metabolism is the main route of sertraline elimination and its clearance was expected to increase with ART co-administration because our patients received a triple efavirenz or nevirapine-based treatment for HIV. Efavirenz and nevirapine are non-nucleotide reverse transcriptase inhibitors (NNRTI) that are known to induce cytochrome P450 metabolizing enzymes responsible for sertraline metabolism (134, 135).

It is challenging to separate out a predictive PD index of sertraline effect in the current study. Our patients were on the CM standard therapy and the observed reduction in $\log_{10}$ CFU/ml cannot be solely attributed to sertraline. Thus, cAUC/MIC is a PD index of sertraline in combination with amphotericin B (0·7–1·0 mg/kg per day) and fluconazole (800 mg/day). The PD target can be different for sertraline monotherapy and

55

to determine that, *in vitro*, *ex vivo*, and *in vivo* animal studies are required due to the ethical reasons and the inability to control for host and fungal factors in a clinical setting. Findings from these studies can then be used to propose a rational dosage regimen of sertraline for confirmatory clinical testing.

Although it decreased sertraline exposure, ART did not influence the rate of fungal clearance from CSF. The sertraline added benefit was also the same regardless of the daily dose our patients received. Together, this suggest that the observed clinical sertraline effect is dose- and concentration-independent which contradicts previous evidence from animal studies (136). One possible explanation is the lack of statistical power related to study design, insufficient number of patients, unbalanced arms, and the narrow range of tested sertraline doses. The range of studied sertraline was only 4-fold and fell at the lower range of the dose-response curve as shown in Figure 3-11. to sufficiently estimate dose-response relationships, at least 10-fold range between the highest and lowest studied doses is recommended by the European Medicines Agency (EMA) (137). The dose to MIC ratio at which sertraline effect is half maximal (D_{50}) was estimated to be 500. Assuming MIC is 4 µg/mL, sertraline daily dose required to achieve 50% reduction in fungal counts is calculated to be 2000 mg (**Figure 3-11**). This is 10-fold greater than the maximum daily dose approved by the US Food & Drug Administration (FDA).
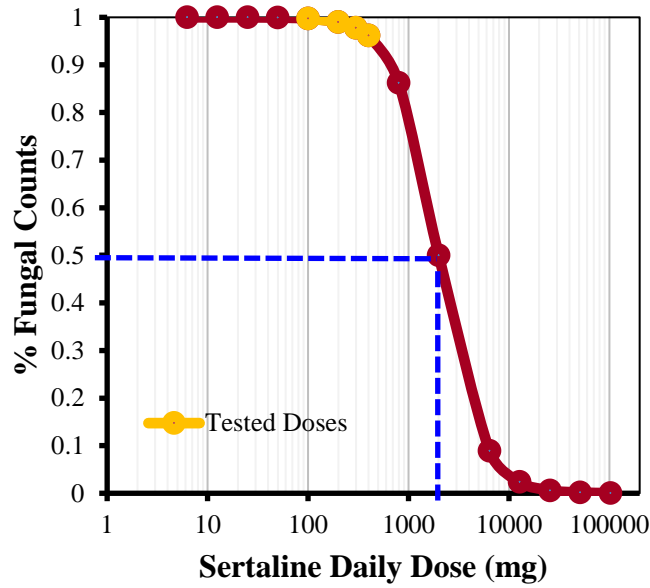
Figure 3-11: Dose-response curve of sertraline. This is the sigmoidal Emax function describing the sertraline effect in equation 4 using the parameter estimates and assuming sertraline MIC is 4 µm/mL.

In addition, it is possible that sertraline effect in human is mediated by different mechanisms than inhibiting protein synthesis of the fungus (111). This idea is supported by the fact that the unbound sertraline concentration is unlikely to reach MIC levels (113). Sertraline is highly-protein bound in plasma and only unbound concentration is able to cross tissue membranes (e.g. blood-brain barrier and fungal cell wall), bind to therapeutic targets, and elicit pharmacological action (138). The highest steady-state total sertraline plasma concentration observed in our patients was 1,078 ng/mL. With 98% protein binding and median of 16.5-fold higher concertation in brain tissue than in blood, the unbound brain sertraline concertation is predicted to be 0.356 µg/mL. This is lower than the lowest determined MIC level (1 µg/mL) for our clinical isolates. Despite consensus that unbound concentration is what really drives drug action *in vivo*, there is unfortunately still a persistent inclination to report total tissue concentrations, arguing

they are better related to drug efficacy. Total tissue concentrations are shown to be poor surrogates for drug efficacy because they are determined after tissue homogenization which is likely unrepresentative of concentration at the site of action (37).

Enhancing fluconazole effect through beneficial pharmacokinetic interaction is one plausible mechanism for the observed clinical effect of sertraline. Fluconazole is a substrate for the efflux transport P-glycoprotein that is widely expressed in gut, blood-brain barrier, renal tubules and other tissues of humans (139–141). Sertraline, on the other hand, is a substrate and inhibitor of P-glycoprotein (142, 143). In theory, the inhibition of P-glycoprotein (P-gp) by sertraline would increase the gut absorption, central nervous system (CNS) penetration producing higher brain concentrations, and decrease renal clearance of fluconazole. Ultimately, sertraline would increase fluconazole exposure particularly in the brain which could possibly explain our results as pointed out by Veringa and his colleagues (144). P-gp-mediated drug-drug interaction at blood brain barrier was confirmed in preclinical species and recently in humans despite the skepticism about the clinical relevance (145, 146).

Increasing 5-HT in plasma is another possible mechanism. 5-HT is shown to have direct and indirect anti-microbial effects against invading pathogens (147, 148). 5-HT possesses antimicrobial properties by itself. It is also a master regulator of innate and adaptive immune response through its wide receptors expressed on immune cells and by receptor independent signaling so-called serotonylation (149). It was shown that depletion of 5-HT in blood and platelets is associated with impaired immune responses as in HIV-infected individuals (150). On the other hand, elevated circulating level of 5-HT is documented in multiple autoimmune inflammatory diseases, such as rheumatoid

58

arthritis, asthma, Crohn's disease, and ulcerative colitis due to either over-production of 5-HT or/and reduced function of 5-HT transporter (SERT) (147). Just like in the brain, SERT in the periphery functions to tightly regulate 5-HT signaling via the reuptake 5-HT back into the cell to terminate and prevent off-target 5-HT effect, protect 5-HT from degradation by monoaminoxidases, and store 5-HT for later release upon subsequent stimulation (151, 152). With that, it is plausible that SERT inhibition by sertraline and simulation of immune response may be the underlying mechanism for the improved fungal clearance in the ASTRO-CM patients.

Survival was not a primary outcome and the study was not powered to find survival difference between sertraline dose arms. However, there was a strong statistical evidence that female patients (p-value <0.0005) and those receiving 100 or 400 mg of sertraline daily (p-value <0.02) had lower survival rate. Our findings could be biased because the analyzed patients represented a nonrandom sample since the analysis only included patients who have plasma measurements and fungal count quantifications (115 out of 137). Results could also be biased by differential co-morbidities or confounding factor that was not accounted for. The first 60 patients were assigned to sertraline daily dose in a non-random fashion. For example, it could be by chance that patients receiving 100 or 400 mg of sertraline daily were sicker, have other opportunistic infections, or just characteristically different than the rest of patients. Though, results should be taken into considerations for further studies to balance patient sample by sex and test at least two different sertraline doses (low and high) to further investigate these findings.

The current study has several limitations. The ASTRO-CM study was not designed for the pharmacometric analyses presented here. Missing data was imputed for

several variables. Single imputations were performed to impute missing weight, dosing time, blood draw time, and clinical characteristics. Pharmacokinetic data were also very sparse and not optimally sampled. Sertraline levels were drawn mostly in the absorption phase on different days. Our patients were diagnosed with multiple medical conditions and on poly-drug therapy. This creates a challenging situation to account for all probable drug-drug interactions. Lastly, sertraline dose groups were not balanced with fewer patients in the 100 mg arm. With these limitations in mind, our findings reflect the available data and should be interpreted cautiously.

In summary, the fungal clearance rate from CSF was increased by sertraline when added to the combination therapy of amphotericin B and fluconazole compared to COAT study. Sertraline effect was unlikely to be mediated via the inhibition of protein synthesis as unbound sertraline concentrations do not reach MIC levels. The effect could be driven by enhancing fluconazole response through the inhibition of P-gp efflux transporter or increasing plasma 5-HT that has antifungal properties and immunomodulatory effects on immune cells. Because the sertraline effect was dose-independent, higher doses than the maximum FDA approved dose may not be needed as they provide little additional benefit come with a greater risk of unwanted adverse events. Further studies are in need to confirm or refine current findings.

4 POPULATION PHARMACOKINETICS OF SERTRALINE: A MODEL-BASED META-ANALYSIS

4.1 SUMMARY

Published mean plasma concentrations of sertraline in healthy adult individuals were extracted from 27 studies and used to develop and validate a population pharmacokinetic model using a model-based meta-analysis (MBMA) approach. Based on non-compartmental analysis (NCA), the increase in C_{max} and AUC_∞ was dose proportional between 50 and 200 mg for single-dose data and between 5 and 200 mg for multiple-dose data. The sertraline single doses of 5 and 25 mg were associated with lower values of C_{max} and AUC_∞ than expected. T_{max} and $t_{1/2}$ did not change across the dose range (5 -200 mg). Sertraline oral bioavailability (F) increased with dose from 5 to 50 mg and then plateaued for single-dose mean data while it was relatively the same across the entire dose range for multiple-dose data. Deconvolution analysis of single-dose data showed that sertraline F was similar to those calculated by NCA and absorption rate constant was a time-dependent process that was best described by a sigmoidal E_{max} function of time after dose. A 2-compartment pharmacokinetic (PK) model with linear elimination, time-dependent absorption, and proportional error adequately described the sertraline literature mean data. Three random effects were used for inter-study variability (ISV), inter-arm variability (IAV), and residual unexplained variability (RUV). The latter two were weighted by the inverse square root of total number of subjects in an arm ($1/\sqrt{n}$). The steady-state (SS) status was associated with higher peripheral volume of distribution (V_3) and F increased with dose nonlinearly for single dose data only.

61

4.2 INTRODUCTION

Sertraline is an orally bioavailable selective serotonin reuptake inhibitor (SSRI) first marketed by Pfizer in 1991 under the brand name Zoloft® for the treatment of major depressive disorder (123). Today, it is approved at 25-200 mg for additional conditions, including panic disorder, obsessive-convulsive disorder, post-traumatic stress disorder, premenstrual dysphoric disorder and social anxiety disorder, and is current being investigated in human for other potential uses (153). Sertraline remains one of the preferred SSRI agents because of its good safety and efficacy profile. It rarely causes serotonin syndrome by itself. When overdosed up to 8,000 mg, symptoms are similar to those associated with therapeutic doses. Over-dose symptoms usually subside within 4 hours and are easily treated with lavage or the administration of activated charcoal when needed (154). Moreover, sertraline has few documented drug-drug interactions of clinical significance due to its minimal inhibition effect on the cytochrome P450 enzyme system (123, 153).

The pharmacokinetics of sertraline, unlike some SSRIs, is reported to be linear up to the maximum studied dose (400 mg) (132). The PK linearity is shown to hold even in overdose cases (155). Following oral administration, sertraline is slowly absorbed from gastrointestinal tract and undergoes extensive first pass metabolism by P450 enzymes to form a pharmacological inactive metabolite, N-desmethylsertraline (134, 156). Absolute oral bioavailability of sertraline remains unknown with inconsistent reports due to the lack of published studies comparing drug exposure of oral to IV administration (123, 157). The maximum plasma concentration (C_{max}) of oral dose is reached 4-8 hours (T_{max}) which is not affected by administration time (morning vs evening) (10). However, the

administration with food increases sertraline C_{max} by 25% and decreases T_{max} from 7.9 to 5.4 hours, yet it results in slightly insignificant and clinically irrelevant increase in area under plasma concentration-time curve (AUC) (158).

Sertraline is a moderate to high clearance drug that is 95-98% bound to plasma proteins; however, it has a long half-life ($t_{1/2}$) that ranges from 22 to 36 hours due to the extensive distribution into body tissues (123, 159). The plasma concentrations at steady state (SS) is highly variable in which 15-fold difference was observed in patients receiving typical therapeutic antidepressant doses (160). Age, gender, hepatic function, and single nucleotide polymorphisms (SNP) of CYP 2C19 were found to affect sertraline pharmacokinetics. Sertraline exposure was higher in elderly, young females, CYP2C19 poor-metabolizers, and individuals with impaired liver function (156, 161–163).

To the authors' knowledge, there is not any published population PK model of sertraline in healthy volunteers. Therefore, the study objective was to use literature plasma concentrations data to develop and validate a population PK model of sertraline in healthy subjects applying model-based meta-analysis (MBMA) approach. This can serve as the starting point for more population-based analyses in different patient populations given the great interest of the medical communities in the use of sertraline as an anticancer, antibacterial, antifungal, and a sensitizing agent of chemotherapies (112, 164–168).

4.3   MATERIALS AND METHODS

4.3.1   Literature Search & Data Extraction.

A systematic literature search in the PubMed database in October 2015 was carried

out to identify published PK studies of sertraline. The search terms included a

combination of the following: sertraline, Zoloft, SSRI, healthy subjects, and

pharmacokinetics. The literature search was restricted to studies which included healthy

subjects aged at least 18 years old, and reported in the English language. The initial

search resulted in 54 articles. After full-paper examination, studies that had the mean

plasma concentration-time profile data tabulated or plotted versus time were selected for

inclusion regardless of the study design. Data including patient demographics were then

extracted and formatted for analysis.

4.3.2   Dose Proportionality Analysis.

Extracted mean plasma concentrations were analyzed by NCA to calculate PK

variables. The sertraline F for each mean plasma concentration-time profile relative to the

IV profile was calculated using the following (equation $4 - 1$):

$$F = \frac{AUC_{po} \times DOSE_{IV}}{AUC_{IV} \times DOSE_{PO}} \qquad (4 - 1)$$

A log-transformed power model with dose as a fixed effect was used to evaluate dose

proportionality for C_{max}, and AUC_∞ (equation $4 - 2$).

$$\text{Log(parameter)} = \log(\alpha) + \beta \log(\text{dose}) + \varepsilon \qquad (4 - 2)$$

The steady-state (SS) status (No/Yes) was adjusted for when testing dose

proportionality for C_{max}. This adjustment was not necessary for AUC_∞ because it was

calculated as AUC$_\tau$ for multiple-dose mean plasma concentration-time profiles. Model fit was assessed by the random scattering of residuals around the horizontal line of zero. The dose proportionality is declared when the estimated β value is not significantly different from 1. Values of β above 1 represent higher (super-proportional) exposure whereas β values below 1 represent lower (sub-proportional) exposure. The dose effect on sertraline $t_{1/2}$ and T$_{max}$ was tested using a linear fixed effects model on log-transformed values adjusted for SS status (equation 4 – 3).

$$\text{Log(parameter)} = \alpha + \beta_1 \text{ Dose} + \beta_2 \text{ SS} + \varepsilon \qquad (4 – 3)$$

4.3.3 Deconvolution Analysis.

The IV mean plasma concentration-time data were analyzed by compartmental analysis. The final estimated exponential terms were assumed to be the same for the oral data. Assuming linear kinetic system, deconvolution analysis was performed on single-dose mean data only to estimate F and input rate into the system. The absorption rate constant (K$_a$) was calculated from the slope of the log absorbable amount of drug in gastrointestinal tract (A) vs time (t) multiplied by -2.303 where A$_o$ represents the absorbable amount of drug at time 0 (equation 4 – 4).

$$\log(A) = \log(A_o) - \left(\frac{K_a}{2.303}\right).t \quad (4 - 4)$$

4.3.4 Pharmacokinetic Modeling.

Using nonlinear mixed-effects regression, mean plasma concentrations were fitted to one and two compartment PK models with linear and nonlinear elimination. Three-level nested random effects were included: inter-study variability (ISV), inter-arm variability

(IAV), and residual unexplained variability (RUV). Exponential models were used for

ISV and IAV while RUV was described by a proportional error. IAV and RUV were

weighted by the inverse square root of the total number of subjects in an arm $(1/\sqrt{n})$.

Guided by the findings of deconvolution analysis, K_a was modeled as a time-dependent

variable using a sigmoidal E_{max} function (equation $4 - 5$).

$$K_a = \frac{Ka_{MAX}\, TAD^\gamma}{T_{50}{}^\gamma + TAD^\gamma} \quad (4-5)$$

TAD is time after dose administration, T_{50} is the TAD when K_a is half maximal, and γ

is a steepness shape parameter for the Ka – TAD curve. The effect of dose, SS status, and

patient demographics including age, weight, and sex were screened visually against

Empirical Bayes parameter estimates of the base model. The statistical significance of

covariates were then tested by the likelihood ratio test (χ^2, $\alpha = 0.01$, df $= 1$), that

corresponds to a reduction in objective function value (OFV) of 6.63 points or greater.

Selection of the final PK model was guided by the OFV, parameter estimates relative to

literature values, diagnostics plots, and Akaike information criterion (AIC). The final

model was validated internally by visual predictive checks (VPC) and the uncertainties of

model parameter estimates were computed by sampling importance resampling (SIR)

method.

4.3.5   Software.

Figures of plasma concentration-time profiles were digitized using WebPlotDigitizer

(version 3.11). NCA were performed in R (version 3.1.0) using PKNCA package and

deconvolution analysis done in Pheonix WinNonlin (version 6.3). Model parameter

estimates and the 95% CI of the log-transformed power and linear models were obtained

by ordinary least square regression in R (version 3.1.0). PK analysis was performed in NONMEM 7.3 (ICON Development Solutions, Ellicott City, MD) using ADVAN 13 with the FOCEI method. The ISV random effect was approximated using $Level and the R-matrix in the $COVARIANCE record. VPC and SIR analyses were implemented in Perl-speaks-NONMEM (PsN). Pirana interface was used to maintain and compare NONMEM and PsN runs.

4.4 RESULTS

4.4.1 Data Extraction.

A total of 60 mean concentration-time profiles extracted from 27 studies provided 748 plasma concentrations of doses ranging from 5 mg to 400 mg (**Table 4-1**). The majority of studies were either randomized crossover PK studies or validation PK studies for developed analytic methods. Eleven mean concentration-time profiles were from multiple-dose studies, 1 mean was from an IV study, and the rest were single-dose studies (**Figure 4-1**). Of the 60 profiles, 6 were the mean of females only, 6 profiles were the mean of equal numbers of females and males, 5 profiles were the mean of females and males in which the proportion of males was greater than 50%. The sex was not reported for 12 mean profiles and the remaining mean profiles were for males only. The median and (range) of mean age and mean body weight were 26 (20-72 years) and 67 (59-80 kg), respectively.

Table 4-1: Summary of PK studies included in the model-based meta-analysis (MBMA)

Study	Description	Subjects	Arms	Doses	Ref
1	Single dose double-blind placebo-controlled cross-over study	10	3	100, 200 & 400 mg	(169)
2	Single dose	24	3	50, 100 & 200 mg	(155)
3	Single dose PK study	10	1	100 mg	(161)
4	Multiple dose PK in elderly and young male and female	24	4	200 mg	(170)
5	Single dose chrono-pharmacokinetic and food effect study	24	4	100 mg	(158)
6	Single dose randomized crossover bioavailability study	24	2	50 mg	(171)
7	Multiple dose PK interaction study with zolpidem	27	2	50 mg	(172)
8	Single dose randomized crossover bioequivalence study	11	2	150 mg	(173)
9	Single dose PK to study CYP2C19 polymorphism effect	6	2	100 mg	(174)
10	Single dose PK validation study for GC-MS method	5	1	50 mg	(175)
11	Single & multiple dose open-label three-period crossover interaction study with donepezil	16	4	50 & 100 mg	(176)
12	Single dose randomized crossover bioequivalence study	24	2	50 mg	(177)
13	Single dose randomized crossover bioequivalence study	24	4	100 mg	(178)
14	Single dose PK validation study for HPLC-EIMS method	20	2	50 mg	(179)
15	Single dose bioequivalence PK validation study for HPLC-TMS method	18	2	50 mg	(180)
16	Single dose randomized crossover bioequivalence study	24	2	50 mg	(181)
17	Single dose bioequivalence PK validation study for HPLC	1	1	100 mg	(182)
18	Single dose randomized crossover bioequivalence study	24	2	50 mg	(183)
19	Single dose bioequivalence PK validation study for HPLC-TMS method	32	2	100 mg	(184)
20	Single dose randomized crossover	24	2	50 mg	(185)

	bioequivalence study				
21	Single dose three-period crossover study	6	3	5, 25 & 50 mg	(186)
22	Single dose bioequivalence PK validation study for LC/MS/MS	18	2	50 mg	(187)
23	Single dose PK study	5	1	100 mg	(188)
24	Single dose crossover PK study	14	2	100 mg	(189)
25	Single dose PK validation study for UPLC-MS/MS method	20	1	100 mg	(190)
26	Multiple dose three-period crossover study	10	3	5, 25 & 50 mg	(191)
27	IV infusion over 12 hours	12	1	100 mg	(192)

4.4.2   Dose Proportionality

The NCA analysis included 56 mean profiles from 25 studies because mean profiles from 2 studies did not have plasma concentrations measured in the elimination phase (**Figure 4-1**). Sertraline PK variables per dose level and color-coded by SS status are presented in **Figure 4-2**. The calculated F increased with dose in a nonlinear fashion for single-dose data, whereas it was relatively the same for multiple-dose data. The dose-proportionality condition (β coefficients were not different from 1) was met for both AUC_∞ and C_{max} across the dose range for multiple-dose data. For single-dose data, the proportionality condition was met only between the dose range of 50-200 mg. There was a disproportional decrease (lower values than expected) in AUC_∞ and C_{max} at lower single doses of 5 and 25 mg. Dose was found to neither affect $t_{1/2}$ nor T_{max} across the entire dose range of 5-200 mg after adjusting for SS status.
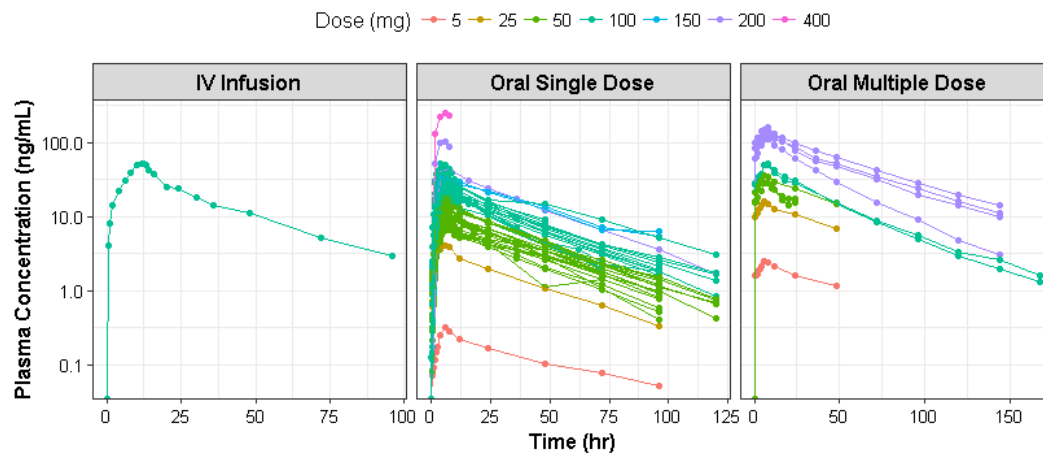
Figure 4-1: Extracted mean concentration-time profiles.
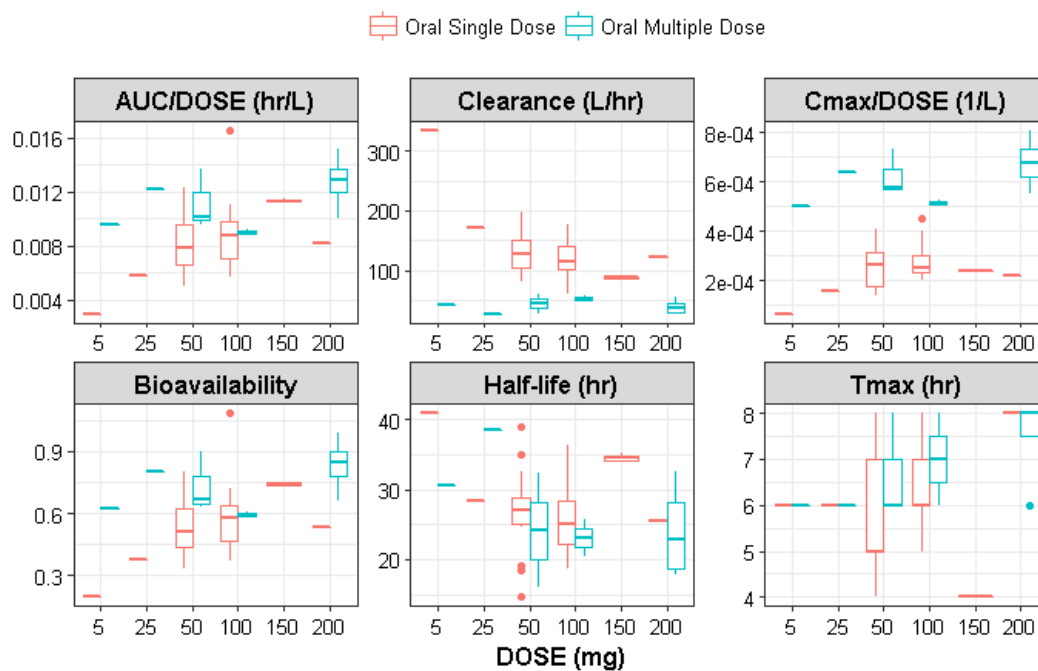
Figure 4-2: Pharmacokinetic variables calculated by NCA. Bioavailability was calculated

using equation 1.

4.4.3 Deconvolution.

The IV mean profile was best fit to a two compartment PK model with a linear

elimination, and a proportional error model. The plasma body clearance (CL), Q, central,

and peripheral volumes (V_2 and V_3, respectively) were estimated to be 66.43 L/hr, 82.75

L/hr, 1011.11 L, and 955.95 L, respectively. The α and β exponential terms were

calculated to be 0.207 1/hr and 0.0275 1/hr.

Deconvolution analysis included 47 mean concentration-time profiles from 21 single-

dose PK studies. The estimated F was comparable to the values calculated from NCA and

presented in **Figure 4-3**. The K_a was found to be time-dependent as shown in **Figure 4-4**.
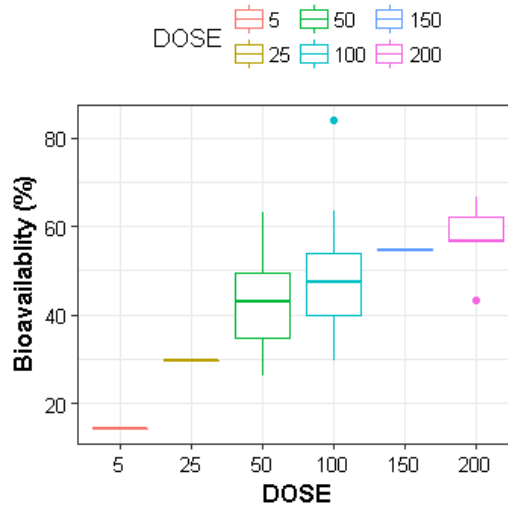
Figure 4-3: Sertraline bioavailability estimated by deconvolution.
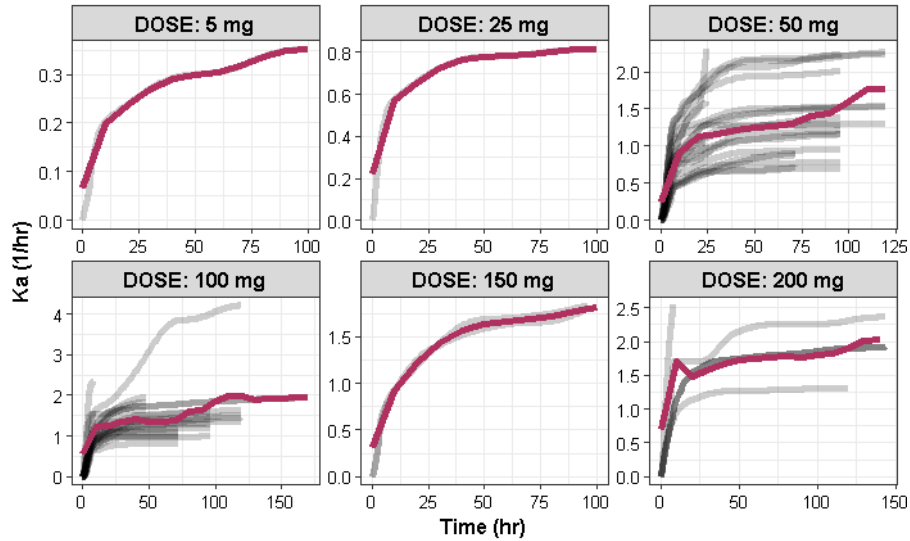
Figure 4-4: Absorption rate constant (K$_a$) relationship with time. Grey and maroon lines are

the individual and the mean Ka, respectively**.**

4.4.4 Pharmacokinetic Model.

A 2-compartment PK model with a linear elimination and proportional error

adequately described the sertraline literature mean data. ISV & IAV were included in CL,

V$_2$ and γ. The SS status increase peripheral volume of distribution (V3) and dose

increased F nonlinearly for single dose data only (equation 4 – 6).

$$F = \frac{DOSE}{D_{50} + DOSE} \quad (4-6)$$

D$_{50}$ is the dose when F is 50%. Diagnostic plots show no evidence of model lack of fit

which is further supported by VPC (**Figure 4-5** & **Figure 4-6**). The parameter estimates

of the selected model and their SIR-based uncertainty are shown in **Table 4-2**.
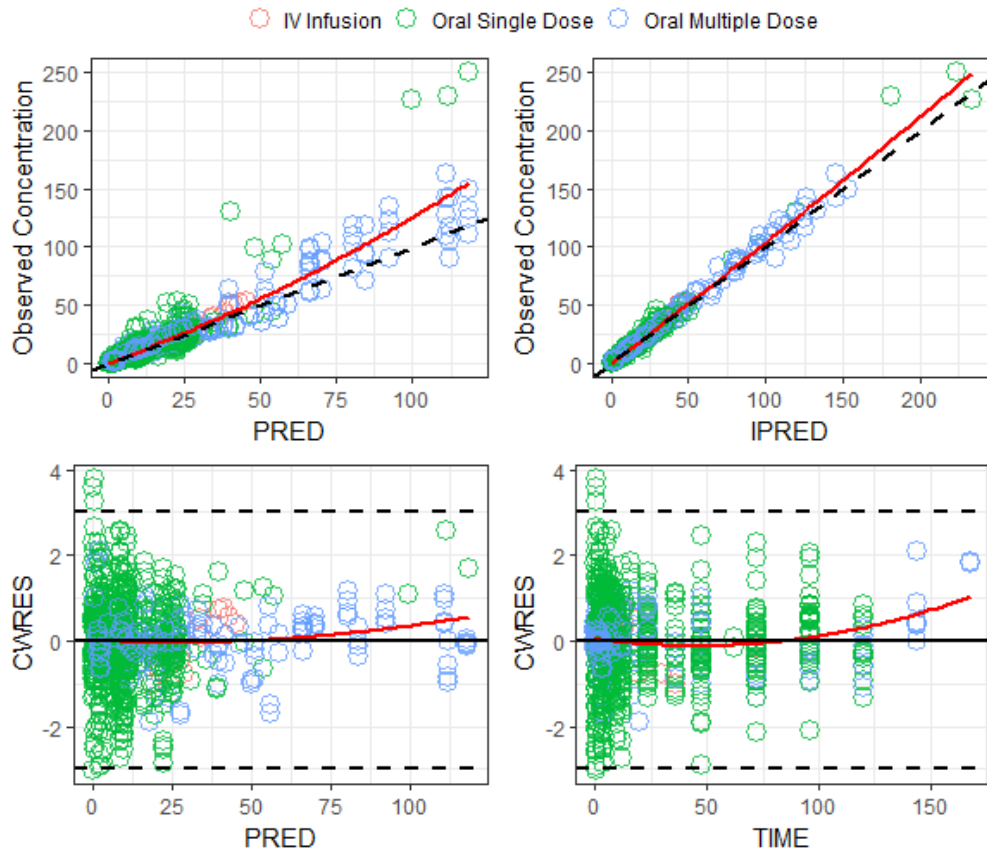
Figure 4-5: Diagnostic plots for the selected MBMA PK model of sertraline. Red lines are Lowess smoothers. CWRES is conditional weighted residuals.
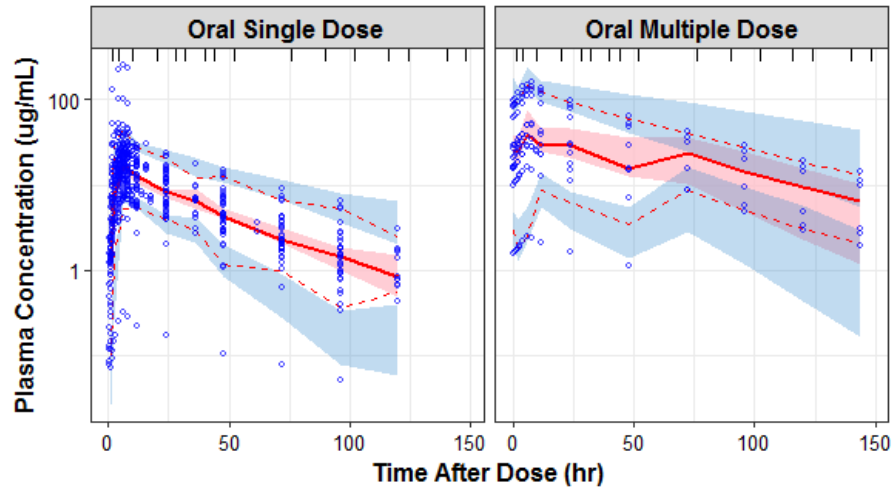
Figure 4-6: Diagnostic plots for the selected MBMA PK model of sertraline. Blue open circle represents the prediction-corrected concentrations, red solid and dashed lines represents the median, 5th and 95th percentile, respectively. Shaded areas are the simulated 95% CI of each percentile.

Table 4-2: Parameter estimates for the selected MBMA PK model of Sertraline

Parameter (unit)		Definition	Estimate (%RSE)	SIR median (95%CI)
CL	(L/hr)	Clearance	59.7 (8)	61.47 (49.17 – 74.01)
V_2	(L)	Central volume of distribution	1200 (12)	1242 (914.2 – 1621)
Q	(L/hr)	Inter-compartmental clearance	161 (11)	163.7 (124.4 – 206.9)
$V_{3\ single}$	(L)	Peripheral volume of distribution for single dose	928 (8)	948.4 (752.9 – 1142)
$V_{3\ multiple}$	(L)	Peripheral volume of distribution for multiple dose	1350 (10)	1371 (1044 – 1755)
Ka_{MAX}	(1/hr)	Maximum absorption rate constant	0.855 (10)	0.86 (0.713 – 1.05)
T_{50}	(hr)	Time when absorption rate is 50% of Ka_{MAX}	3.7 (3)	3.71 (3.23 – 4.31)
γ		Shape parameter of absorption rate	1.37 (3)	1.38 (1.28 – 1.47)
F_{max}		Maximum bioavailability	0.639 (8)	0.661 (0.559 – 0.804)
D_{50}	(mg)	Dose when bioavailability is 50%	15.5 (16)	15.51 (10.5 – 22)
ISV CL	(%CV)	Inter-study variability in CL	30.8 (12)	31.60 (23.50 – 40.91)
ISV V_1	(%CV)	Inter-study variability in V_1	39.8 (16)	40.75 (27.28 – 56.72)
ISV γ	(%CV)	Inter-study variability in γ	54.8 (15)	56.22 (38.92 – 80.26)
IAV CL	(%CV)	Inter-arm variability in CL	30.9 (10)	31.62 (25.32 – 39.28)
IAV V1	(%CV)	Inter-arm variability in V_1	59.9 (13)	60.93 (46.79 – 81.40)
IAV γ	(%CV)	Inter-arm variability in γ	45.7 (12)	46.66 (36.10 – 60.56)
RUV	(%CV)	Proportional residual unexplained variability	19 (6)	19 (17 – 21.4)

4.5 DISCUSSION

In this study, literature mean data of sertraline plasma concentrations were extracted and analyzed by NCA, deconvolution analysis, and MBMA approach. Sertraline C_{max} and AUC_{∞} were dose proportional across the studied doses (5 - 200 mg) for the multiple-dose data whereas dose proportionality was met only between 50 and 200 mg for the single-dose data. F was lower for sertraline single doses of 5 and 25 mg and it is likely the underlying cause of the observed dose disproportionality at lower doses. T_{max} and $t_{1/2}$ of sertraline were dose independent. Deconvolution analysis of single-dose data resulted in similar F estimates from NCA and showed that K_a was time-dependent best described by a sigmoidal E_{max} function of TAD. A 2-comaprment PK model with a linear elimination, time-dependent K_a, and proportional error adequately described the sertraline literature mean data. SS status and sertraline dose after single dose administration increased V_3 and increased F in nonlinear manner, respectively.

The study findings indicate that nonlinear changes in sertraline exposure are due to the changes in F with dose, rather than being mediated through an effect on clearance. This is in disagreement with what was suggested by *in vitro* studies and in adolescent patients (134, 193). The nonlinearity in F can be rationally explained by the inhibition of P-glycoprotein (P-gp) efflux transporter in the gastrointestinal (GI) tract. Sertraline is a substrate and potent inhibitor of P-gp with an IC_{50} value of 31.8 µM that is similar to the well-known inhibitor quinidine (33.8 µM) (142, 143, 194). Given that sertraline can reach GI concentration well above the IC_{50} value (65 to 2612 µM for 5 and 200 mg), this makes GI P-gp inhibition a highly plausible explanation. Even though GI concentrations

are calculated to be twice the IC_{50}, sertraline doses lower than 50 mg had significantly lower F. This is probably because of the low binding affinity (K_i) of sertraline to P-gp that can be compensated for by achieving higher concentrations. This is likely the case with higher doses ($\geq$ 50 mg). It was also suggested that P-gp is easily saturated at therapeutic doses of high permeable drugs like sertraline rendering the effect P-gp clinical irrelevance unless the therapeutic doses are very low (195). Yet, it remains unclear why dose effect on F was absent with repeated dosing that needs further investigation. It might be that repeated dosing of low doses eventually achieves similar P-gp saturation or inhibition caused by high doses. In fact, clinical drug-drug interaction (DDI) studies are required to determine the effect of sertraline therapeutic doses on the pharmacokinetic of P-gp substrate drugs, such as digoxin, because the criterion (the highest approved dose dissolved in 250 ml divide by $IC_{50} \geq 10$) set by the Food Drug Administration in the 2012 draft guidance on DDI is met (196).

According to Biopharmaceutics Classification System (BCS), sertraline is a class II low solubility, high permeability compound whose absorption from the GI tract is limited by solubility (197). Sertraline appears to slowly dissolve in the GI as evident from the initial slow increase of the mean concentration-time profiles on a normal-scale plot (**Figure 4-7**). To account for the time it takes for sertraline to dissolve and be available for absorption, a time-dependent K_a, which was also informed by deconvolution findings, resulted in the best fit of the data. The model fit was significant better and more physiological-sound than a 1st order absorption process with a lag time. A time-dependent K_a resulted in a significant reduction in OFV and improved diagnostic plots. The time-dependent absorption model was also easier to implement as it requires straightforward

coding, less computation time, and it is more likely to coverage than a transit-absorption model (198).
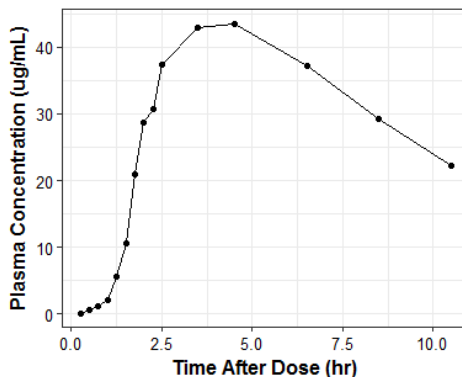
Figure 4-7: A sertraline mean concentration-time profile after 100 mg dose.

SS status was found to significantly increase V_3 indicating a greater tissue distribution of sertraline with repeated dosing. This translates into an increase in elimination $t_{1/2}$ from 26.6 to 32.7 hr. This increase in $t_{1/2}$ is opposite to what was observed in adolescent patients (193). Our analysis did not find sex and age, previously known to be influential, to affect sertraline pharmacokinetics. This can be attributed to the insufficient number of mean profiles of females and the narrow range of mean ages. A major limitation of the current findings that there is few mean concentration-time profiles of doses less than 50 mg leading to high uncertainty of the F-dose relationship at the lower doses.

In conclusion, a population PK model of sertraline in healthy subjects was successfully developed and validated internally by VPC. It was the first model that used IV infusion, single, and multiple oral mean data from 27 studies. F was nonlinearly related to dose after single dose administration only which is likely caused by the inhibition or saturation of P-gp in the GI tract. Repeated dosing of sertraline was associated higher V_3 and longer elimination $t_{1/2}$. Sertraline absorption rate constant was time-dependent and best

described by a sigmoidal function. The PK model can be a useful starting point for other patient populations. Parameter estimates can also be used as inputs for mechanistic models, such as physiological-based PK model (PBPK) in order to increase our understanding of the biological processes that control sertraline disposition.

5 PHYSIOLOGICALLY-BASED PHARMACOKINETIC (PBPK) MODEL OF SERTRALINE TO DETERMINE CLINICAL RELEVANCE OF CONCENTRATIONS AT TARGET TISSUES

5.1 SUMMARY

Significant *in vitro* and *in vivo* evidence supports the potential use of sertraline as an anticancer and antimicrobial agent. Yet, it is unknown whether concentrations following therapeutic doses are achieved in relevant clinical tissues. The study objectives were to develop a PBPK model for sertraline and estimate the probability of achieving effective concentrations in various target tissues, especially in brain and liver. A generic PBPK model consisting of 14 perfusion-limited compartments representing physiological organs of the body linked together by arterial and venous blood and incorporated with clearance, distribution, and absorption models was implemented in R. CL and V parameters were first optimized by scalars from IV data and then used to simulate an oral steady-state profile. The incorporation of a first-order intestinal loss rate constant whose value was dependent on dose and steady state, reduced gastric emptying rate, and saturable hepatic first pass elimination reproduced oral data well. Simulated weights from a truncated normal distribution were used to generate physiological parameters for 1000 *in silico* subjects. Population PBPK simulations were performed and the probabilities of achieving effective steady-state sertraline concentrations in brain, liver and other target tissues were calculated for 50, 100, 200 and 400 mg doses. Predicted unbound concentrations at steady state were unlikely to reach the therapeutic concentrations determined *in vitro*. The estimated probability in 9 clinically relevant tissues was $\leq 50\%$

and zero for therapeutic concentrations 0.25-0.50 and ≥ 1 mg/L, respectively. PBPK simulations indicate therapeutic sertraline doses are unlikely to produce concentrations required for anti-cancer (0.31 – 9 mg/L) and antimicrobial (1 - >200 mg/L) effects in human.

5.2   INTRODUCTION

Physiologically based pharmacokinetic (PBPK) modeling and simulation is a mechanistic quantitative framework that integrates physiological processes with compound physicochemical properties to describe the time-course of absorption, distribution, metabolism, elimination (ADME) of a chemical compound *in vivo*. Thus, two sets of parameters, physiology- and compound-dependent, are required to develop a PBPK model in a species of interest (199, 200). This tool is simple, reliable, fast, cost-effective, and gaining wide acceptance by regulatory agencies as evident by the recent release of PBPK analysis guidance by the U.S. Food and Drug Administration (FDA) (67). The applications of PBPK modeling and simulation are enormous that can be broadly categorized into three major roles from early to late drug development stages: (1) gain mechanistic understanding of the processes affecting the kinetics of the compound; (2) inform clinical development decisions; (3) support regulatory submissions and labeling (201).

Developing the PBPK model is a challenging task and is limited by the availability of input parameters, particularly drug characteristics (202). Although, these parameters can be measured experimentally or predicted by *in silico* models, they remain to be a deterrent to the application of PBPK due to inaccuracy arising from the measurement and

prediction errors. As a consequence of using inaccurate parameter inputs, a simulated profile can fail to follow observed *in vivo* profiles. The mismatch between the simulated and observed profile can be caused by a multitude of factors, especially in oral profiles (199, 203). To identify the parameter inputs that have the most influence on the simulated oral profiles, parameter sensitivity analysis is usually performed. Yet, the selection of parameters on which to focus and the reasonable range of biological plausibility over which parameters can be varied require expert knowledge (199, 201). To overcome the limitation of inaccurate parameter inputs, Peters (195, 203) proposed and validated a strategy using the mismatch pattern between the simulated and observed oral profiles to identify processes that affect oral lineshapes after optimizing clearance (CL) and volume (V) from an intravenous (IV) data by the inclusion of adjustable CL and V scalars to reproduce the observed IV curve.

There is a plethora of *in vitro* and *in vivo* animal evidence supporting the potential use of sertraline as an anticancer and antimicrobial against bacterial, fungal, and viral infections (204–208). Also, synergism is observed when sertraline is combined with chemo- and antimicrobial therapies (112, 120, 164, 168, 209, 210). Sertraline half maximum inhibitory concentration (IC_{50}) for anti-proliferative activity against different cancer cell lines ranged between 1-25 µM (0.31–9 mg/L) and its effect was shown to dose-dependent (112, 166, 167, 211–214). Likewise, antimicrobial properties of sertraline are dose-dependent and its minimum inhibitory concentration (MIC) against wide range of pathogenic microbes vary from 1 to >200 mg/L (109, 206, 207). Whether these concentrations are clinically achieved in target tissues following the administration of therapeutic doses is unknown. The study objectives were to develop and validate a PBPK

model of sertraline in healthy subjects using Peters's novel approach and perform population simulations to estimate the probability of achieving sertraline anticancer and antimicrobial therapeutic concentrations in humans.

5.3   METHODS

5.3.1   PBPK Model Building

A "middle-out" approach that combines mechanistic physiological processes with available *in vivo* information was used to develop and validate a PBPK model for sertraline in healthy subjects (215). A generic PBPK model consisting of 14 compartments representing different physiological organs linked together by arterial and venous blood and incorporated with first-order hepatic clearance, distribution, and advanced compartmental absorption & transit (ACAT) models was implemented in R (version 3.2.5) using mrgsolve package (version 0.8.6) (203, 216). The diagram representation and mass balance differential equations of the integrated PBPK were previously described (203). Because sertraline is a small, highly lipophilic, and permeable compound, perfusion-limited distribution into well-stirred compartments of body organ was assumed (197).

The mean physiological input parameters of a healthy human including organ blood flows (Q_{org}) and organ volumes (V_{org}) for the PBPK model were obtained from literature and are presented in

Table 5-1 (217). Sertraline-specific parameters including molecular weight (MW), lipophilicity (logP), fraction unbound in plasma (fup), its acid dissociation constant (pKa) to calculate tissue-to-blood partition coefficients (Kp) for tissue distribution models, and other parameters were collected from the literature and are summarized in **Table 5-2.** Kp values were predicted from three commonly used *in silico* models (218–220). The hepatic intrinsic clearance (CL_{int}) of sertraline was calculated from the estimated *in vivo* plasma clearance (CL_p), its blood to plasma ratio (BP), and hepatic blood flow (Q_H) using the following equation (221):

$$CL_{int} = \frac{Q_H \times CL_p}{f_{up}\,(Q_H - CL_p/BP)} \quad (5-1)$$

For oral simulations, intestinal solubility (Sol_{if}) was predicted by Mithani's equation that accounts for the increase of solubility due to the presence of bile salts and depends on intrinsic solubility (S_o) and physicochemical properties (222).

$$Sol_{if} = Sol_{water} + Sol_{bile} \quad (5-2)$$

$$Sol_{water} = S_o \times (10^{(pKa - pH)} + 1) \quad (5-3)$$

$$Sol_{bile} = 10^{(2.23 + 0.61 \times logP)} \times Sol_{water} \times MW_{water} \times [bile\ salt] \quad (5-4)$$

Intestinal permeability (P_{eff}) was also predicted by multiplying Caco-2 apparent permeability (P_{app}) by a scaling factor of 25 from which the absorption rate (K_a) was calculated as (203):

$$K_a = \frac{P_{app} \times 25 \times 2}{Radius\ of\ small\ intestine\ (cm)} \quad (5-5)$$

Oral bioavailability (F) was estimated as the product of the fraction absorbed (F_{abs}), the bioavailability of gut (F_g), and the bioavailability of hepatic (F_h). F_g was indistinguishable from F_{abs}, so F was F_{abs} times F_h which is calculated using equation 5 – 6 (221).

$$F = F_{abs} \times F_h = F_{abs} \times \left(1 - \frac{CL_H}{Q_H \times BP}\right) \quad (5-6)$$

Table 5-1: Human physiological tissue parameters

Tissue	Volume (mL/Kg)	Blood Flow Rates (mL/min/Kg)
Adipose	143	3.7
Bone	124	3.6
Brain	20.7	10
Gut	23.6	13
Heart	3.8	2.14
Kidney	4.4	15.7
Liver	24.1	21
Lung	16.7	71
Muscle	429	10.7
Pancreas	1.2	1.9
Skin	111	4.3
Spleen	2.7	1.1
Stomach	2.2	0.56
Testes	0.51	0.04
Arterial blood	25.7	-
Venous blood	51.4	-

Following a stepwise procedure suggested by Peters, CL and Kp scalars were included in the PBPK model and adjusted to fit the observed IV data (203). Because the IV concentration-time profile is primarily dictated by DME wihch presumably remain unchanged regardless of the administration route, the IV-optimized V and CL parameters were fixed and used to simulate an oral profile. The mismatch between simulated and observed oral lineshapes was rationally interpreted by Peter (203) as factors affecting oral profiles including drug-induced gastric emptying delay, gut wall metabolism, P-glycoprotein efflux, chemical degradation, enterohepatic recirculation, and variable absorption across gut wall. She already demonstrated and validated the approach through examples and provided a decision tree to identify these mechanisms affecting oral lineshapes based on the mismatch pattern which we followed in this study.

Table 5-2: PBPK Model input parameters for sertraline

Parameters (unit)	Literature values	Ref	Used Value
Compound type	Monoprotic base	(131)	
Molecular weight (g/mol)	306[a], 343[b]	(131, 197)	306
Lipophilicity, logP	4.9, 5.2, 4.3, 5.15, 5.5	(131, 192, 197, 223, 224)	4.94[g]
Acid dissociation constant, pK_a	9.1, 9.1, 9.16, 9.5, 9.43	(131, 192, 197, 223, 224)	9.26[g]
Fraction unbound in plasma, fup	0.0134 – 0.0161, 0.02, 0.05, 0.023	(123, 131, 170, 223)	0.018[g]
Red blood cells/plasma ratio	1.34	(225)	-
Whole blood/plasma ratio, BP	1.5[c], 0.85, 0.7	(156, 223, 226)	2.925[h]
Intrinsic solubility at pH 7.0 (mg/mL)	0.003[a], 0.18[b]	(192, 197)	0.003
Permeability, P_{app} (10^{-6} cm/s)	5.7, 1.9	(131, 223)	3.80[f]
Intestinal permeability, P_{eff} (10^{-4} cm/s)	1.611	(192)	-
Clinical plasma clearance, CL_p (L/hr)	60[d],66[e], (44,89), 144	(132, 133)	59.7[d]
Clinical volume of distribution, V_{ss} (L/kg)	(28, 30, 36)[d,f], 89[f]	(133)	51.7[g]

a: sertraline, b: sertraline HCl, c: average of rats & dogs BP, d: estimated from a model-based meta-analysis, e:estimated from IV data only, f: calculated by dividing estimated mean total volume by mean body weight, g: mean of literature values, h: the value provided the best fit of IV data and was determined by sensitivity analysis.

5.3.2 Clinical Pharmacokinetics Data

Literature IV infusion and oral sertraline pharmacokinetic data in healthy subjects were used for the PBPK model development and validation. The PBPK model was developed using the IV and single oral dose data that included 48 profiles (1 IV and 47 oral) from 22 PK studies. IV mean data were from a 100 mg dose infused over 12 hours and oral data were from doses ranging from 5 mg to 400 mg. The PBPK model was then validated against the steady-state oral data.

5.3.3 Pharmacokinetic Parameters Calculation and Accuracy Assessment

PK variables (AUC_∞, CL, C_{max}, T_{max}, $t_{1/2}$) of observed and simulated profiles were calculated by non-compartmental analysis in R using PKNCA package (version 0.8.1). The accuracy of predicted PK parameters was assessed by the fold error (FE) calculated as the ratio of the predicted to observed PK parameters. The goodness of fit was also assessed by the mean log fold error (MLFE) taken over all time points (n) and calculated as:

$$MLFE = 10^{\left(\frac{1}{n}\Sigma \log(FE)\right)} \quad (5\text{-}7)$$

When there are multiple observed concentrations at each sampling time point, a reduced χ^2 statistic was used to assess the agreement between the observed and simulated oral profiles and calculated as:

$$\chi^2 = \frac{1}{N} \sum_{i=1}^{N} \frac{(Predicted_i - Observed_i)^2}{Observed\ Variance_i} \quad (5-8)$$

where N is the number of observed concentrations. χ^2 value close to 1 is an indication of a good agreement.

5.3.4 PBPK Simulation

Two published decision trees were followed: the first one was for fitting of IV data and the second was to identify and modify processes affecting the oral profile guided by the mismatch pattern between the observed and simulated data to reproduce the observed curve (195, 203). The initial simulated IV profile in healthy subjects was sensitive to the physiological parameter inputs, predicted Kp values, and BP. Several models generate different physiological parameter values as they are differently scaled to different anthropometric properties (weight vs height) and demographic characteristics (age, gender) (227). For simplicity, physiological parameters solely predicted by body weight (table 1) were used for all simulation in this study. Kp values predicted by the 3 commonly-used *in silico* models only influenced the Kp scalar. Again, for consistency purposes, the values predicted by Rodgers et al. (220) were used in all oral simulation. Sertraline BP was unknown and sensitivity analysis was performed to identify the BP value associated with the best fit which was then fixed and used throughout. Lastly, CL and Kp scalars were adjusted to further improve the fit of IV data as judged by FE and MLFE.

Next, the oral profile under fasting condition of 100 mg dose for which we had the most data was simulated using the CL, V, and BP values from the best IV fit. The simulated AUC was greater than the observed indicating intestinal loss due to gut wall metabolism, P-glycoprotein efflux (P-gp), and chemical degradation. To account for the

intestinal loss, a first-order intestinal loss rate constants (K_{il}) were introduced into all compartments of the ACAT model. K_{il} value was adjusted until the simulated AUC matched the observed value. Despite the agreement of AUC, C_{max} and T_{max} were higher and shorter than the observed indicating drug-induced gastric emptying which was accounted for by decreasing the gastric emptying rate (GER). This modification made the simulated AUC lower than the observed suggesting saturable biliary elimination at the hepatic first passage which was addressed by lowering the CL_{int}. Optimized parameters from the 100 mg dose were used to simulated oral profiles for other doses. Higher K_{il} were needed for 5, 25 and 50 mg to reproduce the observed data and GER was changed for some dose levels to improve the fit of data.

5.3.5   Population PBPK Simulation

Weights of 1000 subjects were simulated from a truncated normal distribution (MEAN=69.33, SD=6.69) to match the observed mean weights of subjects from published PK studies. Using weights, physiological parameters were calculated to generate a virtual population of 1000 healthy individuals. To further account for biological between subject variability, CL was assumed to follow a log-normal distribution with 40% coefficient of variations (CV). In addition, the model included the observed variability in Kp values that was approximated by a log-normal distribution with a mean equal to the predicted value by Rodgers' model and SD = 0.471 (53% CV in a lognormal distribution) (121). After the inclusion of these variabilities, population simulation was performed for all doses of sertraline and the probability of unbound

steady-state concentrations in brain, liver and other tissues being greater of equal to the effective *in vitro* concentration was calculated for 50, 100, 200 and 400 mg doses.

5.4 REULTS

5.4.1 IV Fitting.

The shape of concentration-time profile was highly dependent on the BP ratio. The value of 2.925 guided by sensitivity analysis resulted in a good fit of the observed data irrespective of the model used to predict Kp values (**Figure 5-1A**). The fit was further improved by scaling of CL by1.15 that was also not influenced by the predicted Kp coefficients (**Figure 5-1B**). The Kp scalar was dependent on the prediction model used. The best fit was achieved when Kp scalar was 1, 4.7, and 4.75 for Rodgers & Rowland, Poulin & Theil, and Berezhkovskiy model, respectively (**Figure 5-1B-C**). The goodness of fit was comparable visually for the three Kp models. However, the lowest MLFE of all observed concentrations was achieved with the Kp values predicted by Berezhkovskiy's model (**Table 5-3**).
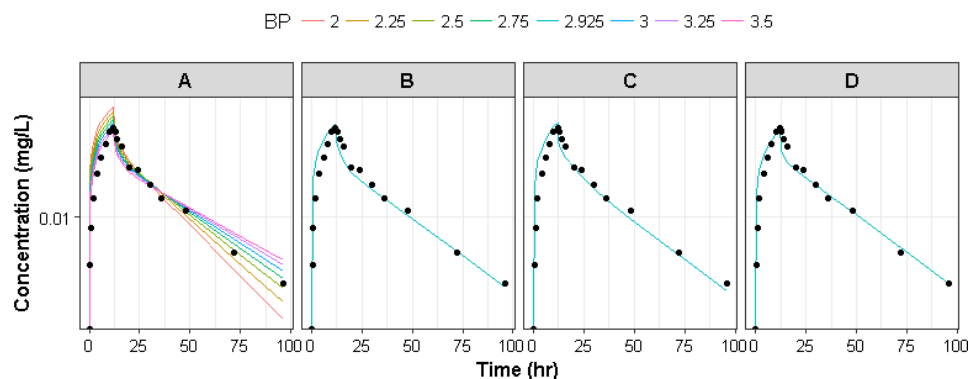
Figure 5-1: PBPK simulation of sertraline IV infusion. Line is simulated concentrations and black circles are observed data. (A) Sensitivity analysis showing the effect of BP on IV profile when Kp values predicted by Rodgers model. (B-D) Optimized simulation (BP =2.925 & CL scalar = 1.15) with Kp values predicted by Rodgers (Kp scalar =1), Poulin (Kp scalar =4.7), and Berezhkovskiy (Kp scalar =4.75) accordingly.

Table 5-3: Goodness of fit comparison using different distribution models

Variable	Observed	Fold Error		
	Values	Rodgers & Rowland*	Poulin & Theil*	Berezhkovskiy*
AUC_∞ (mg.hr/L)	1.53	1.00	1.00	1.00
C_{max} (mg/L)	0.053	1.08	1.10	0.98
$t_{1/2}$ (hr)	24.92	1.00	1.00	1.00
λ (1/hr)	0.028	1.00	1.00	1.00
MLFE	-	1.36	1.42	1.27

* To fit observed data well, BP was 2.925, CL scalar was 1.15, and Kp scalars were 1, 4.7 and 4.75 for Rodgers & Rowland, Poulin & Theil, Berezhkovskiy, respectively.

5.4.2 Oral Simulation.

Simulated from the best IV fit parameters, the oral profile of 100 mg appeared to have a higher AUC, higher C_{max}, and shorter time to reach C_{max} (T_{max}) than the observed data (**Figure 5-2A**). The addition of K_{il} (0.02421 /hr) matched the simulated AUC to the observed value, but it failed to correct C_{max} and T_{max} (**Figure 5-2B**). When compared to the simulated profile, the observed data seems to have lower rate of absorption causing absorption rate-limited elimination, a phenomenon commonly known as flip-flap kinetics and characterized by lower C_{max}, longer T_{max} and terminal $t_{1/2}$. This inconsistency between observed and simulated profiles is an indication of drug-induced impairment of gastric emptying. The reduction of GER by a scaling factor of 0.045 improved the fit significantly (**Figure 5-2C**) (228). Yet, the fit lowered the simulated AUC with significant under-prediction of terminal concentrations suggesting saturable elimination of hepatic first pass effect with oral dosing. The under-prediction was corrected by reducing CL scalar from 1.15 to 1.051 (**Figure 5-2D**).
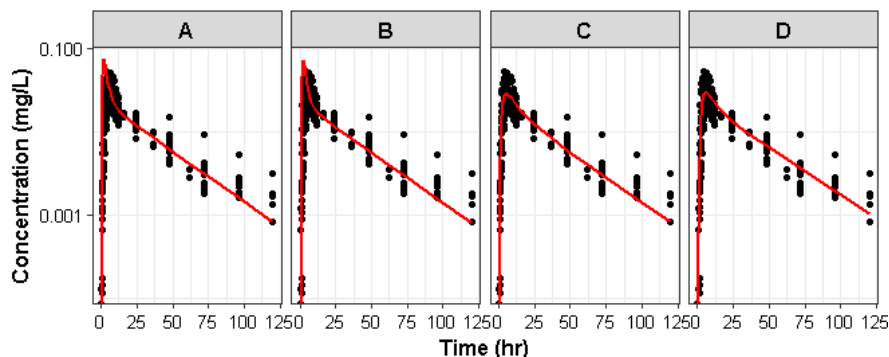
Figure 5-2: PBPK oral simulation of sertraline 100 mg. Line is simulated concentrations and black circles are observed data. (A) Simulated profile using optimized IV parameters. (B) Simulated profile including intestinal loss constant rate (K_{il} =0.02421 1/hr). (C) Simulated profile including intestinal loss and scaled GER by 0.045. (D) Simulated profile including intestinal loss, adjusted GER, and reduced CL scalar from 1.5 to 1.051 to account for saturable elimination at the first pass effect with oral dosing.

Using the best fit parameters of 100 mg oral data, simulated profiles of doses from 5 mg to 400 mg reasonably capture the observed data (**Figure 5-3A**). However, C_{max} and T_{max} were different than observed values for some doses with noticeable over-prediction for 50, 25 and 5 mg doses. The lower the dose was, the higher the over-prediction was. To improve the fit, GER was modified for each dose (**Figure 5-3B**) and the K_{il} was increased for 50, 25, and 5 mg until data were well captured (**Figure 5-3C**). The final parameters for each dose and the assessment of prediction accuracy are presented in **Table 5-4**. In addition, predicted F was close to the estimated values by our model-based meta-analysis (MBMA) performed earlier (**Figure 5-4**).
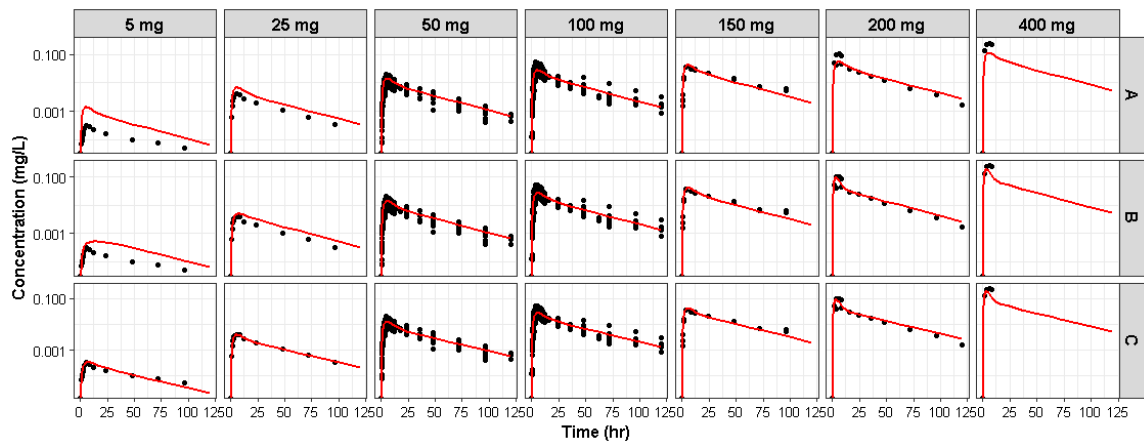
Figure 5-3: PBPK oral simulation of various doses of sertraline after single dose. Line is simulated concentration and black circles are observed data. (A) Simulated profiles using optimized parameters for 100 mg dose. (B) Simulated profiles with adjusted GER. (C) Simulated profiles with higher K_{il} for lower doses < 100 mg to account for the nonlinearity in bioavailability estimated from our earlier MBMA.

Table 5-4: PBPK parameters and prediction accuracy

Variable	5 mg	25 mg	50 mg	100 mg	150 mg	200 mg	400 mg
Adjusted Parameters							
CL scalar*	1.051	1.051	1.051	1.051	1.051	1.051	1.051
Kp scalar	1	1	1	1	1	1	1
GER factor	0.01	0.026	0.045	0.045	0.045	0.15	0.2
K_{li} (1/hr)	0.10	0.080	0.050	0.0242	0.0242	0.0242	0.0242
Fold Error							
AUC (mg.hr/L)	0.96	1	0.95	1.00	0.84	1.07	-
CL (L/hr)	1.04	1	1.06	1.00	1.19	0.94	-
C_{max} (mg/L)	1.1	1.05	1.00	1.07	1.17	1.00	0.86
T_{max} (hr)	1	1	1.00	0.83	1	0.67	0.67
$t_{1/2}$ (hr)	0.65	0.93	0.91		0.77	1.04	-
λ (1/hr)	1.55	1.07	1.10		1.30	0.96	-
Goodness of Fit							
MLFE	1.33	1.00	1.35	1.40	1.07	1.23	0.59
χ^2 statistic	-	-	1.35	1.42	-	-	-

* Reduced from 1.15 to 1.051 to account for the saturable hepatic first pass elimination
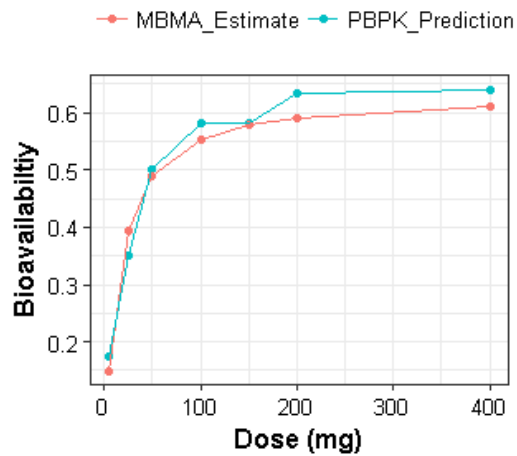
Figure 5-4: Sertraline oral bioavailability.

The simulation of steady-state profiles using the parameters optimized from single-dose data (Table 3) predicted observed data well for 100 and 200 mg while it under-predicted the concentrations for 50, 25 and 5 mg dose with various degrees (**Figure** 5-5) . Better predictions for lower doses were obtained when K_{il} was changed back to, the value of higher doses (**Figure** 5-5).
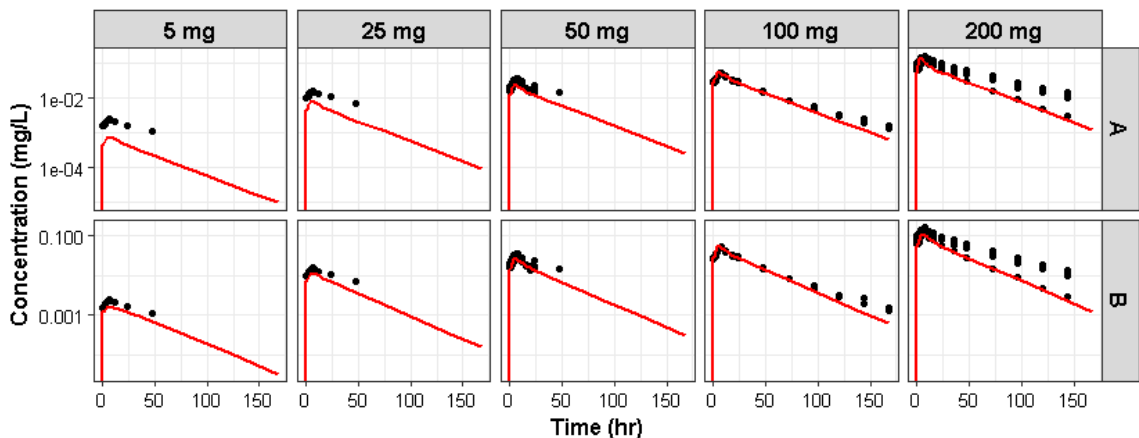
 Figure 5-5: PBPK oral simulation of various doses of sertraline at steady state. Line is simulated concentrations and black circles are observed data. (A) Simulated profiles using optimized parameters from single dose. (B) Simulated profiles excluding nonlinearity in bioavailability in which K_{il} was 0.02421 for all doses.

5.4.3   Probability Prediction of Therapeutic Concentrations.

The median and 95% prediction interval of population PBPK simulation for single and multiple doses captured the observed data well (**Figure 5-6**). Further, steady-state simulations showed the predicted median of sertraline unbound concentration was much higher in liver, kidney, heart, and lung, than in brain even though they are all highly perfused organs (**Figure 5-7**). Likewise, concentration was higher in bone, a less perfused organ, than in the brain. Time-concentration profiles of all organs were similar

to plasma, except the muscle profile. The concentration increased slowly and had considerably longer T_{max} (**Figure 5-7**). The calculated probability of unbound C_{max} concentration at steady state being greater than or equal to therapeutic concentrations of 0.25-0.5 mg/L and ≥ 1 mg/ L was $\leq 50\%$ and zero, respectively (**Figure 5-8**).
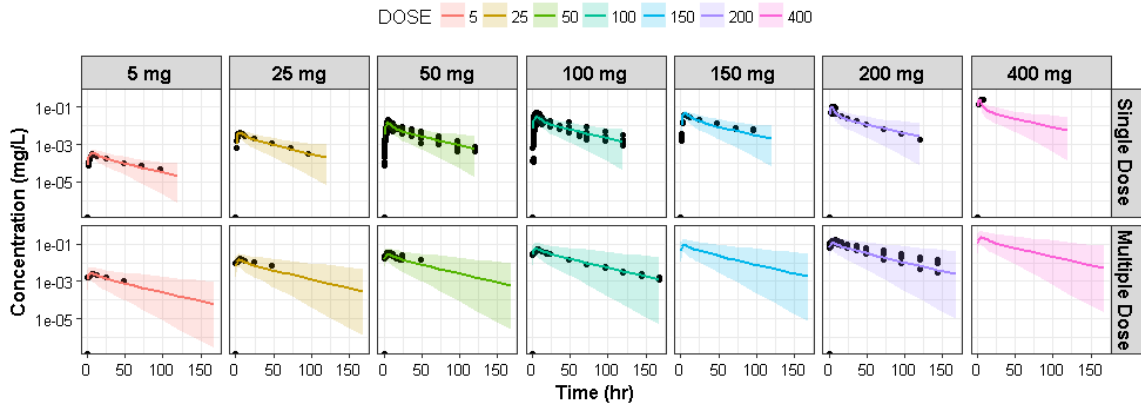
Figure 5-6: Median and 95% prediction interval of population simulation of sertraline.

Black circles are observed data.
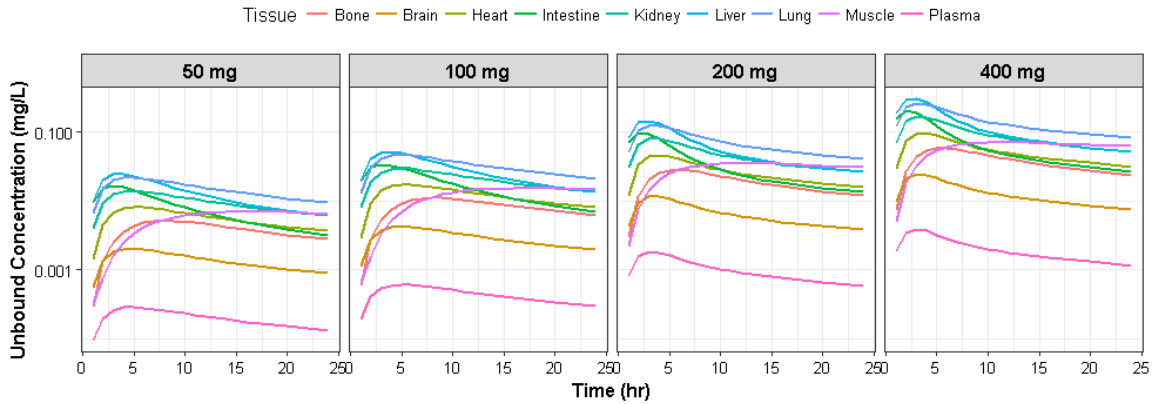
Figure 5-7: Predicted median of steady-state unbound concentrations of different sertraline doses in different tissues.
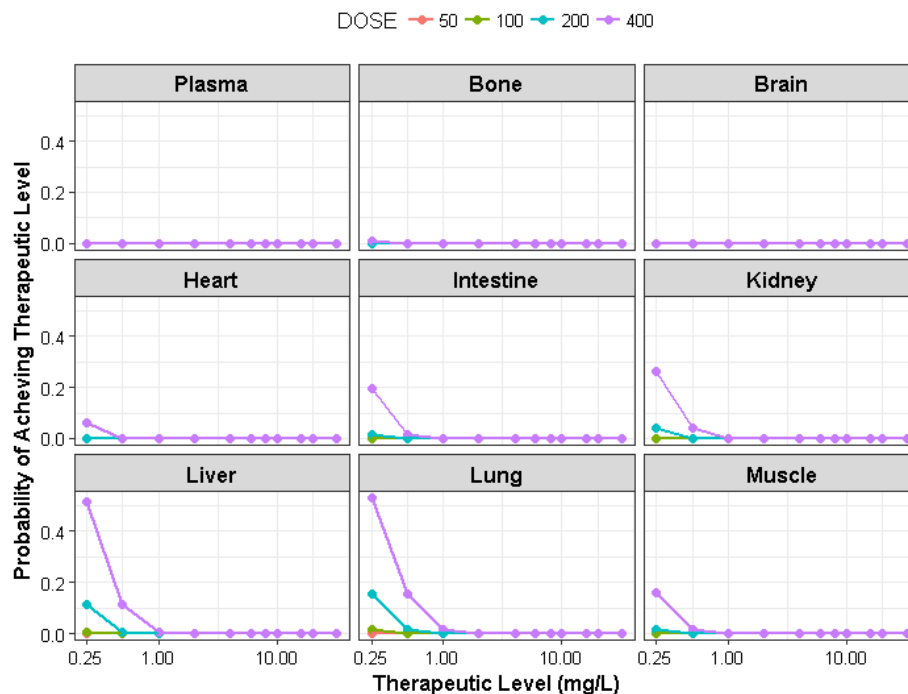
Figure 5-8: Probability of sertraline unbound C_{max} concentrations reaching therapeutic levels in different tissues

5.5 DISCUSSION

This study assessed the potential clinical use of sertraline as an anticancer and antimicrobial using PBPK modeling and simulation. Sertraline CL and V were first optimized from IV data by CL and Kp scalars. Then, the optimized parameters were used to understand mechanisms that affect the oral profile. Introduction of K_{il}, lowering GER, and saturable hepatic first pass effect were introduced into the PBPK model to reproduce observed data. K_{il} was dose-dependent after a single oral dose administration. It decreased with the increase amount of administrated dose and leveled at $\geq$ 100 mg. With repeated dosing, the dependency of K_{il} on dose was lost. Predicted unbound concentrations at steady state in different organs were unlikely to reach therapeutic

98

concentrations determined *in vitro*. The probability was estimated ≤ 50% and zero for therapeutic concentrations 0.25-0.50 and ≥ 1 mg/L.

The reported sertraline CL in rat, dog and human is close to and higher than Q_H (132, 133, 156, 229). Not only does this indicate sertraline is a high clearance drug, but also that it has higher affinity for blood cells than plasma. It is mathematically impossible for CL to exceed Q_H only if BP > 1 as shown in equation 5 – 1 (221). Sertraline BP in previous PBPK models was incorrectly assumed or calculated to be ≤ 1. This could possibly lead to over-prediction of blood CL and under-prediction of F. Informed by sensitivity analysis, we used 2.925 for BP. This value is in line with the values in rat (1.7) and dog (1.5) which all are > 1.

Of the three models, Kp values predicted by Rodgers seems to describe sertraline *in vivo* distribution well from its physicochemical properties since the Kp scalar was 1. On the other hand, Poulin and Berezhkovskiy models needed Kp scalars of 4.7 and 4.75 to correctly account for the observed distribution. This is probably because they fail to account for all specific protein binding in tissues. The $V_{ss,}$ calculated as the sum of scaled Kp times V_{org} for all organs plus the plasma volume, was comparable across all models and ranged from 29 to 33 L/kg. This estimate is in agreement with the reported value in animals (25 L/Kg) and our MBMA estimate in table 1. However, V_{ss} is much higher than the value (8.2 L/Kg) reported by a previous PBPK model (123, 131).

Despite having high CL exceeding Q_H, sertraline exhibits lower C_{max}, longer T_{max} and longer terminal $t_{1/2}$. This could not be accounted for by the large V only. It was likely due to the flip flop kinetics where sertraline elimination is limited by its absorption rate. Since is sertraline is a Biopharmaceutics Classification System (BCS) class 2 compound

characterized by high-permeability and low-solubility, its absorption was expected to be solubility-limited (192). However, neither solubility nor dissolution rate were found to significantly affect sertraline oral profile. Unlike Sutton who modulated P_{eff} to fit the individual data, we followed Peter's recommendation to reduce GER to capture the data because our calculated P_{eff} (1.90×10^{-4} cm/s) was close to the fitted value (1.61×10^{-4} cm/s) by Sutton (192) . When Sun's equation used, our P_{eff} (1.43×10^{-4} cm/s) was also similar to Sutton's value (230). This increased our confidence to modify GER rather than P_{eff}.

Sertraline F was nonlinearly dependent on dose after single dose administration. This is caused by the differential intestinal loss attributed to the sum effect of gut metabolism, P-gp efflux, precipitation, and chemical degradation. Sertraline is a known substrate and inhibitor of P-gp as well as a substrate for CYP enzymes (134, 194). Both P-gp and CYP enzymes are highly expressed in enterocytes of the gut (231, 232). The concerted action of minor P-gp efflux and major metabolism by CYP enzymes are the probable cause of sertraline nonlinear F. At lower doses ($\leq$ 25 mg), intestinal loss is large likely due to the P-gp efflux and CYP intestinal metabolism. At higher doses ($\geq$ 50 mg), higher luminal concentrations are achieved, that are greater than sertraline Michaelis-Menten constants (K_m) for N-demethtylation (98 μM) and N-deamination (114 μM). This would lead to saturation of P-gp and CYP enzymes and ultimately to small intestinal loss we observed (134, 233). Likewise, hepatic first pass effect seems to be saturated as a result of the high hepatic concentrations achieved with an oral administration (217). This is why we needed to reduce CL scalar of IV data from 1.51 to 1.05 in order to reproduce oral data. Accounting for nonlinear elimination as suggested by *in vitro* studies also improved F

predictions that match our MBMA results (Figure 4) (134). This also allowed us to

estimate F_{abs} to be 0.81 for 200 mg, instead of assuming it was 1. F_{abs} estimation was in

agreement with the value reported (0.77) by Sutton (131, 192) . With repeated dosing,

sertraline F was no longer dependent on dose. This could be that CYP saturation is

eventually achieved with the repeated dosing of low doses due to the accumulation of

sertraline in gut and liver tissues.

Our simulation indicates that unbound sertraline concentration at steady state was

unlikely to reach therapeutic levels in 9 different tissues including brain and liver. Yet,

clinical benefit of sertraline against cancer and *Cryptococcus* was shown (108, 204, 234,

235). We believe the observed effect is mediated through the stimulation of immune

system rather than directly killing the cancerous cells and *Cyprtococcus.* Sertraline is

shown to have dose-dependent immune-modulatory effect through altering plasma level

of serotonin that acts as a hormone, auto- paracrine, and intercellular signaling messenger

to control a wide range of critical physiological functions including mounting and

orchestrating immune responses (147).

In this study, we developed a sertraline PBPK model in healthy subjects that quantifies

intestinal loss, F_{abs}, and F. The model well-described single- and multiple-dose data from

wide range of doses (5-400 mg). Overall, the model-predictions were in agreement to

literature values. Based on our stimulation, therapeutic doses of sertraline do not produce

clinical concentrations required for anti-cancer and antimicrobial effects. Thus, it is

unlikely that the observed clinical effect is directly mediated by sertraline. Further

investigations are needed to shed light on the true mechanism of action by which

sertraline could possibly exert its anti-cancer and anti-microbial action. In addition, our

model can be used to predict sertraline concentration-time profile in any patient

population by simply updating the physiology-dependent parameters that represent the

population of interest.

6 AMIKACIN PHARMACOKINETIC-PHARMACODYNAMIC (PK-PD) ANALYSIS IN PEDIATRIC CANCER PATIENTS

6.1 SUMMARY

We performed PK-PD and simulation analyses to evaluate standard 15 mg/kg/day amikacin in children with cancer and to determine an optimal dosing strategy. A population pharmacokinetic model was developed from clinical data collected in 34 pediatric patients and used in a simulation study to predict the population probability of various dosing regimens to achieve accepted safety- ($fC_{min} < 10$ mg/L) and efficacy-linked (fC_{max}/MIC ratio ≥ 8) targets. In addition, an adaptive resistance PD (ARPD) model of amikacin against *Pseudomonas aeruginosa* was built based on literature time-kill curve data and linked to the PK model to perform PK-ARPD simulation and compare results with the probability approach. Using the probability approach, an amikacin dose of 60 mg/kg administered once daily is expected to achieve the target fC_{max}/MIC in 80% of pediatric patients weighing 8-70 kg with a 97.5% probability and almost all patients were predicted to have $fC_{min} < 10$ mg/L. However, PK-ARPD simulation predicted that 60 mg/kg/day is unlikely to suppress bacterial resistance with repeated dosing. Furthermore, PK-ARPD results suggested that amikacin 90 mg/kg given in two divided doses (45 mg/kg BID) are expected to hit safety and efficacy targets, and associated with a lower rate of bacterial resistance. The disagreement between the two methods is due to the inability of the probability approach in predicting development of drug resistance with repeated dosing. This originates from the use of PK-PD indices based on the MIC that neglects measurement errors, ignores the time-course dynamic nature of bacterial

growth and rate of killing, and incorrectly assumes the MIC to be constant during treatment.

6.2 INTRODUCTION

Bacterial resistance to currently available antibiotics is a growing health problem worldwide as it compromises the efficacy of modern antibiotic therapies and endangers millions of human lives (236). According to the U.S. Centers of Disease Control and Prevention (CDC), antibiotic-resistant bacteria infect 2 million people in the United States annually and directly cause 23,000 deaths every year (237). Appropriate dosing is a major determinant of successful drug therapy and, for anti-infective medications, sub-optimal dosing can lead to greater harm than just therapeutic failure. Considerable evidence from *in vitro* and *in vivo* work links antibiotics sub-optimal dosing to the emergence of bacterial resistance (42, 238). An inverted U-shaped function is found to describe the relationship between drug exposure and selection of resistant bacteria that initially rises and then declines with increasing exposure, until reaching a threshold that prevents amplification of resistant bacteria (238).

The optimization of antibiotic dosing could potentially prevent the emergence of resistance or at least delay it. To do so, an understanding of pharmacokinetic-pharmacodynamic (PK-PD) relationships of a drug against a bacterial pathogen is key (31). For example, the licensure of daptomycin, a lipopeptide antibiotic active against gram-positive bacteria, failed in the 1970s because of poor PK-PD understanding. In 2003, the same drug was approved by Food and Drug Administration (FDA) for clinical

104

uses after switching from fixed dose three-times-a-day to weight-based once-daily dosing (42).

Likewise, amikacin, an aminoglycoside antibiotic used either alone or in combination with β–lactams to treat serious gram-negative infections, was first approved at 15 mg/kg of body weight in 1-3 divided doses a day (29–31). Over time as amikacin PK-PD became better understood, dosing changed to larger once daily doses in order to maximize efficacy and limit toxicity (30, 239–241). Amikacin is an antibiotic that exhibits a concentration-dependent bactericidal activity and better clinical outcomes were associated with a high free, unbound plasma concentration to minimum inhibitory concentration ratio (fC_{max}/MIC). Because a bacterial population is not homogeneous but a mixture of distinct populations having their own MIC levels, a population MIC value named MIC_{90} and defined as the drug concentration that inhibits the growth of 90% of bacteria is used in the fC_{max}/MIC target. Generally, fC_{max}/MIC ratio of 8 to 10 has shown to result in at least a 90% therapeutic success rate and believed to suppress bacterial resistance (242–245). Similarly, amikacin safety was linked to the steady-state unbound trough plasma concentration (fC_{min}) being below 10 and ideally less than 5 mg/L (245). Nephrotoxicity is found to be lower with once daily administration since it limits repeated exposure of amikacin and provides longer interdose intervals that allow kidneys to excrete the drug. There is no doubt that dose optimization of antibiotics is of paramount importance and a promising approach to improve therapeutic outcomes, limit adverse events and combat bacterial resistance.

Two of several methods are widely used for the selection of optimal dosing: probability of target attainment (PTA) and PK-PD simulation. PTA was first proposed by

Drusano's team in which drug exposure in a virtual patient population of interest was simulated based on a population PK model developed from similar patients (94). The simulated time-course PK profiles were then used to compute a PK-PD index of interest (fC_{max}/MIC; $fAUC_{24}$/MIC: the area under unbound concentration-time curve over 24 hr to MIC ratio; and $\%fT_{>MIC}$: the cumulative percentage of the dosing interval that the unbound concentration is above MIC) and the PTA of achieving the selected PK-PD target within the population for a given dosing regimen. The acceptable PTA level is still debatable. PTA of 90% or higher is advocated as it is associated with higher probability to achieve desired clinical outcomes. PK-PD simulation is similar to the PTA except that time-concentration drug profile is linked to a dynamic PD model based on *in vitro* or *in vivo* time-curve kill data of a drug-bacterium combination of interest to select a dose that is likely to eradicate bacteria.

The aim of this study is to use a modeling and simulation approach to suggest an optimal dosing regimen of amikacin in pediatric cancer patients through the application of pharmacometric principles. A population pharmacokinetic model was developed from data collected in children with cancer and used in a simulation study to predict the PTA of various dosing regimens to achieve commonly accepted PK-PD targets for efficacy and safety of an fC_{max}/MIC $\geq$ 8 and fC_{min} < 10 mg/L, respectively. In addition, an adaptive resistance PD (ARPD) model of amikacin against *Pseudomonas aeruginosa* was built based on literature time-kill curve data and linked to the PK model to perform PK-ARPD simulation of the same dosing regimens explored in the PTA simulations and to suggest a regimen associated with maximum bacterial killing and minimum development of resistance.

6.3   MATERIALS AND METHODS

6.3.1   Patients.

This study included children with cancer and suspected or documented gram-negative bacterial infection admitted to the in-patient ward of National Cancer Institute (NCI), Cairo, Egypt during the period of June 2009 to December 2009. Patients were diagnosed with different types of malignancies broadly categorized into hematological and solid cancers that were treated with different chemotherapy protocols accordingly. All patients were treated empirically with amikacin 15 mg/kg once daily infused intravenously over 1 hr, which was the standard of care dose. Patient demographics and pertinent clinical characteristics were collected and recorded. The study was reviewed and approved by the Hospital Ethical Committee. Parental informed consent and child informed assent when appropriate were obtained prior to the study inclusion.

6.3.2   Sample Collection & Analytical Assay.

Two blood samples were drawn from a peripheral vein: one was taken at the end of infusion time (1 hr) while the second sample was drawn at least 2 hr following the first sample. Amikacin serum concentrations were measured by amikacin enzyme multiple immunoassay technique (Emit ® 2008), supplied by Syva company (CA, USA). The assay was linear from $0 - 50\ \mu g/mL$ with reported between-run and within-run coefficients of variation (CV) 3.9% and 5.8%, respectively. Two controls were assayed in every 24-hr period and amikacin serum concentrations were calculated automatically by the Emit 2008 analyzer (Syva Co, Dade Behring Inc., Cupertino, CA, USA).

6.3.3   Pharmacokinetic Analysis.

Amikacin concentrations from all patients were fitted simultaneously to one and two-compartment PK models with linear elimination using nonlinear mixed-effects regression analysis. An exponential random effect model and proportional error model were used to estimate between subject variability (BSV) and residual unexplained variability (RUV), respectively. To explain variability in model parameters, the effect of patient demographics and clinical characteristics were screened visually as potential covariates with particular concern on the effects of male vs female, hematological vs solid malignancies, afebrile vs febrile (defined as an oral temperature > 38.5 °C or non-oral, axillary or temporal, temperature > 38 °C on two separate readings at least 1 hr apart) (246), and normal albumin level vs hypoalbuminemia defined as a serum albumin < 3.5 g/dL. The statistical significance of a covariate was tested using the likelihood ratio test (χ^2, $\alpha = 0.01$, df $= 1$) in which a reduction in objective function value (OFV, a measure of goodness of fit similar to a sum of squares) of 6.63 or greater is observed after the inclusion of a covariate. The final PK model was selected based on the OFV, biological plausibility of parameter estimates and diagnostics plots. The parameter standard errors and uncertainty distributions were computed by sampling importance resampling (SIR) (90) and model performance was qualified using a prediction-corrected visual predictive check (pcVPC) (125).

6.3.4   PTA Calculation.

The Empirical Bayesian Estimates (EBEs) from the final PK model and amikacin protein binding were used to calculate fC_{max} and fC_{min} for a single dose. They

consequently were used to estimate the PTA of achieving the safety and efficacy targets of 15 mg/kg/day dosing in the study patients.

In addition, the population PK model was also used to estimate the population PTA to achieve $fC_{max}/MIC \geq 8$ and $fC_{min} < 10$ mg/L for different amikacin dosing regimens. Monte Carlo Simulation (MCS) was used to simulate 500 trials of 100 patients for each combination of amikacin weight-based total daily dose (15, 30, 60, and 90 mg/kg) and dosing interval (Q8h, Q12h and Q24h). Weights of pediatric patients were simulated from a truncated log-normal distribution (mean = 3.23, SD=0.55) to match the observed weights of patients in the study. To account for parameter uncertainty, BSV and the extent of correlation among the estimated values of model parameters, the full variance-covariance matrix obtained by SIR was incorporated into the MCS. Taking into consideration a fixed 10% protein binding of amikacin, the PTA (expressed as a %) of $fC_{max}/MIC \geq 8$ and $fC_{min} < 10$ mg/L for each trial was calculated for a range of assumed MIC values: 1, 2, 4, 8, 16, and 32 mg/L. For each of the 500 simulated trials for each dose and dosing interval combination, the median, 5th and 95th percentiles of PTAs were calculated.

6.3.5 *In Vitro* **Pharmacodynamic Analysis.**

A PubMed literature search was performed and identified time-kill curve studies of amikacin against *Pseudomonas aeruginosa* in which figures were digitized using WebPlotDigitizer (version 3.11) (247). The extracted bacterial counts, measured as colony-forming unit per mL of medium (CFU/mL), from static and dynamic studies were

fitted together to a bacterial dynamic growth model with adaptive resistance (equations 6 – 1:3) (42).

$$\frac{dN}{dt} = K_g \times \left(1 - \frac{N}{N_{max}}\right) \times N - DE \times N \quad (6-1)$$

$$DE = \frac{E_{max} \, C_p}{AD \times EC_{50} + C_p} \quad (6-2)$$

$$AD = 1 + \beta \left[1 - e^{(-\alpha.C_p.t)}\right] \quad (6-3)$$

Bacterial growth (eq.1) follows a logistic model in which N is total bacterial counts at time t; K_g is the first-order bacterial growth rate constant; N_{max} is the maximum bacterial count; and DE is the drug effect and it equals 0 when there is no drug. In the presence of amikacin (eq.2), DE was characterized by a maximal killing effect (E_{max}) and EC_{50} which is the unbound amikacin plasma concentration (C_p) needed to produce 50% of the E_{max}. C_p was simulated from a 1-comparment PK model with half-lives ($t_{1/2}$) and peak concentrations identical to what were reported in the *in vitro* studies. To allow for adaptive resistance to develop, EC_{50} was multiplied by an adaptation factor (AD) that causes EC_{50} to increase with time and C_p. The adaptation factor (eq. 6 – 3) is a fractional multiplier in which β represents the maximum fractional increase in EC_{50} when unbound concentration and time become large; and α is the adaptation rate constant that allows adaptation to transition from 1 when drug concentration is zero to (1 + β).

In this meta-analysis of literature data, random effect terms for inter-study variability (ISV), inter-arm variability (IAV) and $\log_{10}$–based additive RUV were included in the model. The ISV random effect was approximated in NONMEM using $Level and R matrix in the $COVARIANCE record. Below limit of detection observations were ignored in the modeling process. The criteria and methods used to

develop the PK model were used to select and assess the final PD model, except that VPC was not performed due to the sparse nature of extracted literature data.

6.3.6 PK-ARPD Simulations.

The literature-based *in vitro* ARPD model was linked to the final PK model to perform PK-ARPD simulation for the same dosing regimens explored in PTA simulation. A virtual pediatric patient population of 1000 subjects with different weights sampled from the same truncated log-normal distribution above was generated for each dose and dosing interval combination. In PK-ARPD simulation, parameter uncertainty and BSV were only included in the PK parameters while typical values were used for the PD model because of the unsuccessful covariance step.

6.3.7 Software.

All non-linear-mixed-effects modeling analyses were performed in NONMEM 7.3 (ICON Development Solutions, Ellicott City, MD) using ADVAN13 and the first-order conditional estimation method with interaction (FOCEI). Data manipulation and plotting were done in R (version 3.2.5). Perl-speaks-NONMEM (PsN) was utilized to perform the VPC and SIR analyses. MCS was performed with the R-based mrg*solve* package (version 0.7.1). The Pirana interface was used to maintain and compare NONMEM and PsN runs.

6.4   RESULTS

6.4.1   Pharmacokinetic Model.

The PK analysis included 34 Egyptian pediatric patients whose demographics and clinical characteristics of patients are summarized in **Table 6-1**. A total of 68 amikacin plasma concentrations (2 samples per subject) were collected for modeling. The data were best fit by a two-compartment PK model with first-order elimination and BSV on clearance (CL) and volume distribution of central compartment (V_1). All parameters were allometrically scaled to a 70-kg subject as follows:

$$CL = \theta_1 \times \left(\frac{Weight}{70}\right)^{0.75} \times e^{\eta_1} \quad (5-4)$$

$$Q = \theta_3 \times \left(\frac{Weight}{70}\right)^{0.75} \quad (5-5)$$

$$V_1 = \theta_2 \times \left(\frac{Weight}{70}\right) \times e^{\eta_2} \quad (5-6)$$

$$V_2 = \theta_4 \times \left(\frac{Weight}{70}\right) \quad (5-7)$$

Compared to a one-compartment, the two-compartment model was associated with better diagnostic plots and a reduction in OFV by 19.74 points. No other covariates were found to influence the PK parameters. The adequacy of the final model was supported by diagnostics plots and pcVPC (**Figure 6-1** & **Figure 6-2**). Parameter estimates of the final PK model and their SIR-based 95% confidence interval (CI) are presented in **Table** 6-2.

Table 6-1: Summary of patient demographic and clinical characteristics

Characteristic	N = 34
Age, n, median (range)	34, 9 (1 – 18) years
Sex, n (%)	
Male	14 (41)
Female	20 (59)
Weight, n, median (range)	34, (8 – 70) kg
Height, n, median (range)	34, 127.5 (75 – 169) cm
Body Surface area, median (range)	34, 0.94 (0.41 – 1.74) m^2
CrCL, n, median (range)*	34, 207.85 (58.06 – 418) mL/min
BUN, n, median (range)	31, 21 (7 – 93) mg/dL
Hemoglobin b, n, median (range)	34, 8.60 (6.23 – 11.70) mg/dL
Albumin, n, median (range)	19, 3.55 (2.00 – 4.30) g/L
ALT, n, median (range)	17, 22 (5 – 135) unit/L
AST, n, median (range)	17, 23 (9 – 176) unit/L
Bilirubin n, median (range)	33, 0.44 (0.15 – 1.50) mg/dL
Concomitant medication, n (%)	
Vancomycin	12 (35)
Amphotericin B	20 (50)
Fever, n (%)	6 (18)
Malignancy, n (%)	
Hematological	26 (76)
Solid	7 (21)

*CrCL is creatinine clearance and is calculated by Schwartz equation
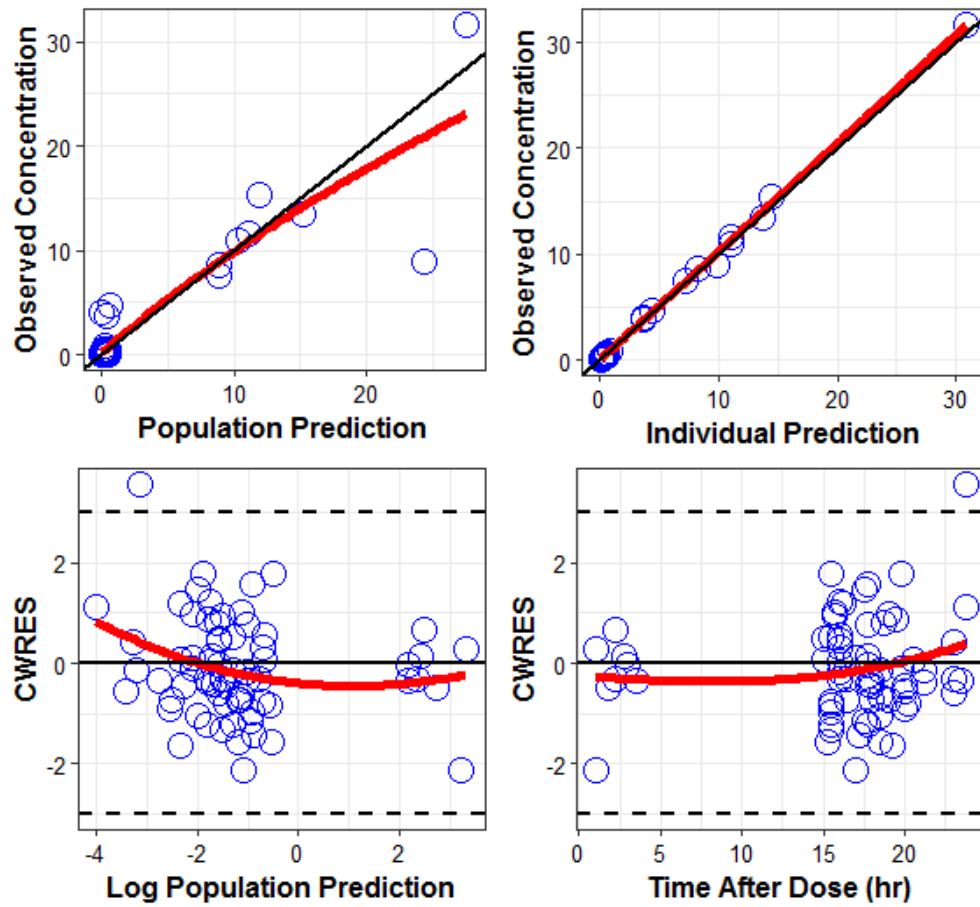
Figure 6-1: Diagnostic plots of the selected amikacin PK model. Red lines are Lowess

smoothers. CWRES is conditional weighted residuals.
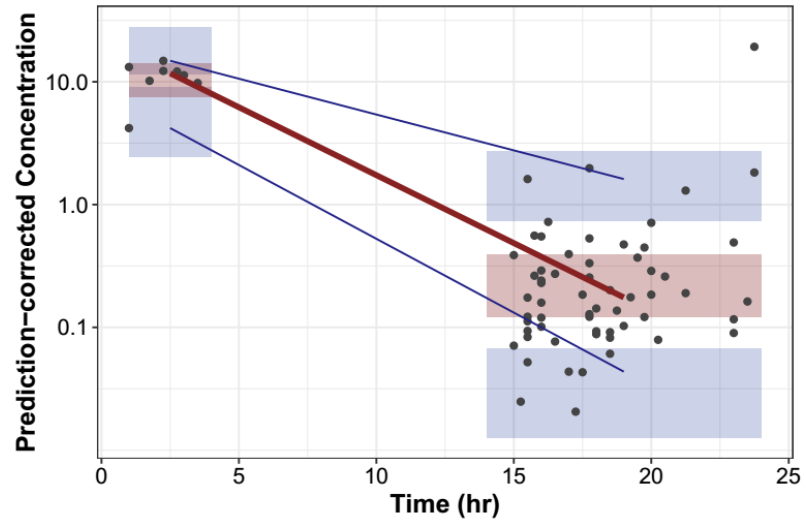
Figure 6-2: Prediction-corrected visual predictive checks of the selected amikacin PK model. Black solid circle represents the prediction-corrected concentrations, red and blue solid lines represents the median, 5th and 95th percentile, respectively. Shaded areas are the simulated 95% CI of each percentile.

Table 6-2: Parameter estimate of the selected amikacin PK model

Parameter (unit)	Definition	Estimate (RSE %)	SIR median (95% CI)
CL* (L/hr/70kg)	Clearance	11.1 (10)	11.1 (9.28 – 13.2)
V_1* (L/70kg)	Central volume of distribution	30.2 (21)	30.70 (16.3 – 43.0)
Q* (L/hr/70kg)	Inter-compartmental clearance	4.26 (42)	4.48 (2.52 – 8.81)
V_2* (L/70kg)	Peripheral volume of distribution	14.9 (13)	15.41 (12.37 – 19.80)
BSV CL (%CV)	Between subject variability in CL	33.0 (22)	33.6 (25.1 – 46.6)
BSV V_1 (%CV)	Between subject variability in V_1	63.1 (22)	67.7 (35.6– 106)
RE (%CV)	Proportional residual error	2.28 (28)	2.39 (1.37 – 4.83)

* Parameters are allometrically scaled to a 70-kg person

6.4.2 PTA.

The single dose median and range of fC_{max} and fC_{min} in Egyptian patients estimated by EBEs were 23.7 (8.69 – 27.7) mg/L and 0.044 (0.0075 – 2.70) mg/L, respectively. The fC_{max} was the estimated concentration at the end of infusion and fC_{min} was the estimated concentration at 24 hr from the start of infusion. The calculated PTA of $fC_{max}/MIC = 8$ was zero for MIC_{90} of 4 and 8 mg/L (248, 249). All patients had an estimated unbound trough concentration substantially below the target trough concentration of 10 mg/L.

The median and range of simulated weights were 25.5 (8 – 70) kg and they are similar to the observed values reported in **Table 6-1**. The predicted PTA was plotted against MIC values, color-coded by total daily dose, and stratified by dosing intervals (**Figure 6-3**). PTA of $fC_{max}/MIC \geq 8$ is higher for higher doses of amikacin for any given MIC level and dosing interval. A total daily dose of amikacin given in divided doses resulted in significantly lower PTA than when given once a day. The width of 95% CI around PTA increased with amikacin doses when given at the same frequency. The 95% CI was the widest for 90 mg/kg and the narrowest for 15 mg/kg when given once a day. On the contrary, the width of 95% CI increased as the frequency of dosing (number of doses per day) decreased. The 95% CI of PTA was wider for 90 mg/kg when administrated once rather than twice or thrice daily. The overall probability of fC_{min} being below 10 mg/L ranged from 95 to 100% for all simulated dosing regimens.
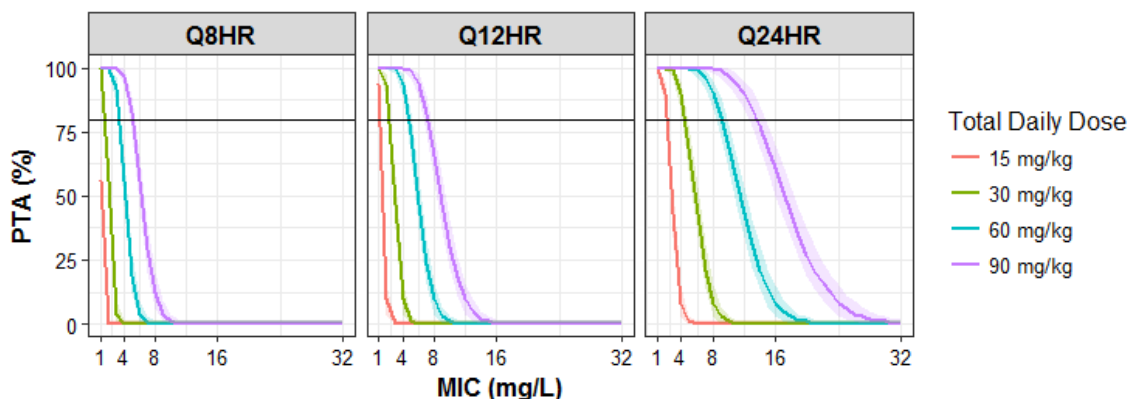
Figure 6-3: PTA of achieving $fC_{max}/MIC \geq 8$ versus MIC for amikacin dosing of 15, 30, 60 and 90 mg/kg when given in one (Q24HR) or divided doses (Q8HR or Q12HR). Each PTA line is the median of 500 Monte Carlo simulations of 100 patients with different weight randomly sampled from a truncated log-normal distributed to match the observed weights of patients included in the study. Shaded areas around each PTA line represent the 95% CI. Horizontal line indicates 80% PTA.

6.4.3 *In Vitro* Pharmacodynamic Model.

The PubMed search identified 10 studies in which in vitro time-kill curve data of amikacin against *Pseudomonas aeruginosa* were available. Eight studies were included in the development of the *in vitro* ARPD model after excluding 2 studies (31, 33, 250–255). One excluded study was an *in vivo* experiment and the other study had a design quite different from the others. One included study was static while the rest were dynamic experiments of single and multiple dosing up to 48 hr (**Table 6-3**).

Table 6-3: Summary of *in vitro* time-curve kill studies included in the final PD analysis

Study	Experiment	Strain	MIC	LOD	C_{max}	$T_{1/2}$	Ref
1	Static	27853	4	NR	0, 2, 8, 32 & 128	-	(254)
2[b,f]	Dynamic	27853/16690	2/2	2	0 & 80	2.1	(253)
3[c,f]	Dynamic	27853/27853R	2/2	2	0, 40, & 80	2.3	(252)
4[c]	Dynamic	27853	3.13	2	0, 80	2.35	(251)
5[a,b,f]	Dynamic	64/244	8/16	NR	24, & 72	2.2	(33)
6[a,c,d]	Dynamic	27853	8	1	0, 24, & 72	2	(250)
7[b]	Dynamic	27853	3.7	NR	10	2.4	(255)
8	Dynamic	99063	NR	NR	0	-	(31)

a: drug was infused over 1 hr instead of being bolused, b: single dose experiment over 24 hr, c: multiple dose experiment up to 48 hr, d: 1-compartment infection model used instead of 2-comparment model, f: studies included more than one stain of *Pseudomonas aeruginosa*. NR: not reported. The unit for MIC and C_{max} is mg/L, LOD is $\log_{10}$ CFU/mL and $T_{1/2}$ is hr.

Overall, there were 302 data points in which 21 observations (6.9%) were at or below the limit of detection (LOD). The final analysis included 281 data points after excluding the below LOD observations. The final ARPD model included additive ISV and IAV on N_o (initial bacterial count), exponential ISV on K_g and E_{max} and one additive RUV for static and dynamic experiments separately. Goodness of fit plots did not show any model deficiency (**Figure 6-5**). The parameter estimates of the ARPD model and their uncertainty distributions were successfully computed by SIR and are presented in **Table 6-4**.
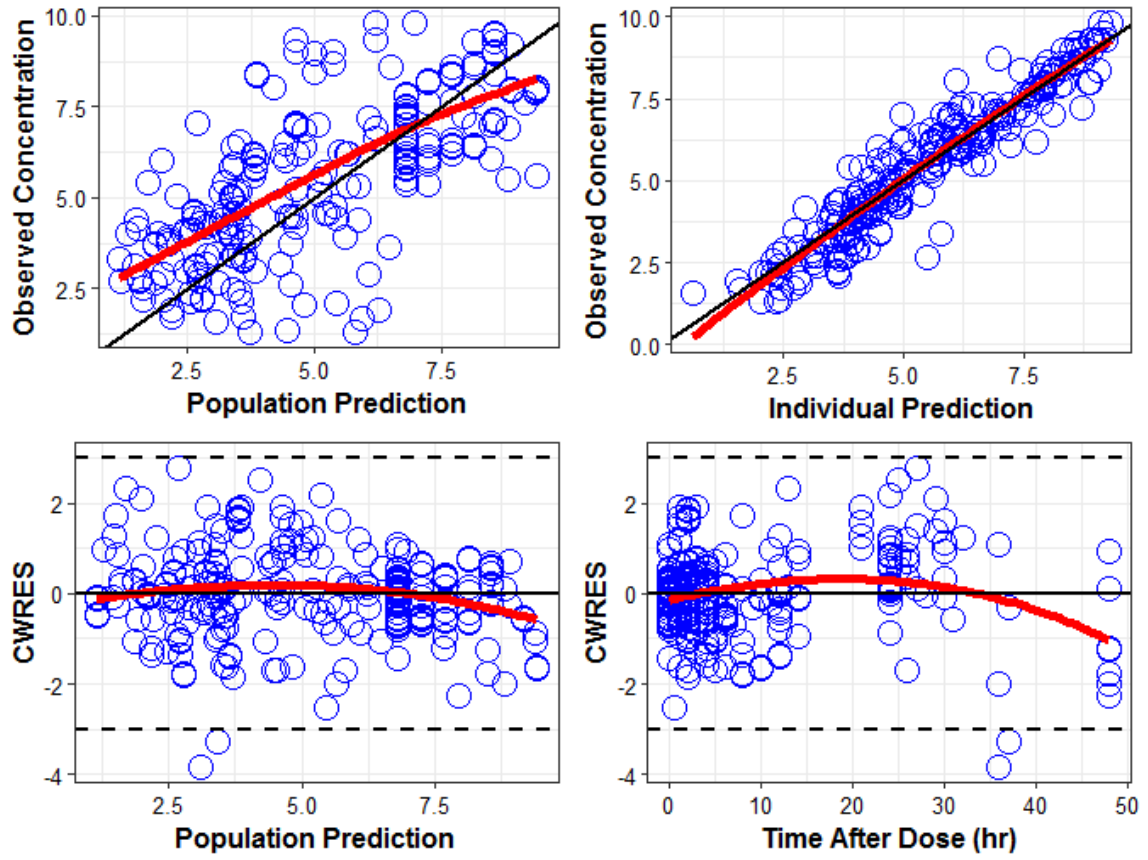
Figure 6-4: Diagnostics plots for the final ARPD model. Red line are Lowess smoothers.

CWRES is conditional weighted residuals.

Table 6-4: Parameter estimates for the final ARPD model

Parameter (unit)	Definition	Estimate	SIR median (95%CI)
N_0 $(10^{CFU/mL})$	Initial bacterial count	6.80	6.79 (6.45 – 7.10)
K_g (hr^{-1})	Bacterial growth rate constant	1.04	1.03 (0.89 – 1.13)
N_{max} $(10^{CFU/mL})$	Maximum bacterial count	9.41	9.61 (8.96 – 10.29)
E_{max} (hr^{-1})	Maximum killing rate constant	9.38	9.38 (7.36 – 11.91)
EC_{50} (mg/L)	Plasma drug concentration to achieve 50% maximum killing rate	3.49	3.46 (2.52 – 4.79)
α (L/mg.hr)	Rate of bacterial adaptation constant	0.0143	0.0143 (0.013 – 0.016)
β	Maximum bacterial adaptation	29.2	30.4 (23.8 – 38.3)
ISV N_0 (SD)	Inter-study variability in N_0	0.91	0.914 (0.769 – 1.02)
ISV K_g (%CV)	Inter-study variability in K_g	23	23.0 (21.7 – 24.8)
ISV E_{max} (%CV)	Inter-study variability in E_{max}	33.9	34.0 (31.8 – 36.2)
IAV N_0 (SD)	Inter-arm variability in N_0	0.14	0.14 (0.12 – 0.16)
RUV_{static}	Log_{10} residual error for static studies	0.859	0.85 (0.61 – 1.02)
$RUV_{dynamic}$	Log_{10} residual error for dynamic studies	0.570	0.58 (0.47 – 0.67)

6.4.4   PK-ARPD Simulations.

Amikacin unbound plasma concentration-time profiles, fC_{max}, and fC_{min} distributions were similar to those obtained in PTA simulations. In general, the probability of $fC_{min} < 10$ mg/L decreased with higher amikacin doses given more

frequently as shown in the top panels of **Figure 6-5** . Significant reduction of bacterial

counts occurred with the first dose of amikacin followed by bacterial regrowth. The

magnitude of initial bacterial reduction and time to regrowth were higher and longer with

higher doses of amikacin for a given dosing interval. This pattern is clearly evident with

the daily dosing as shown in the bottom right plot of **Figure 6-5**. Administering the same

amikacin amount in divided doses was also associated with lower initial bacterial

reduction. A reduction in bacterial killing with subsequent doses of the same amount was

also observed, indicating development of bacterial resistance. This is a documented

phenomenon for aminoglycoside antibiotics and it is well-captured by the current ARPD

model (42, 98). The loss of bacterial killing is the highest for 15 mg/kg dose and rate of

resistance was faster when the same daily dose was given more frequently in divided

doses. Predicted bacterial counts below LOD (2 $\log_{10}$ or 10^2 CFU/mL) was achieved by

90 mg/kg administered either at once or in divided doses. The 60 mg/kg also resulted in

bacterial count below LOD but only when administered daily and not in divided doses.

Lower doses (15 – 30 kg/mg) failed to drive bacterial count to the LOD level.
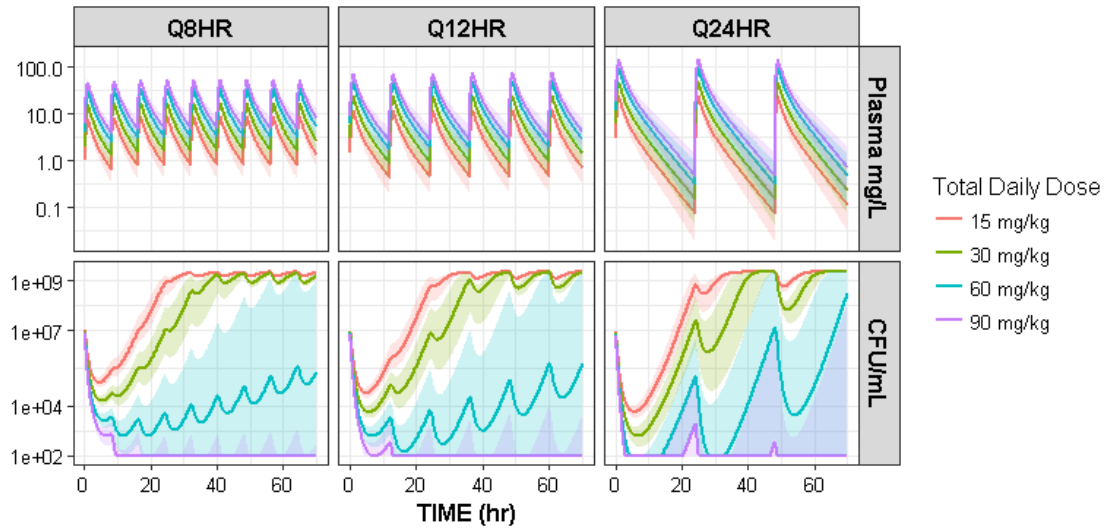
Figure 6-5: PK-ARPD simulations of 1000 patients for amikacin dosing of 15, 30, 60 and 90 mg/kg when given in one (Q24HR) or divided doses (Q8HR or Q12HR). Weights of patient were sampled from a truncated log-normal distributed to match the observed weights of patients in the study. Top panel is the predicted unbound amikacin plasma concentration time-profiles from the PK model after 1-hr infusion. Bottom panel shows bacterial time-kill curves predicted by the ARPD model given the predicted unbound amikacin plasma concentration time-profiles. Lines are the median and shaded areas are 95% CI.

6.5   DISCUSSION

The simulation results suggest that 15 mg/kg/day is a safe but suboptimal dose of amikacin in our pediatric cancer patients. Not a single patient in the study was calculated using the EBEs and percent of protein binding to achieve the $fC_{max}/MIC \geq 8$. The ramification of a low dose is not only limited to high probability of therapeutic failure in a patient, but also associated with significant collateral damage that affects our societies as a whole through the selection of drug-resistant bacteria (256). Our PTA simulation study suggests that once daily administration of larger amikacin doses are expected to be

associated with higher PTA and lower risk of toxicities overall. The rationale for once daily dosing is to maximize bactericidal effects driven by higher fC_{max}/MIC and prolong post-antibiotic effects, and to allow longer interdose intervals resulting in lower fC_{min}. Based on the PTA simulation, a minimum amikacin dose of 60 mg/kg administrated once daily is expected to achieve the target $fC_{max}/MIC \geq 8$ in 80% of pediatric patients weighing 8-70 kg with a 97.5% probability and the safety target < 10 mg/L in almost all patients.

This dosing recommendation is consistent with other studies that suggest higher single daily doses of amikacin ≥ 40 mg/kg in different patient populations including pediatric cancer patients (142, 164–166). In 1998, the amikacin dose of 20 mg/kg administered once a day was recommended for immuno-compromised pediatric patients including those with cancer (241). A recent study presented in the 2017 American Society for Clinical Pharmacology & Therapeutics (ASCPT) conference has suggested a high dose of 40 mg/kg for a 5-year old patient weighing 20 kg and having creatinine clearance (CrCL) of 120 mL/min per 1.73 m^2 of body surface area (35). The increase in recommended dose from 20 to 40 mg/kg daily is likely due to the documented increase in amikacin MIC_{90} from 4 to 8 mg/L against *Pseudomonas aeruginosa* over the past decades (249, 257). Craig has shown that the magnitude of PK-PD index does not change for resistant bacteria when one corrects for the increase in MIC (258). Higher doses are needed to produce higher exposure and reach the effective PK-PD target as a compensation of the increase in MIC. According to a recent study, the amikacin MIC_{90} is currently at 16 mg/L (259). The consistent increase in amikacin MIC_{90} over time is

caused at least partly if not entirely by the repeated exposure of suboptimal concentrations that selects for the pre-existing less-susceptible bacterial populations.

There are several possible explanations for the study findings. Our PK model was based on limited data (64 observations, 2 data points per subject) from Egyptian patients and did not find CrCL and age to be significant covariates as has been shown previously (35). Despite that, the estimated CL (4.33 L/hr), V_1 (8.63 L), Q (1.66 L/hr), V_2 (4.26 L) and $t_{1/2}$ (3 hr) for a typical patient of 20 kg are similar to reported literature values (35, 241, 260, 261). It is documented that oncology patients do have altered amikacin kinetics characterized by increased clearance and volume of distribution (261–264). This is attributed to the disease condition, severity, and drugs used for treatment. Yet, the kinetic changes are not uniform and they can be predicted by a single or combined variables, such as malignancy type, degree of neutropenia, disease state, total exposure or type of chemotherapy (264). This is in agreement with our results that did not find any influential clinical covariate. It is also important to note that the majority of our patients had hematological malignancy. With that, our results may not apply to children with different types of cancer. The generalization of study findings to other population is also limited due to the heterogeneity in renal functions.

Another justification for our results is that uncertainty of typical PK parameters, BSV, and variability of body weights were accounted for in the MCS when estimating the mean and 95% CI of PTA to achieve $fC_{max}/MIC \geq 8$ and $fC_{min} < 10$ mg/L. It is noted that higher uncertainty of and variability in PK parameters generally leads to higher uncertainty of PTA resulting in higher optimal dose prediction (95). However, this approach is strongly advised by Colin in the support of quality and proper clinical-

125

decision making for anti-infective optimal dosing (95). He stated that the lower boundary of PTA 95% CI can be conservatively used to select an appropriate dosing regimen for a given MIC where there is 97.5% probability that the unknown PTA exceeds a certain cut-off (e.g. 80% in our case) in a patient population. The high uncertainty in PK parameter estimates caused by the sparse nature of our data, high BSV, high level of confidence (95% vs 90%), and random selection of weight together can explain the higher predicted optimal dose of 60 instead of 40 mg/kg/day suggested by Liu (35).

Despite the merits of PTA with the parameter uncertainty approach, it lacks the ability to account for the adaptive resistance of bacteria upon exposure to amikacin (42, 98). The PTA approach is based on MIC that provides no information about the kinetics of drug effect and the persistent activity when drug concentrations are below the MIC since it is determined at single time point (265). This is a major limitation that can lead to incorrect dosing recommendation. PK-ARPD simulation shows that the 60 mg/kg/day dose suggested by PTA is unlikely to suppress bacterial resistance. Upon repeated dosing, bacterial resistance is expected to dominate over the killing effect that is initially predicted. This is demonstrated in figure 5; after the initial reduction, predicted median bacterial account at the end of every day increases in a linear fashion. The steepness of slope decreases as the dosing frequency increases suggesting slower rate of resistance. The predicted increase in bacterial count is driven by both the drop in amikacin concentration with time during dosing intervals and the loss of amikacin efficacy with repeated exposure. The PK-ARPD simulation also shows that safety and development of resistance goes hand in hand creating a double-sword situation. Large single doses are safer for patients with greater initial killing but they are likely to be selective for the

emergence of resistant bacterial population. When complete bacterial eradication (bacteriological cure) is not achieved, less susceptible bacterial sub-populations with increased MIC will grow and predominate as amikacin unbound concentration falls below the MIC threshold. A compromise between efficacy on one hand and acceptable safety and less chance of bacterial resistance on the other hand is achieved with twice-daily dosing where there is enough time between doses for kidneys to excrete amikacin while limiting the amount of time when drug concentration is below the MIC and maintaining an acceptable fC_{max}/MIC ratio.

PK-ARPD simulation predicted 90 mg/kg/day given in two divided doses are needed to sustain median bacterial counts below the LOD until the end of day 3. Predicted median bacterial counts remained below LOD until day 7 (data not shown), but we only presented the results up to day 3 since it is the time it takes to get an informative microbiological report back to adjust therapy accordingly. Taking safety into account, 90 mg/kg administered in two divided doses (45 mg/kg BID) is probably safer for empirical treatment than given in three divided doses (30 mg/kg TID) that is predicted to have fC_{min} > 10 mg/L. With twice a day dosing, fC_{min} is predicted to be < 10 mg/L and provides sufficient time for drug excretion before next dose to avoid drug accumulation. Furthermore, our stimulation shows that the probability of resistance is lower with twice daily dosing (45 mg/kg BID) than with a single dose (90 mg/kg QD).

PK-ARPD simulation also shows the administration of amikacin in divided doses is generally expected to facilitate bacterial resistance more than killing, unless the divided dose is high enough ($\geq$ 20 mg/kg TID or $\geq$ 40 mg/kg BID) (data not shown). The simulation results (Figure 5) also show that bacterial regrowth rate is the same

127

irrespective of dose and it peaks at the time of the next dose. This is consistent with amikacin affecting only growing bacteria while leaving less-drug susceptible bacteria in the stationary phase unaffected (266). This may explain the adaptive resistance seen with aminoglycosides despite their bactericidal effect. A limitation of our PK-ARPD simulation is that the *in vitro* ARPD model does not take into account for the role of immune system of the host. In the antimicrobial world, the observed effect *in vivo* is a combination of both drug effect and the host immune response. With that in mind, it is very possible that even lower doses than what our simulation suggested could be effective.

The disagreement in dose recommendation between PTA and PK-ARPD approach in our simulations highlights the inability of PTA in predicting development of drug resistance. Nielsen highlighted several limitations associated with the PTA approach in details which are beyond the scope of this manuscript (59). Importantly, she pointed out that PTA limitations originate from the use of MIC-based PK-PD indices as targets for safety and efficacy. All PK-PD indices rely on the MIC which is a threshold that neglects measurement errors and ignores the dynamic nature of bacterial growth and killing rate occurring over the incubation period. She also mentioned that MIC is incorrectly assumed to stay constant during the treatment period. In addition, the MIC-based PK-PD indices are surrogate end-points of the true clinical outcome to achieve the complete eradication of pathogenic bacteria, bacteriological cure.

With that, PK-PD modeling and simulation is preferred over MIC-based PTA. It is a better approach for amikacin to describe the time-course relationship among dose, concentration, bacterial killing and resistance that happen simultaneously. The PK-ARPD

models can also be used to predict the efficacy-linked PK-PD indices (267). However, although PK-PD modeling and simulation shows superiority over the MIC-based PTA approach, it remains underused in the development and improvement of antibiotic dosing regimens despite (59). When adapted, the PK-PD approach would result in more appropriate dosing of antibiotics which is likely to help in battling growing bacterial resistance.

In conclusion, oncology pediatric patients do have altered amikacin pharmacokinetics which probably necessitates higher doses to achieve the therapeutic target. Based on our simulation findings, daily mono-dose administration of 15 mg/kg may not be optimal in the study patients. In addition, a dose recommendation suggested by PTA is likely incorrect because it uses surrogate indices of clinical outcomes that are not sufficiently sensitive for determining optimal dosage regimens for total bacteriological cure. We find PK-PD modeling and simulation superior on theoretical basis because it provides deeper insight about the intricate time-course relationship among dosing regimens, plasma concentration and wanted as well as unwanted outcomes. Our PK-ARPD simulation suggests that 45 mg/kg BID is likely to achieve safety and efficacy targets, and is expected to be associated with lower rate of bacterial resistance. Study results can be used to justify a controlled clinical trial to evaluate suggested doses against currently doses used in clinical setting.

7   RECAPITULATION

This thesis demonstrated through examples the vital role pharmacometric modeling and simulation can play both in drug development and pharmacotherapy. Despite being in its infancy, pharmacometrics has emerged quickly as an indispensable tool to rationalize the drug development process and support decision making throughout the path from *in vitro* experiments, to laboratory animals, to human studies and to market. The implementation of the approach has increased the productivity and efficiency of drug development leading to higher success rates of late-stage trials, lower cost, and accelerated drug approval. Similarly, pharmacometrics can conserve the efficacy of currently available antimicrobial therapies and reduce the emergence of microbial resistance through dosing optimization. Unfortunately, the approach remains underutilized in pharmaceutical industry and is almost non-existent in investigator-led clinical research for multiple reasons that should no longer be hurdles for the implementation and full exploitation of pharmacometric-based analyses.

In Chapter 3, re-analysis of the ASTRO-CM pilot study using the pharmacometric-based approach was performed to describe the dose-exposure, exposure-response and response-outcome relationships of sertraline antifungal properties when combined with the standard induction CM therapy that consisted of amphotericin B and fluconazole. Sertraline kinetics was affected by patient body weight and the concomitant anti-retroviral therapy NNRTI, efavirenz and navirapine (**Table 3-2**). This was expected because of their known induction effect on drug-metabolizing P450 enzymes. The PK-PD index exploration showed that cAUC/MIC ≥ 10 mg/L was associated with 50% reduction in initial fungal count (**Figure 3-5**). However, this association was strictly visual and did

not account for correlations of data within a subject. The addition of sertraline increased the rate of fungal clearance from CSF by 41% compared to the COAT study in which patients received the CM standard therapy without sertraline. The effect of sertraline was dose and exposure-independent with a similar increase in the CSF fungal clearance observed across study arms (**Table 3-3**). Despite a more rapid fungal clearance from the CSF, short-term survival did not seem to be improved. An exploratory survival analysis did not show any benefit of adjunctive sertraline; rather, a higher 2-week mortality rate was observed in 100 mg and 400 mg sertraline arms compared to the other arms (no sertraline and 200-300 mg sertraline daily) and among female patients (**Table 3-4**).

Our findings contradicted the evidence from *in vitro* and *in vivo* animal studies that suggested dose-dependent antifungal effect of sertraline. The lack of dose-effect could be due to the insufficient number of patients and low statistical power. Under the assumption that sertraline has dose-dependent activity, the dose-response curve was explored while accounting for serial correlation in the data. Findings indicated that studied sertraline doses (100 – 400 mg) were at the lower range of dose-response curve and 2000 mg daily dose would be required to achieve 50% reduction in CSF fungal burden (**Figure 3-11**). Together with the fact that sertraline has immunomodulatory action, results suggested the observed clinical effect might be mediated through the stimulation of immune responses and not through the direct effect on the fungus. This hypothesis is highly plausible and is further supported by the fact that predicted unbound sertraline concentrations are unlikely to reach therapeutic levels needed for antifungal activities. Future studies are essential to test this hypothesis, to shed some light on the

possible underlying mechanisms of sertraline observed clinical benefit, and to whether or not sertraline affects the immune system.

In addition, the antifungal activity of sertraline main metabolite, N-desmethysertrlaine, is unknown and can be determined to assess its potential contribution to the observed effect. More *in vitro* and *in vivo* animal experiments are critical to discern sertraline true mechanism of action, mode of killing (time- vs concentration-dependent), and efficacy-predicting PK-PD index that can help strategize the dosing regimen. From such studies, much can be learned and doses can be rationally selected for testing in clinical studies to maximize the success rate and the amount of knowledge gained. Time-kill curve experiments, routinely performed studies, are far more powerful in exploring the dynamic microbial growth and rate of killing by drug over a wide range of antimicrobial concentrations. This can be intimidating to perform due to the slow-growing nature of *Cryptococcus*, but a similar experiment has been successfully done and guided fluconazole optimal dosing.

The sparse nature of ASTRO-CM pharmacokinetic data precluded fitting a more complex model to explore the underlying causes of sertraline nonlinear exposure in patients. Therefore, an MBMA of published sertraline pharmacokinetic studies was performed to fully characterize sertraline kinetics in healthy subjects (Chapter 4). After single dose administration, bioavailability was found to increase nonlinearly with dose (**Figure 4-2**). Additionally, repeated dosing of sertraline resulted in greater tissue distribution evident by the increase in peripheral distribution (V_3) (**Table 4-2**).

Furthermore, a PBPK model for sertraline was developed and validated against literature data and used to provide insight regarding the potential clinical uses of

sertraline as an anticancer and antimicrobial therapy. Simulation of oral dosing indicated that steady-state C_{max} unbound concentrations of sertraline in different target tissues do not reach the levels required for antitumor and antimicrobial activities (**Figure 5-8**). This is in total agreement with our previous prediction (Chapter 3) and published studies that undermine sertraline antifungal use for the same reason. The PBPK model also supported dose-dependent bioavailability after single dose administration that was suggested by our MBMA (**Figure 5-4**). Saturable hepatic elimination after oral administration was first predicted by *in vitro* studies and now captured by the PBPK model (**Figure 5-2**).

Putting the pieces together, there is little evidence of additional clinical benefits (higher efficacy) for sertraline doses above 200 mg a day. It is the maximum FDA-approved dose and doses above that if they do not come with greater risk of adverse events, will at least be of un-necessary cost to health care systems and patients. This was supported by multiple analyses we conducted and our findings are consistent with previous publications. Thus, the lowest possible efficacious dose should be considered as it is the best choice for the aforementioned safety and economic reasons. Meanwhile, resources should be directed toward more *in vitro* work to allow for the full characterization of the exposure-response relationships of sertraline antifungal action and elucidation of the mechanism by which it exerts its action.

Lastly in chapter 6, the PTA and PK-PD simulation approach were implemented to propose an optimal amikacin dose against *Pseudomonas aeruginosa* infections in children with cancer. Our simulation shows that the approved dose of 15 mg/Kg in 1-3 divided doses a day is sub-optimal and may be the reason behind the increasing MICs during the past several decades. The MIC-based PTA method indicated at least 60 mg/kg

once daily is needed to achieve the efficacy target (fC_{max}/MIC $\geq$ 8 mg/L) in 80% of pediatric cancer patients (**Figure 6-3**). However, this approach wrongly assumes that MIC remains constant over time and, thus, it fails to account for the adaptive bacterial resistance that develops upon exposure. This phenomenon was well captured by the PK-PD modeling and simulation approach that suggested 45 mg/Kg twice daily instead (**Figure 6-5**). Higher and less frequent dosing was associated with higher initial killing of susceptible bacteria and faster domination of resistant-bacterial populations maybe because they provide sufficient time for bacteria to replicate after drug concentration drops below MIC and before the next dose is due. Therefore, twice daily dosing (45 mg/kg BID) was predicted to be better than once daily (90 mg QD) in suppressing the emergence of bacterial resistance without compromising safety associated with frequent dosing. However, this proposed dosing regimen is a simulation-based recommendation that needs clinical testing before it can be adapted in clinical practice.

8   REERENCES

1.   Paul SM, Mytelka DS, Dunwiddie CT, Persinger CC, Munos BH, Lindborg SR, Schacht AL. 2010. How to improve R&D productivity: the pharmaceutical industry's grand challenge. Nat Rev Drug Discov 9:203.

2.   Collins FS. 2011. Reengineering translational science: the time is right. Sci Transl Med 3:90cm17.

3.   Dimasi JA, Grabowski HG, Hansen RW. 2016. Innovation in the pharmaceutical industry: New estimates of R&D costs. J Health Econ 47:20–33.

4.   Laura P, Piddock J V, Piddock LJ V. 2012. The crisis of no new antibiotics—what is the way forward? Lancet Infect Dis 12:249–53.

5.   World Health Organization. 2014. Antimicrobial resistance global report on surveillance.

6.   O'Neill J. 2014. Antimicrobial Resistance : Tackling a crisis for the health and wealth of nations. Rev Antimicrob Resist 1–16.

7.   Dall C. 2017. Pan-resistant CRE reported in Nevada. Cent Infect Dis Res Policy, Univ Minnesota,.

8.   Kaitin KI, DiMasi JA. 2011. Pharmaceutical Innovation in the 21st Century: New Drug Approvals in the First Decade, 2000–2009. Clin Pharmacol Ther 89.

9.   Kinch MS, Patridge E, Plummer M, Hoyer D. 2014. An analysis of FDA-approved drugs for infectious disease: antibacterial agents. Drug Discov Today 19:1283–1287.

10.   Silver LL. 2011. Challenges of antibacterial discovery. Clin Microbiol Rev 24:71–109.

11.   Asín-Prieto E, Rodríguez-Gasc On A, Isla A. 2015. Applications of the pharmacokinetic/pharmacodynamic (PK/PD) analysis of antimicrobial agents.

12.   Flego M, Ascione A, Cianfriglia M, Vella S. 2013. Clinical development of monoclonal antibody-based drugs in HIV and HCV diseases. BMC Med 11:4.

13.   HTB. 2017. HIV pipeline 2017htb supplement.

14.   Koszalka P, Tilmanis D, Aeron |, Hurt C, Aeron CA. 2017. Influenza antivirals currently in late-phase clinical trial. Influ Other Respi Viruses 11:240–246.

15.   The Pew Charitable Trusts. 2017. Antibiotics Currently in Clinical Development.

16.   Pianalto K, Alspaugh J. 2016. New Horizons in Antifungal Therapy. J Fungi 2:26.

17. Dall C. 2017. Antifungal development gets new attention. Cent Infect Dis Res Policy, Univ Minnesota.

18. Hope W, Drusano GL, Rex JH. 2016. Pharmacodynamics for antifungal drug development: an approach for acceleration, risk minimization and demonstration of causality. J Antimicrob Chemother 71:3008–3019.

19. Lalonde R, Kowalski K, Hutmacher M, Ewy W, Nichols D, Milligan P, Corrigan B, Lockwood P, Marshall S, Benincosa L, Tensfeldt T, Parivar K, Amantea M, Glue P, Koide H, Miller R. 2007. Model-based Drug Development. Clin Pharmacol Ther 82:21–32.

20. Kimko H, Pinheiro J. 2014. Model-based clinical drug development in the past, present and future: a commentary. Br J Clin Pharmacol 79:108–16.

21. Peck CC, Rubin DB, Sheiner LB. 2003. Hypothesis: A single clinical trial plus causal evidence of effectiveness is sufficient for drug approval. Clin Pharmacol Ther 73:481–490.

22. Walsh TJ, Goodman JL, Pappas P, Bekersky I, Buell DN, Roden M, Barrett J, Anaissie EJ. 2001. Safety, tolerance, and pharmacokinetics of high-dose liposomal amphotericin B (AmBisome) in patients infected with Aspergillus species and other filamentous fungi: maximum tolerated dose study. Antimicrob Agents Chemother 45:3487–96.

23. Ellis M, Spence D, de Pauw B, Meunier F, Marinus A, Collette L, Sylvester R, Meis J, Boogaerts M, Selleslag D, Krcmery V, von Sinner W, MacDonald P, Doyen C, Vandercam B. 1998. An EORTC international multicenter randomized trial (EORTC number 19923) comparing two dosages of liposomal amphotericin B for treatment of invasive aspergillosis. Clin Infect Dis 27:1406–12.

24. Cornely OA, Maertens J, Bresnik M, Ebrahimi R, Ullmann AJ, Bouza E, Heussel CP, Lortholary O, Rieger C, Boehme A, Aoun M, Horst H-A, Thiebaut A, Ruhnke M, Reichert D, Vianelli N, Krause SW, Olavarria E, Herbrecht R. Liposomal Amphotericin B as Initial Therapy for Invasive Mold Infection: A Randomized Trial Comparing a High–Loading Dose Regimen with Standard Dosing (AmBiLoad Trial).

25. Al-Nakeeb Z, Petraitis V, Goodwin J, Petraitiene R, Walsh TJ, Hope WW. 2015. Pharmacodynamics of amphotericin B deoxycholate, amphotericin B lipid complex, and liposomal amphotericin B against Aspergillus fumigatus. Antimicrob Agents Chemother 59:2735–45.

26. Viele K, Connor JT. 2015. Dose-Finding Trials. JAMA 314:2294.

27. Ventola CL. 2015. The antibiotic resistance crisis: part 1: causes and threats. P T 40:277–83.

28. Connors KP, Kuti JL, Nicolau DP, Connors KP, Nicolau DP, Kuti JL, Nicolau DP. 2013. Optimizing Antibotic Pharmcodynamics for Clinical Practice. Pharm Anal Acta 4.

29. Teva Parenteral Medicines I. Amikacin sulfate package insert.

30. White BP, Lomaestro B, Pai MP. 2015. Optimizing the initial amikacin dosage in adults. Antimicrob Agents Chemother 59:7094–7096.

31. Burgess DS. 2005. Use of pharmacokinetics and pharmacodynamics to optimize antimicrobial treatment of Pseudomonas aeruginosa infections. Clin Infect Dis 40 Suppl 2:S99-104.

32. Taccone FS, Laterre P-F, Spapen H, Dugernier T, Delattre I, Layeux B, De Backer D, Wittebole X, Wallemacq P, Vincent J-L, Jacobs F. 2010. Revisiting the loading dose of amikacin for patients with severe sepsis and septic shock. Crit Care 14:R53.

33. Dudley MN, Zinner SH. 1991. Single daily dosing of amikacin in an in-vitro model. J Antimicrob Chemother 27 Suppl C:15–9.

34. Burdet C, Pajot O, Couffignal C, Armand-Lefèvre L, Foucrier A, Laouénan C, Wolff M, Massias L, Mentré F. 2015. Population pharmacokinetics of single-dose amikacin in critically ill patients with suspected ventilator-associated pneumonia. Eur J Clin Pharmacol 71:75–83.

35. Liu X, Smits A, Wang Y, Wead S, Kagan R, Healy3 D, Cock P De, Allegaert K, Sherwin C. 2017. Dosing optimization of amikacin in pediatric patients with burn injuries and those with oncology conditions. The American Society for Clinical Pharmacology and Therapeutics (ASCPT) Annual Meeting, Washington DC, March 15-18.

36. Tufs center for the study of drug development. 2013. Causes of clinical failures vary widely by therapeutic class, phase of study.

37. Toutain PL, Del Castillo JRE, Bousquet-Melou A. 2002. The pharmacokinetic – pharmacodynamic approach to a rational dosage regimen for antibiotics. Res Vet Sci 5288:105–114.

38. McCormack JP, Allan GM, Virani AS. 2011. Is bigger better? An argument for very low starting doses. CMAJ 183:65–9.

39. Cross Ms J, Lee H, Westelinck Pharmd A, Mba JN, Grudzinskas C, Peck C. 2002. Postmarketing drug dosage changes of 499 FDA-approved new molecular entities, 1980–1999. Pharmacoepidemiol Drug Saf 11:439–446.

40. Toutain P-L. 2002. Pharmacokinetic/pharmacodynamic integration in drug development and dosage-regimen optimization for veterinary medicine. AAPS

PharmSci 4:E38.

41. Ambrose PG. 2017. Antibacterial drug development program successes and failures: a pharmacometric explanation The superiority quest. Curr Opin Pharmacol 36:1–7.

42. Tam VH, Ledesma KR, Vo G, Kabbara S, Lim TP, Nikolaou M. 2008. Pharmacodynamic modeling of aminoglycosides against Pseudomonas aeruginosa and Acinetobacter baumannii: Identifying dosing regimens to suppress resistance development. Antimicrob Agents Chemother 52:3987–3993.

43. Davies G, Hope W, Khoo S. 2013. Opinion: The Pharmacometrics of Infectious Disease. Pharmacometrics Syst Pharmacol.

44. Williams PJ, Ette EI. Pharmacometrics: Impacting Drug Development and Pharmacotherapy, p. 1–21. *In* Pharmacometrics. John Wiley & Sons, Inc., Hoboken, NJ, USA.

45. Cole ST. 2014. Who will develop new antibacterial agents? Philos Trans R Soc Lond B Biol Sci 369:20130430.

46. Ambrose PG, Hammel JP, Bhavnani SM, Rubino CM, Ellis-Grosse EJ, Drusano GL. 2012. Frequentist and Bayesian Pharmacometric-Based Approaches To Facilitate Critically Needed New Antibiotic Development: Overcoming Lies, Damn Lies, and Statistics. Antimicrob Agents Chemother 56:1466–1470.

47. Corey GR, Kollef MH, Shorr AF, Rubinstein E, Stryjewski ME, Hopkins A, Barriere SL. 2014. Telavancin for hospital-acquired pneumonia: clinical response and 28-day survival. Antimicrob Agents Chemother 58:2030–7.

48. Ledford H. 2012. FDA under pressure to relax drug rules. Nature 492:19–19.

49. Food and Drug Administration. 2004. Challenge and Opportunity on the Critical Path to New Medical Products.

50. Miller R, Ewy W, Corrigan BW, Ouellet D, Hermann D, Kowalski KG, Lockwood P, Koup JR, Donevan S, El-Kattan A, Li CS, Werth JL, Feltner DE, Lalonde RL. 2005. How Modeling and Simulation Have Enhanced Decision Making in New Drug Development. J Pharmacokinet Pharmacodyn 32.

51. Mid E, Marshall S, Burghaus R, Cosson V, Cheung S, Chenel M, DellaPasqua O, Frey N, Hamr en B, Harnisch L, Ivanow F, Kerbusch T, Lippert J, Milligan P, Rohou S. 2016. Good Practices in Model-Informed Drug Discovery and Development: Practice, Application, and Documentation. CPT Pharmacometrics Syst Pharmacol 5:93–122.

52. Sheiner LB, Fnzncisco S. 1997. Learning versus confirming in clinical drug development 61.

53. Ventola CL. 2015. The antibiotic resistance crisis: part 2: management strategies and new agents. P T 40:344–52.

54. Woodcock J. 2014. Three encouraging steps towards new antibotics. Food Drug Adm.

55. Asín-Prieto E, Rodríguez-Gasc On A, Isla A. 2015. Applications of the pharmacokinetic/pharmacodynamic (PK/PD) analysis of antimicrobial agents. J Infect Chemother 21:319–329.

56. Milligan P, Brown M, Marchant B, Martin S, van der Graaf P, Benson N, Nucci G, Nichols D, Boyd R, Mandema J, Krishnaswami S, Zwillich S, Gruben D, Anziano R, Stock T, Lalonde R. 2013. Model-Based Drug Development: A Rational Approach to Efficiently Accelerate Drug Development. Clin Pharmacol Ther 93:2013.

57. Lepak AJ, Andes DR. 2014. Antifungal Pharmacokinetics and Pharmacodynamics. Cold Spring Harb Perspect Med 5:a019653–a019653.

58. van der Graaf P. 2012. CPT: Pharmacometrics and Systems Pharmacology. Cit CPT Pharmacometrics Syst Pharmacol 8.

59. Nielsen EI, Friberg LE. 2013. Pharmacokinetic-pharmacodynamic modeling of antibacterial drugs. Pharmacol Rev 65:1053–90.

60. Tylutki Z, Polak S, Wiśniowska B. 2016. Top-down, Bottom-up and Middle-out Strategies for Drug Cardiac Safety Assessment via Modeling and Simulations. Curr Pharmacol reports 2:171–177.

61. McKinnon PS, Dvais SL. 2004. Pharmacokinetic and Pharmacodynamic Issues in the Treatment of Bacterial Infectious Diseases. Eur J Clin Microbiol Infect Dis 23:271–288.

62. Hyatt JM, McKinnon PS, Zimmer GS, Schentag JJ. 1995. The Importance of Pharmacokinetic/Pharmacodynamic Surrogate Markers to Outcome. Clin Pharmacokinet 28:143–160.

63. Schentag JJ. 1999. Antimicrobial Action and Pharmacokinetics/Pharmacodynamics: The Use of AUIC to Improve Efficacy and Avoid Resistance. J Chemother 11:426–439.

64. Sánchez-Recio MM, Colino CI, Sánchez-Navarro A. 2000. A retrospective analysis of pharmacokinetic/pharmacodynamic indices as indicators of the clinical efficacy of ciprofloxacin. J Antimicrob Chemother 45:321–8.

65. Author M, Craig WA. 1998. Pharmacokinetic/Pharmacodynamic Parameters: Rationale for Antibacterial Dosing of Mice. Source Clin Infect Dis 26:1–10.

66.   Andes D, Craig WA. 2002. Animal model pharmacokinetics and pharmacodynamics: a critical review. Int J Antimicrob Agents 19:261–268.

67.   Food and Drug Administration. 2016. Physiologically Based Pharmacokinetic Analyses — Format and Content Guidance for Industry.

68.   Food and Drug Administration. 1999. Guidance for Industry: Guidance for Industry Population Pharmacokinetics.

69.   Food and Drug Administration. 2003. Guidance for Industry: Exposure-Response Relationships — Study Design, Data Analysis, and Regulatory Applications.

70.   Food and Drug Administration. 2009. Guidance for Industry End-of-Phase 2A Meetings.

71.   Food and Drug Administration, Infectious Diseases Society of America. 2007. Issues in the design and conduct of clinical trials of antibacterial drugs in the treatment of community-acquired pneumonia.

72.   European Medicines Agency. 2011. Guideline on the evaluation of medicinal products indicated for treatment of bacterial infections.

73.   Nielsen EI, Friberg LE. 2013. Pharmacokinetic-Pharmacodynamic Modeling of Antibacterial Drugs. Pharmacol Rev Pharmacol Rev 65:1053–1090.

74.   Barrett JS, Fossler MJ, Cadieu KD, Gastonguay MR. 2008. Pharmacometrics: A Multidisciplinary Field to Facilitate Critical Thinking in Drug Development and. J Clin Pharmacol J Clin Pharmacol 48:632–649.

75.   Lee JY, Garnett CE, Gobburu JVS, Bhattaram VA, Brar S, Earp JC, Jadhav PR, Krudys K, Lesko LJ, Li F, Liu J, Madabushi R, Marathe A, Mehrotra N, Tornoe C, Wang Y, Zhu H. Impact of Pharmacometric Analyses on New Drug Approval and Labelling Decisions A Review of 198 Submissions Between 2000 and 2008.

76.   Bhattaram V, Bonapace C, Chilukuri D, Duan J, Garnett C, Gobburu J, Jang S, Kenna L, Lesko L, Madabushi R, Men Y, Powell J, Qiu W, Ramchandani R, Tornoe C, Wang Y, Zheng J. Impact of Pharmacometric Reviews on New Drug Approval and Labeling Decisions—a Survey of 31 New Drug Applications Submitted Between 2005 and 2006.

77.   Li F, Nandy P, Chien S, Noel GJ, Tornoe CW. 2010. Pharmacometrics-based dose selection of levofloxacin as a treatment for postexposure inhalational anthrax in children. Antimicrob Agents Chemother 54:375–9.

78.   Trivedi A, Lee RE, Meibohm B. 2013. Applications of pharmacometrics in the clinical development and pharmacotherapy of anti-infectives. Expert Rev Clin Pharmacol 6:159–70.

79. Koch G, Krzyzanski W, Juan @bullet, Pérez-Ruixo J, Schropp J. 2014. Modeling of delays in PKPD: classical approaches and a tutorial for delay differential equations. J Pharmacokinet Pharmacodyn 41:291–318.

80. Upton RN, Mould DR. 2014. Basic concepts in population modeling, simulation, and model-based drug development: part 3-introduction to pharmacodynamic modeling methods. CPT pharmacometrics Syst Pharmacol 3:e88.

81. Standing JF. 2017. Understanding and applying pharmacometric modelling and simulation in clinical practice and research. Br J Clin Pharmacol 83:247–254.

82. Karlsson KE, Vong C, Bergstrand M, Jonsson EN, Karlsson MO. 2013. Comparisons of Analysis Methods for Proof-of-Concept Trials. CPT pharmacometrics Syst Pharmacol 2:e23.

83. Dosne A-G. 2016. Improved Methods for Pharmacometric Model-Based Decision-Making in Clinical Drug Development.

84. Holford N, Karlsson M. 2007. Time for Quantitative Clinical Pharmacology: A Proposal for a Pharmacometrics Curriculum. Clin Pharmacol Ther 82:103–105.

85. Kang D, Schwartz JB, Verotta D. 2004. A sample size computation method for non-linear mixed eeects models with applications to pharmacokinetics models. Stat Med Stat Med 23:2551–2566.

86. Ueckert S, Mats Karlsson BO, Andrew Hooker BC. 2016. Accelerating Monte Carlo power studies through parametric power estimation. J Pharmacokinet Pharmacodyn 43:223–234.

87. Vong C, Bergstrand M, Nyberg J, Karlsson MO. 2012. Rapid Sample Size Calculations for a Defined Likelihood Ratio Test-Based Power in Mixed-Effects Models. AAPS J 14:176–186.

88. Dosne A-G, Bergstrand M, Mats @bullet, Karlsson O. 2016. A strategy for residual error modeling incorporating scedasticity of variance and distribution shape. J Pharmacokinet Pharmacodyn 43:137–151.

89. Petersson KJF, Hanze E, Savic RM, Karlsson MO. 2009. Semiparametric Distributions With Estimated Shape Parameters. Pharm Res 26:2174–2185.

90. Dosne A-G, Bergstrand M, Harling K, Karlsson MO. 2016. Improving the estimation of parameter uncertainty distributions in nonlinear mixed effects models using sampling importance resampling. J Pharmacokinet Pharmacodyn 43:583–596.

91. Hu C, Zhang J, Zhou H. 2011. Confirmatory analysis for phase III population pharmacokinetics. Pharm Stat 10.

92.	Hu C, Moore KHP, Kim YH, Sale ME. 2004. Statistical Issues in a Modeling Approach to Assessing Bioequivalence or PK Similarity with Presence of Sparsely Sampled Subjects. J Pharmacokinet Pharmacodyn 31:321–339.

93.	Dosne AG, Bergstrand | M, Karlsson | M O, Renard | D, Heimann | G. 2017. Model averaging for robust assessment of QT prolongation by concentration-response analysis. Stat Med 26:3844–3857.

94.	Drusano GL, Preston SL, Hardalo C, Hare R, Banfield C, Andes D, Vesga O, Craig WA. 2001. Use of preclinical data for selection of a phase II/III dose for evernimicin and identification of a preclinical MIC breakpoint. Antimicrob Agents Chemother 45:13–22.

95.	Colin P, Eleveld DJ, Jonckheere S, Van Bocxlaer J, De Waele J, Vermeulen A. 2016. What about confidence intervals? A word of caution when interpreting PTA simulations. J Antimicrob Chemother 71: 2502-2508.

96.	Mouton JW, Brown DFJ, Apfalter P, Cantón R, Giske CG, Ivanova M, MacGowan AP, Rodloff A, Soussy C-J, Steinbakk M, Kahlmeter G. 2012. The role of pharmacokinetics/pharmacodynamics in setting clinical MIC breakpoints: the EUCAST approach. Clin Microbiol Infect 18:E37–E45.

97.	Müller M, Dela Peña A, Derendorf H. 2004. Issues in Pharmacokinetics and Pharmacodynamics of Anti-Infective Agents: Kill Curves versus MIC. Antimicrob Agents Chemother 48:1441–1453.

98.	Barclay ML, Begg EJ, Chambers ST. 1992. Adaptive resistance following single doses of gentamicin in a dynamic in vitro model. Antimicrob Agents Chemother 36:1951–1957.

99.	Keel RA, Zhanel GG, Zelenitsky S, Nicolau DP. 2011. Pharmacodynamic profiling of antimicrobials against Gram-negative respiratory isolates from Canadian hospitals. Can J Infect Dis Med Microbiol = J Can des Mal Infect la Microbiol medicale 22:132–6.

100.	Mouton JW, Dudley MN, Cars O, Derendorf H, Drusano GL. 2005. Standardization of pharmacokinetic/pharmacodynamic (PK/PD) terminology for anti-infective drugs: an update. J Antimicrob Chemother 55:601–607.

101.	Whitney CG, Heffelfinger JD. 2000. Management of Community-Acquired Pneumonia in the Era of Pneumococcal Resistance. Arch Intern Med 160:1399–1408.

102.	Bulik CC, Bader JC, Zhang L, Van Wart SA, Rubino CM, Bhavnani SM, Sweeney KL, Ambrose PG. 2017. PK–PD Compass: bringing infectious diseases pharmacometrics to the patient's bedside. J Pharmacokinet Pharmacodyn 44:161–177.

103.   Tillotson G. 2017. PK-PD Compass, a novel computerized decision support system. Lancet Infect Dis 17:908.

104.   La Hoz RM, Pappas PG. 2013. Cryptococcal infections: Changing epidemiology and implications for therapy. Drugs 73:495–504.

105.   Bicanic T, Meintjes G, Wood R, Hayes M, Rebe K, Bekker L-G, Harrison T. 2007. Fungal Burden, Early Fungicidal Activity, and Outcome in Cryptococcal Meningitis in Antiretroviral-Naive or Antiretroviral-Experienced Patients Treated with Amphotericin B or Fluconazole 45.

106.   Jarvis JN, Bicanic T, Loyse A, Namarika D, Jackson A, Nussbaum JC, Longley N, Muzoora C, Phulusa J, Taseera K, Kanyembe C, Wilson D, Hosseinipour MC, Brouwer AE, Limmathurotsakul D, White N, Van Der Horst C, Wood R, Meintjes G, Bradley J, Jaffar S, Harrison T. 2014. Determinants of mortality in a combined cohort of 501 patients with HIV-associated cryptococcal meningitis: Implications for improving outcomes. Clin Infect Dis 58:736–745.

107.   Park BJ, Wannemuehler KA, Marston BJ, Govender N, Pappas PG, Chiller TM. 2009. Estimation of the current global burden of cryptococcal meningitis among persons living with HIV/AIDS. Aids 23:525–30.

108.   Rhein J, Morawski BM, Hullsiek KH, Nabeta HW, Kiggundu R, Tugume L, Musubire A, Akampurira A, Smith KD, Alhadab A, Williams DA, Abassi M, Bahr NC, Velamakanni SS, Fisher J, Nielsen K, Meya DB, Boulware DR, Ndyetukira JF, Ahimbisibwe C, Kugonza F, Sadiq A, Kandole TK, Luggya T, Kaboggoza J, Laker E, Butler EK, Dyal J, Neborak JM, King AM, Fujita AW, Yueh N, Namudde A, Halupnick R, Jawed B, Vedula P, Peterson M, Bohjanen PR, Kambugu A. 2016. Efficacy of adjunctive sertraline for the treatment of HIV-associated cryptococcal meningitis: An open-label dose-ranging study. Lancet Infect Dis 16:809–818.

109.   Trevino-Rangel RDJ, Villanueva-Lozano H, Hernandez-Rodriguez P, Martinez-Resendez MF, Garcia-Juarez J, Rodriguez-Rocha H, Gonzalez GM. 2016. Activity of sertraline against Cryptococcus neoformans: In vitro and in vivo assays. Med Mycol 54:280–286.

110.   Smith KD, Achan B, Hullsiek KH, Mcdonald TR, Okagaki LH, Alhadab AA, Akampurira A, Rhein JR, Meya DB, Boulware DR, Nielsen K. 2015. Increased Antifungal Drug Resistance in Clinical Isolates of Cryptococcus neoformans in Uganda. Antimicrob Agents Chemother 59:7197–7204.

111.   Zhai B, Wu C, Wang L, Sachs MS, Lin X. 2012. The antidepressant sertraline provides a promising therapeutic option for neurotropic cryptococcal infections. Antimicrob Agents Chemother 56:3758–3766.

112.   Lin C-JJ, Robert F, Sukarieh R, Michnick S, Pelletier J. 2010. The antidepressant sertraline inhibits translation initiation by curtailing mammalian target of

rapamycin signaling. Cancer Res 70:3199–208.

113. Young TJ, Oliver GP, Pryde D, Perros M, Parkinson T. 2003. Antifungal activity of selective serotonin reuptake inhibitors attributed to non-specific cytotoxicity. J Antimicrob Chemother 51:1045–7.

114. Heller I, Leitner S, Dierich MP, Lass-Flörl C. 2004. Serotonin (5-HT) enhances the activity of amphotericin B against Aspergillus fumigatus in vitro. Int J Antimicrob Agents 24:401–404.

115. Mayr A, Hinterberger G, Dierich MP, Lass-Flörl C. 2005. Interaction of serotonin with Candida albicans selectively attenuates fungal virulence in vitro. Int J Antimicrob Agents 26:335–7.

116. Hernandez ME, Mendieta D, Pérez-Tapia M, Bojalil R, Estrada-Garcia I, Estrada-Parra S, Pavón L. 2013. Effect of selective serotonin reuptake inhibitors and immunomodulator on cytokines levels: an alternative therapy for patients with major depressive disorder. Clin Dev Immunol 2013:267871.

117. Rainey MM, Korostyshevsky D, Lee S, Perlstein EO. 2010. The antidepressant sertraline targets intracellular vesiculogenic membranes in yeast. Genetics 185:1221–33.

118. Nayak R, Xu J. 2010. Effects of sertraline hydrochloride and fluconazole combinations on Cryptococcus neoformansand Cryptococcus gattii. Mycology 1:99–105.

119. Perfect JRR, Dismukes WEE, Dromer F, Goldman DLL, Graybill JRR, Hamill RJJ, Harrison TSS, Larsen RA a, Lortholary O, Nguyen MM-H, Pappas PGG, Powderly WGG, Singh N, Sobel JDD, Sorrell TCC. 2010. Clinical Practice Guidelines for the Management of Cryptococcal Disease: 2010 Update by the Infectious Diseases Society of America. Clin Infect Dis 50:291–322.

120. Spitzer M, Griffiths E, Blakely KM, Wildenhain J, Ejim L, Rossi L, De Pascale G, Curak J, Brown E, Tyers M, Wright GD. 2014. Cross-species discovery of syncretic drug combinations that potentiate the antifungal fluconazole. Mol Syst Biol 7:499–499.

121. Lewis RJ, Angier MK, Williamson KS, Johnson RD. 2013. Analysis of sertraline in postmortem fluids and tissues in 11 aviation accident victims. J Anal Toxicol 37:208–216.

122. Orlando M, Burnam MA, Beckman R, Morton SC, London AS, Bing EG, Fleishman JA, Health R. 2002. Re-estimating the prevalence of psychiatric disorders in a nationally representative sample of persons receiving care for HIV: results from the HIV Cost and Services Utilization Study. Int J Methods Psychiatr Res 11:75–82.

123. DeVane CL, Liston HL, Markowitz JS. 2002. Clinical Pharmacokinetics of Sertraline. Clin Pharmacokinet 41:1247–1266.

124. Boulware DR, Meya DB, Muzoora C, Rolfes MA, Huppler Hullsiek K, Musubire A, Taseera K, Nabeta HW, Schutz C, Williams DA, Rajasingham R, Rhein J, Thienemann F, Lo MW, Nielsen K, Bergemann TL, Kambugu A, Manabe YC, Janoff EN, Bohjanen PR, Meintjes G. 2014. Timing of Antiretroviral Therapy after Diagnosis of Cryptococcal Meningitis. N Engl J Med 370:2487–2498.

125. Bergstrand M, Hooker AC, Wallin JE, Karlsson MO. 2011. Prediction-corrected visual predictive checks for diagnosing nonlinear mixed-effects models. AAPS J 13:143–51.

126. Dyal J, Akampurira A, Rhein J, Morawski BM, Kiggundu R, Nabeta HW, Musubire AK, Bahr NC, Williams DA, Bicanic T, Larsen RA, Meya DB, Boulware DR, Team AT. 2016. Reproducibility of CSF quantitative culture methods for estimating rate of clearance in cryptococcal meningitis 361–369.

127. CLSI. 2008. Reference Method for Broth Dilution Antifungal Susceptibility Testing of Yeasts ; Approved Standard — Second Edition Serving the World ' s Medical Science Community Through Voluntary Consensus.

128. Plan EL. 2014. Modeling and Simulation of Count Data.

129. Holford N. 2013. A Time to Event Tutorial for Pharmacometricians 1–8.

130. Keizer RJ, Karlsson MO, Hooker A. 2013. Modeling and Simulation Workbench for NONMEM: Tutorial on Pirana, PsN, and Xpose. CPT pharmacometrics Syst Pharmacol 2:e50.

131. Templeton IE, Chen Y, Mao J, Lin J, Yu H, Peters S, Shebley M, Varma M V. 2016. Quantitative Prediction of Drug-Drug Interactions Involving Inhibitory Metabolites in Drug Development: How Can Physiologically Based Pharmacokinetic Modeling Help? CPT pharmacometrics Syst Pharmacol 5:505–515.

132. Cooper JM, Duffull SB, Saiao AS, Isbister GK. 2015. The pharmacokinetics of sertraline in overdose and the effect of activated charcoal. Br J Clin Pharmacol 79:307–15.

133. Li CH, Pollock BG, Lyketsos CG, Vaidya V, Drye LT, Kirshner M, Sorisio D, Bies RR. 2012. Population Pharmacokinetic Modeling of Sertraline Treatment in Patients With Alzheimer Disease: The DIADS-2 Study. J Clin Pharmacol XX.

134. Obach RS, Cox LM, Tremaine LM. 2005. Sertraline is metabolized by multiple cytochrome p450 enzymes, monoamine oxidases, and glucuronyl transferases in human: an in vitro study 33:262–270.

135. Therapeutics E, Chiba K. 1999. Short Communication Sertraline N - Demethylation Is Catalyzed by Multiple Isoforms of Human Cytochrome ABSTRACT : 27:763–766.

136. Pierre Loulergue, Olivier Mir, Pierre Rocheteau, Fabrice Chrétien RG. 2016. Sertraline-induced increase in VEGF brain levels and its activity in cryptococcal meningitis. Lancet Infect Dis 16:891.

137. European Medicines Agency. 2015. Report from dose finding workshop. London, UK.

138. Lepak AJ, Andes DR. 2014. Antifungal pharmacokinetics and pharmacodynamics. Essentials Clin Mycol Second Ed 121–134.

139. Thiebaut F, Tsuruot T, Hamadat H, Gottesman MM, Pastan IRA. 1987. Cellular localization of the multidrug-resistance gene product P-glycoprotein in normal human tissues 84:7735–7738.

140. Schinkel AH. 1999. P-Glycoprotein, a gatekeeper in the blood–brain barrier 36:179–194.

141. Wang EJ, Lew K, Casciano CN, Clement RP, Johnson WW. 2002. Interaction of common azole antifungals with P glycoprotein. Antimicrob Agents Chemother 46:160–165.

142. Kapoor A, Iqbal M, Petropoulos S, Ho HL, Gibb W, Matthews SG. 2013. Effects of Sertraline and Fluoxetine on P-Glycoprotein at Barrier Sites: In Vivo and In Vitro Approaches. PLoS One 8:3–8.

143. Weiss J, Dormann S-MG, Martin-Facklam M, Kerpen CJ, Ketabi-Kiyanvash N, Haefeli WE. 2003. Inhibition of P-glycoprotein by newer antidepressants. J Pharmacol Exp Ther 305:197–204.

144. Anette Veringa, Kim C M van der Elst, Jeremy N Day, Guy E Thwaites J-WCA enaar. 2016. Sertraline for HIV-associated cryptococcal meningitis. Lancet Infect Dis 16:1111–12.

145. Kalvass JC, Polli JW, Bourdet DL, Feng B, Huang S-M, Liu X, Smith QR, Zhang LK, Zamek-Gliszczynski MJ. 2013. Why Clinical Modulation of Efflux Transport at the Human Blood–Brain Barrier Is Unlikely: The ITC Evidence-Based Position. Clin Pharmacol Ther 94:80–94.

146. Eyal S, Hsiao P, Unadkat JD. 2009. Drug interactions at the blood-brain barrier: fact or fantasy? Pharmacol Ther 123:80–104.

147. Shajib MS, Khan WI. 2015. The role of serotonin and its receptors in activation of immune responses and inflammation. Acta Physiol (Oxf) 213:561–74.

148. Speth C, Rambach G, Lass-Flörl C. 2014. Platelet immunology in fungal infections. Thromb Haemost 112:632–639.

149. Mercado CP, Ziu E, Kilic F. 2011. Communication between 5-HT and small GTPases. Curr Opin Pharmacol 11:23–8.

150. Larsson M, Hagberg L, Norkrans G, Forsman A. 1989. Indole amine deficiency in blood and cerebrospinal fluid from patients with human immunodeficiency virus infection. J Neurosci Res 23:441–446.

151. Meredith EJ, Chamba A, Holder MJ, Barnes NM, Gordon J. 2005. Close encounters of the monoamine kind: immune cells betray their nervous disposition. Immunology 115:289–95.

152. Baganz NL, Blakely RD. 2013. A dialogue between the immune system and brain, spoken in the language of serotonin. ACS Chem Neurosci 4:48–63.

153. 2017. Zoloft(R). Prescribing Information. Pfizer, New York, NY.

154. Lau GT, Horowitz BZ. 1996. Sertraline overdose. Acad Emerg Med 3:132–6.

155. Warrington SJ. 1991. Clinical implications of the pharmacology of sertraline. Int Clin Psychopharmacol 6 Suppl 2:11–21.

156. Sanders J, Chen L, Burka L, Matthews H. 2000. Metabolism and disposition of the 5-hydoxytryptamine Uptake Blocker Sertraline in the Rat and Dog. Xenobiotica 30:263–272.

157. C. Lindsay DeVance. 1994. Pharmacokinetics of the Newer Antidepresssant: Clinical Relavence. Am J Meicine 97:6A–13S–6A–23S.

158. Ronfeld RA, Wilner KD, Baris BA. 1997. Chronopharmacokinetics and the Effect of Coadministration with Food. Clin Pharmacokinet 32:50–55.

159. Hiemke C, Härtter S. 2000. Pharmacokinetics of selective serotonin reuptake inhibitors. Pharmacol Ther 85:11–28.

160. Gupta RN, Dziurdzy SA. 1994. Therapeutic Monitoring of Sertraline 40:498–499.

161. Démolis JL, Angebaud P, Grangé JD, Coates P, Funck-Brentano C, Jaillon P. 1996. Influence of liver cirrhosis on sertraline pharmacokinetics. Br J Clin Pharmacol 42:394–397.

162. Lau GT, Horowitz Z. 1996. Sertraline Overdose 31:132–136.

163. Rudberg I, Hermann M, Refsum H, Molden E. 2008. Serum concentrations of sertraline and N-desmethyl sertraline in relation to CYP2C19 genotype in psychiatric patients. Eur J Clin Pharmacol 64:1181–8.

164. Ayaz M, Subhan F, Ahmed J, Khan A-U, Ullah F, Ullah I, Ali G, Syed N-I-H, Hussain S. 2015. Sertraline enhances the activity of antimicrobial agents against pathogens of clinical relevance. J Biol Res (Thessalonikē, Greece) 22:4.

165. Whellan DJ, Ellis SJ, Kraus WE, Hawthorne K, Piña IL, Keteyian SJ, Kitzman DW, Cooper L, Lee K, O'Connor CM. 2009. In vitro novel combinations of psychotropics and anti-cancer modalities in U87 human glioblastoma cells. Ann Intern Med 151:414–420.

166. Gil-ad I, Zolokov A, Lomnitski L, Taler M, Bar M, Luria D, Ram E, Weizman A. 2008. Evaluation of the potential anti-cancer activity of the antidepressant sertraline in human colon cancer cell lines and in colorectal cancer-xenografted mice 277–286.

167. Reddy KK, Lefkove B, Chen LB, Govindarajan B, Carracedo A, Velasco G, Carrillo CO, Bhandarkar SS, Owens MJ, Mechta-Grigoriou F, Arbiser JL. 2008. The antidepressant sertraline downregulates Akt and has activity against melanoma cells. Pigment Cell Melanoma Res 21:451–456.

168. Drinberg V, Bitcover R, Rajchenbach W, Peer D. 2014. Modulating cancer multidrug resistance by sertraline in combination with a nanomedicine. Cancer Lett 354:290–8.

169. Saletu B, Grünberger J, Linzmayer L. 1986. On central effects of serotonin re-uptake inhibitors: quantitative EEG and psychometric studies with sertraline and zimelidine. J Neural Transm 67:241–66.

170. Ronfeld R a., Tremaine LM, Wilner KD. 1997. Pharmacokinetics of sertraline and its N-demethyl metabolite in elderly and young male and female volunteers. Clin Pharmacokinet 32 Suppl 1:22–30.

171. Moraes MOE, Lerner FE, Perozin M, Moraes MOE, Frota Bezerra FA, Sucupira M, Corso G, De Nucci G. 1998. Comparative bioavailability of two sertraline tablet formulations in healthy human volunteers after a single dose administration. Int J Clin Pharmacol Ther 36:661–5.

172. Allard S, Sainati SM, Roth-Schechter BF. 1999. Coadministration of short-term zolpidem with sertraline in healthy women. J Clin Pharmacol 39:184–91.

173. Zhu CJ, Wu JF, Qu ZW, Chen LM, Zhang JT, Zhang, J TZhu CJ, Wu JF, Qu ZW, Chen LM, Zhang JT. 1999. Bioequivalence evaluation of two sertraline tablet formulations in healthy male volunteers after a single dose administration. Int J Clin Pharmacol Ther 37:120–4.

174. Wang JH, Liu ZQ, Wang W, Chen XP, Shu Y, He N, Zhou HH. 2001. Pharmacokinetics of sertraline in relation to genetic polymorphism of CYP2C19. Clin Pharmacol Ther 70:42–7.

175. Kim KM, Jung BH, Choi MH, Woo JS, Paeng K-J, Chung BC. 2002. Rapid and sensitive determination of sertraline in human plasma using gas chromatography-mass spectrometry. J Chromatogr B Analyt Technol Biomed Life Sci 769:333–9.

176. Nagy CF, Kumar D, Perdomo CA, Wason S, Cullen EI, Pratt RD. 2004. Concurrent administration of donepezil HCl and sertraline HCl in healthy volunteers: Assessment of pharmacokinetic changes and safety following single and multipe oral doses. Br J Clin Pharmacol Suppl 58:25–33.

177. Koytchev R, Ozalp Y, Erenmemisoglu A, van der Meer MJ, Alpan RS. 2004. Serotonin reuptake inhibitors: bioequivalence of sertraline capsules. Arzneimittelforschung 54:629–33.

178. Almeida S, Portolés A, Terleira A, Filipe A, Cea E, Caturla MC. 2005. Comparative bioavailability/ bioequivalence of two different sertraline formulations: a randomised, 2-period x 2-sequence, crossover clinical trial in healthy volunteers. Arzneimittelforschung 55:191–7.

179. He L, Feng F, Wu J. 2005. Determination of sertraline in human plasma by high-performance liquid chromatography-electrospray ionization mass spectrometry and method validation. J Chromatogr Sci 43:532–535.

180. Chen X, Duan X, Dai X, Zhong D. 2006. Development and validation of a liquid chromatographic/tandem mass spectrometric method for the determination of sertraline in human plasma. Rapid Commun Mass Spectrom 20:2483–9.

181. Tassaneeyakul W, Kanchanawat S, Gaysonsiri D, Vannaprasath S, Paupairoj P, Kittiwattanagul K, Tippabhotla SK, Khuroo A, Panigrahy BK, Reyar S, Monif T. 2008. Comparative bioavailability of two sertraline tablet formulations after single-dose administration in healthy Thai volunteers. Int J Clin Pharmacol Ther 46:151–6.

182. Farshchi A, Ghiasi G, Bahrami G. 2009. High Performance Liquid Chromatography Determination of Sertraline in Human. Iran J Pharm Sci 5:171–8.

183. Niyomnaitham S, Chatsiricharoenkul S, Sathirakul K, Pongnarin P, Kongpatanakul S. 2009. Bioequivalence study of 50 mg sertraline tablets in healthy Thai volunteers. J Med Assoc Thail 92:September-.

184. Patel BN, Sharma N, Sanyal M, Shrivastav PS. 2009. Analysis of second-generation antidepressant drug, sertraline and its active metabolite, N-desmethyl sertraline in human plasma by a sensitive and selective liquid chromatography-tandem mass spectrometry method. J Chromatogr B Anal Technol Biomed Life Sci 877:221–229.

185. Kang H-A, Cho H-Y, Young-Bok L. 2011. Bioequivalence of Traline Tablet to Zoloft Tablet (Sertraline HCl 50 mg). J Pharm Investig 41:317–22.

186. Park MK, Shin KH, Kim KP, Kim TE, Yoon SH, Cho JY, Shin SG, Jang IJ, Yu KS. 2011. Open label, three period, single sequence, study of 5, 25, 50 mg sertraline pharmacokinetics in healthy male Korean volunteers. Int J Clin Pharmacol Ther 49:672–678.

187. Zhang M, Gao F, Cui X, Zhang Y, Sun Y, Gu J. 2011. Development and validation of an improved method for the quantitation of sertraline in human plasma using LC-MS-MS and its application to bioequivalence studies. J Chromatogr Sci 49:89–93.

188. Roerig JL, Steffen K, Zimmerman C, Mitchell JE, Crosby RD, Cao L. 2012. Preliminary comparison of sertraline levels in postbariatric surgery patients versus matched nonsurgical cohort. Surg Obes Relat Dis 8:62–66.

189. Ruderman EBW. 2013. Effects of Acute Aerobic Exercise on the Pharmacokinetics of the Anti-anxiety / Anti-depressant Effects of Acute Aerobic Exercise on the Pharmacokinetics of the.

190. Yue X-H, Wang Z, Tian D-D, Zhang J-W, Zhu K, Ye Q. 2015. Determination of Sertraline in Human Plasma by UPLC–MS/MS and its Application to a Pharmacokinetic Study. J Chromatogr Sci bmv128.

191. Shin KH, Kim KP, Lim KS, Kim JW, Lee YS, Yang BY, Lee JS, Jung JM, Yoon SH, Jang IJ, Yu KS. 2012. A positron emission tomography microdosing study with sertraline in healthy volunteers. Int J Clin Pharmacol Ther 50:224–232.

192. Sutton SC. 2009. Role of physiological intestinal water in oral absorption. AAPS J 11:277–285.

193. AXELSON DA, PEREL JM, BIRMAHER B, RUDOLPH GR, NUSS S, BRIDGE J, BRENT DA. 2002. Sertraline Pharmacokinetics and Dynamics in Adolescents. J Am Acad Child Adolesc Psychiatry 41:1037–1044.

194. Wang J-S, Zhu H-J, Gibson BB, Markowitz JS, Donovan JL, DeVane CL. 2008. Sertraline and its metabolite desmethylsertraline, but not bupropion or its three major metabolites, have high affinity for P-glycoprotein. Biol Pharm Bull 31:231–4.

195. Peters SA. 2008. Identification of Intestinal Loss of a Drug through Physiologically Based Pharmacokinetic Simulation of Plasma Concentration-Time Profiles. Clin Pharmacokinet 47:245–259.

196. Food and Drug Administration. 2012. Guidance for Industry Drug Interaction Studies — Study Design, Data Analysis, Implications for Dosing, and Labeling Recommendations.

197. Sutton SC. 2009. The use of gastrointestinal intubation studies for controlled release development. Br J Clin Pharmacol 68:342–354.

198. Savic RM, Jonker DM, Kerbusch T, Karlsson MO. 2007. Implementation of a transit compartment model for describing drug absorption in pharmacokinetic studies. J Pharmacokinet Pharmacodyn 34:711–726.

199. Maharaj A, Edginton A. 2014. Physiologically Based Pharmacokinetic Modeling and Simulation in Pediatric Drug Development. CPT Pharmacometrics Syst Pharmacol.

200. Jones HM, Gardner IB, Watson KJ. 2009. Modelling and PBPK simulation in drug discovery. AAPS J 11:155–66.

201. Zhuang X, Lu C. 2016. PBPK modeling and simulation in drug research and development. Acta Pharm Sin B 6:430–440.

202. Lu J, Goldsmith M-R, Grulke CM, Chang DT, Brooks RD, Leonard JA, Phillips MB, Hypes ED, Fair MJ, Tornero-Velez R, Johnson J, Dary CC, Tan Y-M. Developing a Physiologically-Based Pharmacokinetic Model Knowledgebase in Support of Provisional Model Construction.

203. Peters SA. 2008. Evaluation of a Generic Physiologically Based Pharmacokinetic Model for Lineshape Analysis. Clin Pharmacokinet 47:261–275.

204. Radin DP, Patel P. 2017. A current perspective on the oncopreventive and oncolytic properties of selective serotonin reuptake inhibitors. Biomed Pharmacother 87:636–639.

205. Barrows NJ, Campos RK, Powell S, Reddisiva Prasanth K, Schott-Lerner G, Soto-Acosta R, Galarza-Muñoz G, Mcgrath EL, Urrabaz-Garza R, Gao J, Wu P, Menon R, Saade G, Fernandez-Salas I, Rossi SL, Vasilakis N, Routh A, Bradrick SS, Garcia-Blanco MA. 2016. A screen of FDA-approved drugs for inhibitors of Zika virus infection HHS Public Access. Cell Host Microbe 20:259–270.

206. Kalaycı S, Demirci S, Fikrettin Ş. 2014. Antimicrobial Properties of Various Psychotropic Drugs Against Broad Range Microorganisms. Curr Psychopharmacol 3:195–202.

207. Samanta A, Chattopadhyay D, Sinha C, Dulal Jana A, Ghosh S, Mandal A, Banerjee A, Hendricks O, B. Christensen J, Elisabeth Kristiansen J. 2012. Evaluation of In Vivo and In Vitro Antimicrobial Activities of a Selective Serotonin Reuptake Inhibitor Sertraline Hydrochloride. Anti-Infective Agents 10:95–104.

208. Lieb J. 2008. Defeating cancer with antidepressants. Ecancermedicalscience 2:88.

209. Nayak R, Xu J. 2010. Effects of sertraline hydrochloride and fluconazole combinations on *Cryptococcus neoformans* and *Cryptococcus gattii*. Mycology 1:99–105.

210. Hallett RM, Girgis-Gabardo A, Gwynne WD, Giacomelli AO, Bisson JNP, Jensen JE, Dvorkin-Gheva A, Hassell JA, Hallett RM, Girgis-Gabardo A, Gwynne WD, Giacomelli AO, Bisson JNP, Jensen JE, Dvorkin-Gheva A, Hassell JA, Hallett RM, Girgis-Gabardo A, Gwynne WD, Giacomelli AO, Bisson JNP, Jensen JE, Dvorkin-Gheva A, Hassell JA. 2016. Serotonin transporter antagonists target tumor-initiating cells in a transgenic mouse model of breast cancer. Oncotarget 7:53137–53152.

211. Gwynne WD, Hallett RM, Girgis-Gabardo A, Bojovic B, Dvorkin-Gheva A, Aarts C, Dias K, Bane A, Hassell JA, Gwynne WD, Hallett RM, Girgis-Gabardo A, Bojovic B, Dvorkin-Gheva A, Aarts C, Dias K, Bane A, Hassell JA, Gwynne WD, Hallett RM, Girgis-Gabardo A, Bojovic B, Dvorkin-Gheva A, Aarts C, Dias K, Bane A, Hassell JA. 2017. Serotonergic system antagonists target breast tumor initiating cells and synergize with chemotherapy to shrink human breast tumor xenografts. Oncotarget 5:32101–32116.

212. Paper F. 2017. TCTP as a therapeutic target in melanoma treatment. Br J Cancer 1–10.

213. Amit BH, Gil-Ad I, Taler M, Bar M, Zolokov A, Weizman A. 2009. Proapoptotic and chemosensitizing effects of selective serotonin reuptake inhibitors on T cell lymphoma/leukemia (Jurkat) in vitro. Eur Neuropsychopharmacol 19:726–734.

214. Kuwahara J, Yamada T, Egashira N, Ueda M, Zukeyama N. 2015. Comparison of the Anti-tumor Effects of Selective Serotonin Reuptake Inhibitors as Well as Serotonin and Norepinephrine Reuptake Inhibitors in Human Hepatocellular Carcinoma Cells 38:1410–1414.

215. Tylutki Z, Polak S, Wiśniowska B. 2016. Top-down, Bottom-up and Middle-out Strategies for Drug Cardiac Safety Assessment via Modeling and Simulations. Curr Pharmacol reports 2:171–177.

216. Agoram B, Woltosz WS, Bolger MB. 2001. Predicting the impact of physiological and biochemical processes on oral drug bioavailability. Adv Drug Deliv Rev 50 Suppl 1:S41-67.

217. Peters SA. 2012. Physiologically-Based Pharmacokinetic (PBPK) Modeling and Simulations: Principles, Mehtods and Application in Pharmaceutical Industry. John Wiley & Sons, Inc., Hoboken, NJ, USA.

218. Poulin P, Theil F-P. 2002. Prediction of pharmacokinetics prior to in vivo studies. 1. Mechanism-based prediction of volume of distribution. J Pharm Sci 91:129–56.

219. Berezhkovskiy LM. 2004. Volume of Distribution at Steady State for a Linear Pharmacokinetic System with Peripheral Elimination. J Pharm Sci 93:1628–1640.

220. Rodgers T, Leahy D, Rowland M. 2005. Physiologically Based Pharmacokinetic Modeling 1: Predicting the Tissue Distribution of Moderate-to-Strong Bases. J

Pharm Sci 94:1259–1276.

221. Yang J, Jamei M, Yeo KR, Rostami-Hodjegan A, Tucker GT. 2007. Misuse of the Well-Stirred Model of Hepatic Drug Clearance. Drug 35:501–502.

222. Mithani SD, Bakatselou V, TenHoor CN, Dressman JB. 1996. Estimation of the increase in solubility of drugs as a function of bile salt concentration. Pharm Res 13:163–7.

223. Siccardi M, Marzolini C, Seden K, Almond L, Kirov A, Khoo S, Owen A, Back D. 2013. Prediction of drug-drug interactions between various antidepressants and efavirenz or boosted protease inhibitors using a physiologically based pharmacokinetic modelling approach. Clin Pharmacokinet 52:583–592.

224. Tihanyi K, Noszal B, Takacs-Novak K, Deak K. 2006. Physico-Chemical Profiling of Antidepressive Sertraline: Solubility,Ionisation, Lipophilicity. Med Chem (Los Angeles) 2:385–389.

225. Vatassery GT, Holden LA, Hazel DK, Dysken MW. 1997. Analysis of sertraline and desmethylsertraline in human plasma and red blood cells. Clin Biochem 30:565–568.

226. Uchimura T, Kato M, Saito T, Kinoshita H. 2010. Prediction of human blood-to-plasma drug concentration ratio. Biopharm Drug Dispos 31:n/a-n/a.

227. Bosgra S, van Eijkeren J, Bos P, Zeilmaker M, Slob W. 2012. An improved model to predict physiologically based model parameters and their inter-individual variability from anthropometry. Crit Rev Toxicol 42:751–767.

228. Peters SA, Hultin L. 2008. Early identification of drug-induced impairment of gastric emptying through physiologically based pharmacokinetic (PBPK) simulation of plasma concentration-time profiles in rat. J Pharmacokinet Pharmacodyn 35:1–30.

229. Melis V, Usach I, Peris JE. 2012. Determination of sertraline in rat plasma by HPLC and fluorescence detection and its application to in vivo pharmacokinetic studies. J Sep Sci 35:3302–3307.

230. Sun D, Lennernas H, Welage LS, Barnett JL, Landowski CP, Foster D, Fleisher D, Lee K-D, Amidon GL. 2002. Comparison of human duodenum and Caco-2 gene expression profiles for 12,000 gene sequences tags and correlation with permeability of 26 drugs. Pharm Res 19:1400–16.

231. VONRICHTER O, BURK O, FROMM M, THON K, EICHELBAUM M, KIVISTO K. 2004. Cytochrome P450 3A4 and P-glycoprotein expression in human small intestinal enterocytes and hepatocytes: a comparative analysis in paired tissue specimens. Clin Pharmacol Ther 75:172–183.

232. Kaminsky LS, Fasco MJ. 1991. Small intestinal cytochromes P450. Crit Rev Toxicol 21:407–22.

233. Kwon H, Lionberger RA, Yu LX. 2004. Impact of P-glycoprotein-mediated intestinal efflux kinetics on oral bioavailability of P-glycoprotein substrates. Mol Pharm 1:455–65.

234. Chan H-L, Chiu W-C, Chen VC-H, Huang K-Y, Wang T-N, Lee Y, McIntyre RS, Hsu T-C, Lee CT-C, Tzang B-S. 2017. SSRIs associated with decreased risk of hepatocellular carcinoma: A population-based case-control study. Psychooncology 1–6.

235. Mørch LS, Dehlendorff C, Baandrup L, Friis S, Kjaer SK. 2017. Use of antidepressants and risk of epithelial ovarian cancer. Int J Cancer.

236. Ventola CL. 2015. The antibiotic resistance crisis: part 1: causes and threats. P T A peer-reviewed J Formul Manag 40:277–83.

237. Centers for Disease Control and Prevention Office of Infectious Diseases. 2013. Antibiotic resistance threats in the United States, 2013.

238. Tam VH, Louie A, Deziel MR, Liu W, Drusano GL. 2007. The relationship between quinolone exposures and resistance amplification is characterized by an inverted U: a new paradigm for optimizing pharmacodynamics to counterselect resistance. Antimicrob Agents Chemother 51:744–7.

239. Murry KR, McKinnon PS, Mitrzyk B, Rybak MJ. 1999. Pharmacodynamic characterization of nephrotoxicity associated with once-daily aminoglycoside. Pharmacotherapy 19:1252–60.

240. Nicolau DP, Freeman CD, Belliveau PP, Nightingale CH, Ross JW, Quintiliani R. 1995. Experience with a once-daily aminoglycoside program administered to 2,184 adult patients. Antimicrob Agents Chemother 39:650–5.

241. Krivoy N, Postovsky S, Elhasid R, Ben Arush MW. 1998. Pharmacokinetic analysis of amikacin twice and single daily dosage in immunocompromised pediatric patients. Infection 26:396–8.

242. Lacy MK, Nicolau DP, Nightingale CH, Quintiliani R. The Pharmacodynamics of Aminoglycosides.

243. Moore RD, Lietman PS, Smith CR. 1987. Clinical response to aminoglycoside therapy: importance of the ratio of peak concentration to minimal inhibitory concentration. J Infect Dis 155:93–9.

244. Craig WA. 1998. State-of-the-Art Clinical Article: Pharmacokinetic/Pharmacodynamic Parameters: Rationale for Antibacterial Dosing of Mice and Men. Clin Infect Dis 26:1–10.

245. Martínez Illamola S. 2012. Development of a population pharmacokinetic model to determine the optimal doses of amikacin in the treatment of neonatal sepsis.

246. Newby B, Acpr Bs, Prevost D, Lotocka-Reysner H. Assessment of gentamicin 7 mg/kg once daily for pediatric patients with febrile neutropenia: a pilot project.

247. Ankit Rohatgi. 2017. WebPlotDigitizer. 3.11. Austin, Texas, USA.

248. Zelenitsky SA, Rubinstein E, Ariano RE, Zhanel GG, Zhanel GG, Hoban DJ, Adam HJ, Karlowsky JA, Baxter MR, Nichol KA, Lagace-Wiens PRS, Walkty A. 2013. Integrating pharmacokinetics, pharmacodynamics and MIC distributions to assess changing antimicrobial activity against clinical isolates of Pseudomonas aeruginosa causing infections in Canadian hospitals (CANWARD). J Antimicrob Chemother 68:i67–i72.

249. Staneck JL, Glenn S, DiPersio JR, Leist PA. 1989. Wide variability in Pseudomonas aeruginosa aminoglycoside results among seven susceptibility testing procedures. J Clin Microbiol 27:2277–2285.

250. 2016. Amikacin , Ceftazidime , and Flucloxacillin against Suspended and Adherent Pseudomonas aeruginosa and Staphylococcus epidermidis in an in vitro Model of Infection Author (s): Patrice Vergères and Jürg Blaser Published by : Oxford University Press Stable 165:281–289.

251. Cappelletty DM, Kang SL, Palmer SM, Rybak MJ. 1995. Pharmacodynamics of ceftazidime administered as continuous infusion or intermittent bolus alone and in combination with single daily-dose amikacin against Pseudomonas aeruginosa in an in vitro infection model. Antimicrob Agents Chemother 39:1797–1801.

252. McGrath BJ, Lamp KC, Rybak MJ. 1993. Pharmacodynamic effects of extended dosing intervals of imipenem alone and in combination with amikacin against Pseudomonas aeruginosa in an in vitro model. Antimicrob Agents Chemother 37:1931–1937.

253. McGrath BJ, Bailey EM, Lamp KC, Rybak MJ. 1992. Pharmacodynamics of once-daily amikacin in various combinations with cefepime, aztreonam, and ceftazidime against Pseudomonas aeruginosa in an in vitro infection model. Antimicrob Agents Chemother 36:2741–2746.

254. Craig WA, Redington J, Ebert SC. 1991. Pharmacodynamics of amikacin in vitro and in mouse thigh and lung infections. J Antimicrob Chemother 27 Suppl C:29–40.

255. Zinner SH, Blaser J, Stone BB, Groner MC. 1985. Use of an in-vitro kinetic model to study antibiotic combinations 221–226.

256. Paterson DL. 2004. "Collateral Damage" from Cephalosporin or Quinolone Antibiotic Therapy. Clin Infect Dis 38:S341–S345.

257. Zelenitsky SA, Rubinstein E, Ariano RE, Zhanel GG, Canadian Antimicrobial Resistance Alliance. 2013. Integrating pharmacokinetics, pharmacodynamics and MIC distributions to assess changing antimicrobial activity against clinical isolates of Pseudomonas aeruginosa causing infections in Canadian hospitals (CANWARD). J Antimicrob Chemother 68 Suppl 1:67–72.

258. Craig WA. 2014. Introduction to Pharmacodynamics, p. 3–22. *In* Fundamentals of Antimicrobial Pharmacokinetics and Pharmacodynamics. Springer New York, New York, NY.

259. Sutherland CA, Verastegui JE, Nicolau DP. 2016. In vitro potency of amikacin and comparators against E. coli, K. pneumoniae and P. aeruginosa respiratory and blood isolates. Ann Clin Microbiol Antimicrob 15:39.

260. Treluyer J, Merle Y, Tonnelier S. 2002. Nonparametric population pharmacokinetic analysis of amikacin in neonates, infants, and children. Antimicrob agents … 46:1381–1387.

261. Villena R, Rabello M, Pharmd JM, Aravena R, Kopp K, Villarroel M, Santolaya ME. 2011. Pharmacokinetics of amikacin in children with cancer and febrile neutropenia. 49th Annual Meeting of the Infectious Diseases Society of America, Boston, Massachusetts.

262. Davis RL, Lehmann D, Stidley CA, Neidhart J. 1991. Amikacin pharmacokinetics in patients receiving high-dose cancer chemotherapy. Antimicrob Agents Chemother 35:944–947.

263. Tod M, Lortholary O, Seytre D, Semaoun RM, Uzzan B, Guillevin LC, Casassus P, Petitjean O. 1998. Population Pharmacokinetic Study of Amikacin Administered Once or Twice Daily to Febrile, Severely Neutropenic Adults 42:849–856.

264. Romano S, de Gatta MMF, Calvo M V., Caballero D, Dominguez-Gil A, Lanao JM. 1999. Population pharmacokinetics of amikacin in patients with haematological malignancies. J Antimicrob Chemother 44:235–242.

265. Müller M, Dela Peña A, Derendorf H. 2004. Issues in Pharmacokinetics and Pharmacodynamics of Anti-Infective Agents: Distribution in Tissue. Antimicrob Agents Chemother 48:1441–1453.

266. Taber HW, Mueller JP, Miller PF, Arrow AS. 1987. Bacterial uptake of aminoglycoside antibiotics. Microbiol Rev 51:439–57.

267. Nielsen EI, Cars O, Friberg LE. 2011. Pharmacokinetic/pharmacodynamic (PK/PD) indices of antibiotics predicted by a semimechanistic PKPD model: a step toward model-based dose optimization. Antimicrob Agents Chemother 55:4619–30.

9 APPENDIX

A. NONMEM CODE FOR SERTRALINE PK IN HIV PATIENTS

```
$PROBLEM SERTRALINE PK IN HIV PATIENTS

$INPUT C ID PID DATE=DROP TIME TAD AMT DV DMS RA SS II DL EFA
MIC DEATH WT AGE SEX ART IND=DROP INH=DROP SUB=DROP
NET=DROP QCC BILI=DROP ALT=DROP AST=DROP SCR=DROP  ;LOCF
THEN LOCB IMPLEMENTED FOR QCC BILI ALT AST SCR

$DATA scm_im.CSV IGNORE=@
$SUBROUTINES ADVAN2 TRANS2

$PK
IWT = WT
IF(WT.EQ.-99.AND.SEX.EQ.0) IWT=46
IF(WT.EQ.-99.AND.SEX.EQ.1) IWT=54
TVCL = THETA(1) * (1+ART*THETA(4)) * (IWT/70)**0.75
CL = TVCL * EXP(ETA(1))
TVV = THETA (2) * (IWT/70)
V = TVV * EXP(ETA(2))
KA = THETA(3)
S2=V/1000
K = CL/V

$ERROR
IPRED = F
Y = F + F*ERR(1) + ERR(2)

$THETA
(0, 42);CL
(0, 1800);V
(0, 0.3) FIX ;KA
(0, 2);ART_CL

$OMEGA
(0.1) ; IIV CL
(0.1) ; IIV V

$SIGMA
0.1;PROP
100 ;ADD
```

$EST METHOD=1 INTERACTION MAXEVAL=9999

$COV

$TABLE ID PID TIME AMT TAD V CL KA RA AGE WT DL SEX ART IPRED
CWRES ONEHEADER NOPRINT FILE=sdtab32

;XPOSE
$TABLE ID KA CL V ETA1 ETA2 ONEHEADER NOPRINT FILE=patab32
$TABLE ID RA AGE WT ONEHEADER NOPRINT FILE=cotab32
$TABLE ID DL SEX ART ONEHEADER NOPRINT FILE=catab32

B. NONMEM CODE FOR FUNGAL COUNT MODLE

$PROBLEM POISSON MODEL FOR RATE OF FUNGAL CLEARANCE

$INPUT ID TIME DV DOSE AGE SEX WT ART DEATH T2DEATH CL V
SMIC FMIC AMIC SER VMR IND ME INDE
$DATA rate2.csv IGNORE=@

$PRED
```
BASE = THETA(1) ;+ ETA(1)
IF(IND.EQ.0)  LAMB1 = BASE
IF(IND.EQ.1)  LAMB1 = BASE * THETA(2)
IF(IND.EQ.-1) LAMB1 = BASE * THETA(3)

DIF = 1                ;COAT
IF(DOSE.EQ.100) DIF = THETA(5)  ;A 100
IF(DOSE.EQ.200) DIF = THETA(6)  ;A 200
IF(DOSE.EQ.300) DIF = THETA(7)  ;A 300
IF(DOSE.EQ.400) DIF = THETA(8)  ;A 400

TE = THETA(4) * DIF + ETA(1)*SER + ETA(2)*(1-SER)

LAMB = LAMB1 * EXP(-TE*TIME)
LFDV = LOG(EXP(GAMLN(DV+1)))
LOGP = -LAMB + DV*LOG(LAMB) - LFDV

Y=-2*LOGP
;Simulation block
IF (ICALL.EQ.4) THEN
T=0
N=0
DO WHILE (T.LT.1)          ;Loop
CALL RANDOM (2,R)           ;Random number in a uniform distribution
T=T-LOG(1-R)/LAMB
IF (T.LT.1) N=N+1
END DO
DV=N                ;Incrementation of one integer to the DV
ENDIF
```

$THETA
```
(0,0.5)            ;LAMB 0
(0,0.5)            ;LAMB 1
(0,0.5)            ;LAMB -1
(0, 0.5)           ;TE
(0, 1)             ;DIF_A100
```

```
(0, 1)                    ;DIF_A200
(0, 1)                    ;DIF_A300
(0, 1)                    ;DIF_A400

$OMEGA
0.1    ;BSV TE ASTRO_CM
0.1    ;BSV TE COAT

;Sim_start
;$SIM (12345) (678910 UNI) ONLYSIM NOPRED NSUB=100
$EST MAXEVAL=9999 METHOD=COND LAPLACE -2LL PRINT=1

$COV PRINT=E

$TABLE ID TIME LAMB DOSE AGE SEX WT ART DEATH T2DEATH CL V
SMIC FMIC AMIC SER VMR IND ME INDE NOPRINT ONEHEADER
FILE=sdtab4
;$TABLE ID TIME LAMB DOSE AGE SEX WT ART DEATH T2DEATH CL V
SMIC FMIC AMIC SER VMR IND ME INDE NOPRINT ONEHEADER
FILE=simtab4
;Sim_end
```

C. NONMEM CODE FOR SURVIVAL ANALYSIS

$PROBLEM VARYING DEATH HAZARD USING DES

$INPUT ID TIME DV SER DL DOSE AGE SEX WT ART CL V SMIC FMIC
AMIC EVID
;Sim_start

$DATA sur30.csv IGNORE=@ ;IGNORE(SER.EQ.0)
;$DATA simsur30.csv IGNORE=@ ;IGNORE(SER.EQ.0)
;Sim_end

$SUBR ADVAN=6 TOL=9

$MODEL COMP=(HAZARD)

$PK
IF(NEWIND.NE.2) TP=0 ; for RTTE. TP is time of previous event.
; T-TP is time since last event.
; For TTE TP is always 0.
BASE = THETA(1)*EXP(ETA(1)) ;the ETA is a placeholder here

SHP = THETA(2)   ;shape
LAM = BASE*SHP   ;lambda=scale
BETA = SHP-1
BETA1 = THETA(3)   ;SEX EFFECT
X1=0
IF(DOSE.EQ.400.OR.DOSE.EQ.100)X1=1
BETA2 = THETA(4)   ;DOSE100/400 EFFECT

$DES
DEL=1E-6   ; to keep from taking 0**power
DADT(1) = LAM*EXP(BETA*LOG(BASE*(T-TP)+DEL)) *
EXP(BETA1*SEX+BETA2*X1)

$ERROR
IF(NEWIND.NE.2) OLDCHZ=0 ;reset the cumulative hazard
CHZ = A(1)-OLDCHZ   ;cumulative hazard from previous time point in data set
OLDCHZ = A(1)   ;rename old cumulative hazard
SUR = EXP(-CHZ)   ;survival probability
DELX = 1E-6
HAZNOW=LAM*EXP(BETA*LOG(BASE*(TIME-TP)+DELX)) *
EXP(BETA1*SEX+BETA2*X1)
IF(DV.EQ.0) Y=SUR   ;censored event (prob of survival)
IF(DV.NE.0) Y=SUR*HAZNOW ;prob density function of event

161

```
IF(ICALL.EQ.4) THEN          ; for simulation
CALL RANDOM (2,R)
DV=0
RTTE = 0
IF(TIME.EQ.13) RTTE = 1     ; for the censored observation at 13 day
IF(R.GT.SUR) THEN
DV=1
RTTE = 1           ;observed event
ENDIF
ENDIF
```

$THETA
```
(0,0.02)     ; LAMBDA
(0,2)        ; ALPHA
(1)          ; MALE
(1)          ; DOSE100/400
```

$OMEGA
```
0  FIX
```

```
;Sim_start : add/remove for simulation
;$SIMULATION (5988566) (39978 UNIFORM) ONLYSIM NOPREDICTION
SUB=100
```
$EST MAXEVAL=9990 METHOD=0 LIKE PRINT=1

$COV PRINT=E

$TABLE ID TIME BASE DOSE SUR EVID NOPRINT ONEHEADER
FILE=sdtab14
;$TABLE ID TIME Y DV SER DOSE AGE SEX WT ART CL V SMIC FMIC
AMIC EVID NOPRINT ONEHEADER FILE=simtab14
;Sim_end

;XPOSE
$TABLE ID CL V ONEHEADER NOPRINT FILE=patab14
$TABLE ID AGE WT SMIC FMIC AMIC ONEHEADER NOPRINT
FILE=cotab14
$TABLE ID SER DOSE SEX ART ONEHEADER NOPRINT FILE=catab14

D. NONMEM CODE FOR SERTRALINE MODLE-BASED META-ANALYAIS

$PROBLEM SERTRALINE PK META-ANALYSIS IN HEALTHY SUBJECTS

$INPUT ID SID TIME DV AMT RATE SS II M WT AGE SEX DOSE CMT N EVID ARM

$DATA METAN.csv IGNORE=@ ;GNORE(M.EQ.1) ;IGNORE(TIME.GT.144) IGNORE(SID.EQ.7)

$SUBROUTINES ADVAN6 TOL=6

$MODEL
```
COMP(1)    ;GUT
COMP(2)    ;CENTRAL
COMP(3)    ;PERIPHERAL
```

$PK
```
W =1/SQRT(N)

TVCL = THETA(1)
CL = TVCL * EXP(ETA(1)*W + ETA(4))

TVV2 = THETA(2)
V2 = TVV2 * EXP(ETA(2)*W + ETA(5))

TVQ = THETA(3)

Q = TVQ ;* EXP(ETA(3)*W + ETA(11))

TVV3 = THETA(4)
IF(M.EQ.1) TVV3 = THETA(11)
V3 = TVV3 ;* EXP(ETA(4)*W + ETA(12))

TVKAMAX = THETA(5)
KAMAX = TVKAMAX ;* EXP(ETA(5)*W + ETA(13))

TVKA50 = THETA(6)
KA50 = TVKA50 ;* EXP(ETA(6)*W + ETA(14))

TVGAM = THETA (7)
GAM = TVGAM * EXP(ETA(3)*W + ETA(6))

TVF1 = THETA(8) *
DOSE**THETA(10)/(THETA(9)**THETA(10)+DOSE**THETA(10))
```

```
IF(M.EQ.1) TVF1=THETA(8)
F1 = TVF1 ;* EXP(ETA(8)*W + ETA(16))


S2 = V2/1000
K23=Q/V2
K32=Q/V3
```

$DES
```
CP = A(2)/V2
KA = KAMAX * T**GAM/(KA50**GAM + T**GAM)


DADT(1) = -KA*A(1)
DADT(2) = KA*A(1) + K32*A(3) - K23*A(2) - CP*CL
DADT(3) = K23*A(2) - K32*A(3)
```

$ERROR
```
Y= F + F*ERR(1)*W
IPRED = F
```

$THETA
```
(0, 56.4)       ;TVCL
(0, 1140)        ;TVV2
(0, 163)        ;TVQ
(0, 940)        ;TVV3
(0, 0.836)       ;TVKAMAX
(0, 3.65)       ;TVKA50
(0, 1.38)       ;TVGAM
(0, 0.684)        ;TVF1

(0, 20.4)        ;D50
(0, 1)    FIX    ;GDOSE
(0, 1140)        ;TVV2M
```

$OMEGA
```
0.1 ;IAV CL
0.1 ;IAV V2
0.1 ;IAV GAM
```

$OMEGA
```
0.1 ;ISV CL
0.1 ;ISV V2
0.1 ;ISV GAM
```

$SIGMA
```
0.1 ;PROP ERROR
```
$LEVEL
```
SID=(4[1],5[2],6[3])
```

$EST METHOD=1 INTERACTION MAX=9999 PRINT=5 SLOW

$COV MATRIX=R PRINT=E

$TABLE ID TIME CL V2 Q V3 KAMAX KA50 F1 GAM WT AGE SEX M DOSE
IPRED WRES CWRES NOPRINT ONEHEADER FILE=sdtab103

;XPOSE
$TABLE ID CL V2 Q V3 F1 KAMAX KA50 GAM ETA1 ETA2 ETA3 ETA4 ETA5
ETA6 ONEHEADER NOPRINT FILE=patab103
$TABLE ID WT AGE ONEHEADER NOPRINT FILE=cotab103
$TABLE ID SEX M DOSE ONEHEADER NOPRINT FILE=catab103

E. NONMEM CODE FOR AMIKAIN PK IN CHIDLERN WITH CANCER

$PROBLEM AMIKACIN PK IN PEDS

$INPUT ID TIME DV AMT RATE II SS EVID RA AGE SEX WT HT BSA ALB AST ALT BIL DIAG SCR BUN URIC CRCL VAN AMPH TEMP HGB HCT PLT BCLT DCHM DAMK

$DATA AMIKACIN.csv IGNORE=@

$SUB ADVAN3 TRANS4

$PK
TVCL = THETA(1)*(WT/70)**0.75
CL = TVCL*EXP(ETA(1))

TVV1 = THETA(2)*(WT/70)
V1 = TVV1*EXP(ETA(2))

TVQ = THETA(3)*(WT/70)**0.75
Q   = TVQ

TVV2 = THETA(4)*(WT/70)
V2 = TVV2

S1 = V1

$ERROR
IPRED=F
Y = IPRED + (IPRED*ERR(1))

$THETA
(0,5) ;CL
(0,15) ;V1
(0,5) ;Q
(0,30) ;V2

$OMEGA
0.1   ;CL
0.1   ;V

$SIGMA
0.1 ; PROP
$EST METHOD=1 INTERACTION PRINT=5 MAX=9999

$COV

$TABLE ID TIME AMT RATE CL V1 Q V2 PRED CWRES WRES IPRED
ONEHEADER NOPRINT FILE=sdtab1

;XPOSE
$TABLE ID CL V1 Q V2 ETA1 ETA2 ONEHEADER NOPRINT FILE=patab1
$TABLE ID RA AGE WT HT BSA ALB AST ALT BIL DIAG SCR BUN URIC CRCL
HGB HCT PLT DCHM DAMK ONEHEADER NOPRINT FILE=cotab1
$TABLE ID SEX VAN AMPH TEMP BCLT ONEHEADER NOPRINT FILE=catab1

$PROBLEM IN VITRO PD MODEL

$INPUT C SID ID TIME NDV DV LDV AMT CMT ADDL MIC STRAIN
STATIC DRUG HL II BQL EVID CONC RATE RUV4

$DATA PD_DATA2.csv IGNORE@ IGNORE (SID.EQ.3) IGNORE (SID.EQ.8)
IGNORE (BQL.EQ.1)

$SUB ADVAN13 TOL=6

$MODEL
COMP(1) ;CFU
COMP(2) ;CP

$PK
TVN0   = THETA(1)
N0   = 10**(TVN0 + ETA(1) + ETA(4))
A_0(1) = N0

TVKG   = THETA(2)
KG   = TVKG * EXP(ETA(2))

TVNMAX = THETA(3)
NMAX   = 10**(TVNMAX)

TVEMAX = THETA(4)
EMAX   = TVEMAX * EXP(ETA(3))

TVEC50 = THETA(5)
EC50   = TVEC50

ALPHA   = THETA(6)

BETA   = THETA(7)

K   = LOG(2)/HL
IF(HL.EQ.0) K = 0

$DES
N   = A(1)
CP   = A(2)

```
AD      = 1 + BETA*(1-EXP(-CP*ALPHA*T))
DE      = EMAX * CP/(AD*EC50+CP)
IF(DRUG.EQ.0) DE=0

DADT(1) = KG*(1-N/NMAX)*N - DE*N
DADT(2) = -K*A(2)
```

$ERROR
```
IPRED = 0
IF(F.GT.0) IPRED = LOG10(F)
ER = ERR(1)
IF(SID.NE.1) ER = ERR(2)
Y = IPRED + ER
```

$THETA
```
(0,6.8)    ;NO
(0,1.04)   ;KG
(0,9.40)   ;NMAX
(0,9)      ;EMAX
(0,3.5)    ;EC50
(0,0.0143) ;ALPHA
(0,29)     ;BETA
```

$OMEGA
```
0.14      ;IAV NO
```

$OMEGA
```
0.9       ;ISV NO
0.0445    ;ISV KG
0.0916    ;ISV EMAX
```

$LEVEL
```
SID=(4[1])
```

$SIGMA
```
2         ;STATIC
2         ;DYNAMIC
```

$EST METHOD=1 INTERACTION PRINT=5 MAX=9999 SLOW

$COV MATRIX=R

$TABLE ID TIME N0 KG NMAX EMAX EC50 ALPHA BETA SID MIC
STATIC DRUG PRED CWRES WRES IPRED ONEHEADER NOPRINT
FILE=sdtab70

;XPOSE
$TABLE ID N0 KG NMAX EMAX EC50 ALPHA BETA ONEHEADER
NOPRINT FILE=patab70
$TABLE ID ONEHEADER NOPRINT FILE=cotab70
$TABLE ID SID MIC STATIC DRUG ONEHEADER NOPRINT FILE=catab70